POREWATER PRESSURE RESPONSE OF AN ARTIFICIAL ISLAND TO WAVE LOADING

by

MUTHUCUMARASAMY YOGENDRAKUMAR

B.Sc(Eng.), University Of Peradeniya, Sri Lanka, 1980

A THESIS SUBMITTED IN PARTIAL FULFILMENT OF

THE REQUIREMENTS FOR THE DEGREE OF

MASTER OF APPLIED SCIENCE

in

THE FACULTY OF GRADUATE STUDIES

CIVIL ENGINEERING DEPARTMENT

We accept this thesis as conforming

to the required standard

THE UNIVERSITY OF BRITISH COLUMBIA

December 1983

Department of Civil Engineering

The University of British Columbia
2075 Wesbrook Place
Vancouver, Canada
V6T 1W5

Date: January 20, 1984

Dedicated

To Appah and Ammah

ABSTRACT

Plans for the future development of hydrocarbon reserves in the Western Canadian Arctic are based on the use of Caisson retained and Tanker islands as platforms for exploration drilling and future production. At present, the design of these islands are based on current geotechnical engineering design procedures. As exploration progresses towards deeper waters, the need for secure designs is indeed necessary. To be able to achieve this, one requires more sophisticated analytical procedures with the ability to quantify the probable response of these islands to environmental loadings. The chief environmental loads are due to ice, wave and earthquake.

A computer based method of analysis is presented for determining the porewater pressure response of these islands to wave loading. The method considers both dissipation and generation effects during wave loading. It also takes into account of the effect of increasing porewater pressure on soil properties. The computer program was used to analyse three different artificial islands subjected to different patterns of storm waves, each of duration 6 hours. The results of the analyses are presented and discussed.

TABLE OF CONTENTS

LIST OF TABLES

LIST OF FIGURES

ACKNOWLEDGEMENTS

CHAPTER 1

INTRODUCTION

1.1 Conventional Artificial Islands

Dramatic advances have taken place in offshore drilling for both exploration and production of hydrocarbons ever since the first commitment of the oil industry to offshore works. Numerous innovative offshore drilling methods have been proposed to suit offshore environments generally considered to be hostile and remote. These include artificial islands, concrete gravity structures, submersible concrete gravity structures such as the 'Monopad' and the 'Cone'(Stenning et al,1979),bottom-founded mobile rigs and several other types of floating rigs.

Of these innovative methods, artificial drilling islands are the popular mode in offshore drilling in the Mackenzie delta area and the southern Beaufort sea in the Western Canadian Arctic.

Artificial islands are man-made islands and serve as platforms for exploration drilling. The conventional artificial islands can be divided into different main groups depending on the construction techniques.

(1) Islands,known as ice islands, built during winter by trucking on-land gravels and dumping them on the sea bed after removing the ice by cutting it into blocks. Slope protection is provided after completion of the island. Adequate free board is

also provided so that these islands could be used during summer. This type of island is suitable for water depths less than 2 to 3 metres.

(2) Islands built within an underwater retaining wall consisting of sandbags. The fill material required for construction of the island is hauled in by barges from an offshore borrow pit. Slope protection above the water level is usually provided by additional sandbags.

(3) Islands constructed as hydraulic fills with material excavated by suction dredges from an offshore and/or onshore borrow pit and pumped as a slurry through a floating pipeline directly onto the island. Slope protection is provided by a sacrificial beach surrounding the island. This type of island is suitable for intermediate water depths.

The technical feasibility of conventional artificial islands, particularly in the offshore environment of Beaufort sea, is influenced to a great extent by the following factors. Firstly, suitable filling material must be available in abundance close to the island location. Secondly, enough construction power and equipment must be available on site to haul filling material from borrow pits and to complete the construction of the island within the limited time available for construction during the summer season. Thirdly, a reasonable construction season must be available so that drilling equipment can be moved onto the island in time.

The cost for island construction increases substantially in deeper water and at locations where suitable filling material cannot be found locally.

1.2 Caisson Retained Islands

The scarcity of suitable filling material for island construction, the increased cost involved in transporting suitable fill material to the site, coupled with the experience and confidence gained through the performance of existing conventional artificial islands have given rise to the concept of caisson retained artificial islands. These are islands built by ballasting reuseable concrete caissons onto a previously built berm and backfilling the interior by sand and gravel. The concrete caissons form the geometry of the island and are connected at the corners by steel doors to retain the fill. The maximum set down depth of a set of caissons is fixed, generally around 6 to 9 metres and in the case of deeper water, the underwater berm would be constructed to within the maximum set down depth of the water surface. Once exploration is complete, the caissons would be floated onto a new location as a ring. Figure 1.1 shows schematically a typical caisson retained island.

The caisson retained islands, also known as CRI have the advantage that they require much less quantity of fill material than conventional artificial islands. Further, these are not subject to significant erosion during or after construction. It also offers the advantage that it can be constructed more
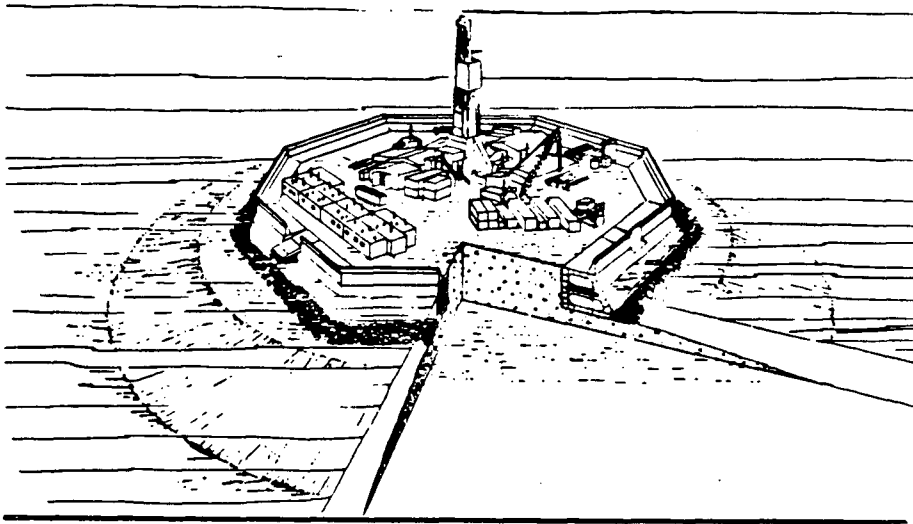
Figure 1.1; Caisson Retained Island

(After De Jong and Bruce, 1978)

speedily. The above factors provide the attraction for its use in the Beaufort sea in the Western Canadian Arctic, where the construction period is extremely limited and uncertain. The possibility that CRI could be converted into a production island with appropriate modifications and approvals and also that it could provide oil storage within caissons are added advantages of the caisson retained islands.

1.3 Scope

The artificial drilling islands built to date in Beaufort sea are for the purpose of gas and oil explorations and therefore, they are, at this stage, temporary in character. Further, all of them have been constructed in shallow waters within the landfast ice zone, except for a few more recent islands that have been constructed in intermediate water depths on the shear zone which separates the landfast ice from the floes of first year and multi-year pack ice. These islands are proven to be resistant to wave and ice attacks.

However, once gas and oil explorations progress towards deeper waters, artificial drilling islands will become exposed to harsher offshore environments. They will have interactions with much more mobile ice packs than encountered before. Also they will be exposed to open-water fetches of up to several thousands kilometres depending on wind direction and ice conditions. Therefore, deep water islands have to be designed on the basis of revised design procedures, generally trending towards greater stringency, to ensure their long term success.

One of the more interesting and perhaps, more important aspect that has to be given consideration in designing artificial islands in both deep and intermediate water depths is the wave induced porewater pressure during a storm and its implications for the stability of the island. It has been realised that the magnitude of wave induced porewater pressure at any location in berm and seafloor depends not only on the intensity of the storm but also on the contemporaneous rates of generation and dissipation of porewater pressure, which in turn depends on the liquefaction, the drainage and compressibility characteristics of soil deposits.

In practice, suitability of fill material for berms is based on the criteria drawn mainly from past experience. Generally sand and/or gravel with an average grain size of 150 microns or greater and with less than 10% silt are accepted to be most suitable for fill material. However, scarcity of such clean sand and gravel in the Beaufort sea area, the economic imperatives coupled with an extremely limited construction period make it almost impossible to have a good quality control on the material dredged for berm construction that would certainly meet the accepted standard for the fill. Therefore, when less permeable fill is used, it is possible that during a storm, the porewater pressure may build up substantially, perhaps even to liquefaction levels, causing great concern for the stability of the islands. It is also possible that residual porewater pressures after a storm can cause substantial reduction in stability of the island. In order to handle these

conditions, a proper understanding of wave induced porewater pressures during and after a storm is essential.

A part of the study carried out in this thesis is directed towards finding answers to such potential problems mentioned above. Basically, various analyses were conducted to establish the level of porewater pressures induced at selected sections of a typical artificial drilling island during a moderate storm. Variation in berm configuration, variation in soil strata comprising the seafloor soil profile and their drainage and compressibility characteristics were also considered in the analyses to determine their significance on the induced porewater pressure. All wave induced porewater pressure analyses were conducted using the computer program STABW3, which was developed by Yogendrakumar, Siddharthan and Finn. It is a modified version of STABW (Siddharthan and Finn, 1979;1982). Some important elements of the program STABW3 are presented in Chapter 3 and 4.

1.4 Thesis Outline

Chapter 2 discusses extensively the important aspects of wave induced residual porewater pressure analysis which include the mechanisms of porewater pressure generation and dissipation during wave loading. It also contains a brief review of existing analytical methods for the determination of wave induced porewater pressures.

Chapter 3 deals with the general theory of wave induced residual porewater pressure analysis. The assumptions of the

theory are examined and the procedures for incorporating the modifications in soil properties caused by increasing porewater pressures are discussed.

The motivation for the development of STABW3 program and the formulation of the finite element equations involved are presented in Chapter 4.

The selection of soil parameters and other relevant data required for wave induced residual porewater pressure analysis are presented in Chapter 5.

Chapter 6 discusses the results of the wave induced residual porewater pressure analysis for different drainage characteristics. The effect of rockfill cover and foundation conditions are presented in Chapter 7 and 8 respectively.

The summary and main conclusions based on the results of the analyses are presented in Chapter 9.

CHAPTER 2

GENERAL ASPECTS OF WAVE INDUCED RESIDUAL POREWATER PRESSURES

2.1 Introduction

The wave induced porewater pressure response is a result of a complex interaction between waves and seafloor. However, with certain assumptions and idealizations with respect to storm characteristics and seafloor characteristics, it is possible to devise a simple analytical tool to evaluate wave induced porewater pressures with an accuracy generally acceptable for engineering purposes. Such assumptions and idealizations are often extensive and are discussed in the next Chapter along with the development of theory.

2.2 Mechanism For Porewater Pressure Generation

The mechanism that is responsible for the generation of residual porewater pressure under the action of waves is well understood. The waves, as they pass by, create dynamic wave pressure on the seafloor. There are numerous wave theories available to compute the amplitude of the pressure wave, each of which has its own assumptions and applicability based primarily on wave characteristics and water depth. Most researchers determine pressure wave amplitude using linear wave theory which assumes the seafloor to be rigid and impermeable. Some aspects of the linear wave theory are presented in Section 3.8. This moving harmonic pressure wave on the seafloor creates shear stresses, cyclic in nature, the magnitude of which depend

on the material properties of the underlying soil forming the soil profile. These cyclic shear stresses generate porewater pressures in the underlying soil due to the creation of volumetric strain potential (Martin, Finn and Seed, 1975).

2.3 Dissipation Effects On Wave Induced Residual Porewater Pressure

Unlike earthquakes, storms last much longer, often several hours. Therefore, unlike in earthquake analyses, the common assumption that an undrained condition prevails cannot be adopted in wave induced residual porewater pressure analyses. The analysis assuming undrained conditions will lead to higher porewater pressure response than will actually occur and as a result undue conservatism in design will result from using this approach. To avoid this, it is necessary to take into account both dissipation as well as the generation of porewater pressure. The net porewater pressure response will be the resultant of the two opposing processes mentioned above.

Diffusion within and drainage out of the free draining boundary, constitute the dissipation effects. These may be substantial in those soils in which drainage can take place easily. Seed and Rahman (1977) have illustrated the significance of incorporating dissipation effects on the wave induced residual porewater pressure response. In general, the changes in porewater pressure response produced by incorporating dissipation effects, will depend primarily on (1) the geometric detail of the soil profile,

(2) the compressibility and permeability characteristics of soil layers forming the soil profile.

2.4 Wave Induced Instability

The artificial drilling islands built to date are temporary in character with design lives of a few years at most. The designs of these islands are based only on fairly simple geotechnical engineering design assessments. As exploration progresses towards deeper waters, the need for more secure designs for both temporary and production islands becomes necessary. To be able to achieve this, one requires more sophisticated geotechnical engineering analytical procedures with the ability to quantify the probable response of the islands to environmental loadings. The chief environmental loads are due to ice, waves and earthquakes. The relative importance of the risk from each of this sources depends on the location of the island. A brief review of the instability arising from wave loading and the methods available in current engineering practice to handle wave related instability are presented herein.

The kinds of instability that arise from wave loading fall into two main categories. The first one is due to the instantaneous stress field generated by a passing wave. If the intensity of the passing wave is strong enough, then the effective stresses associated with the wave loading violate the Mohr-Coulomb failure criterion and consequently failing or yielding will occur in the seafloor or island slope.

The other kind of wave induced instability arises from the cumulative effects of waves which create residual porewater pressures. The consequences of the wave induced porewater pressure are of two types. The first type is liquefaction related. If the induced porewater pressures attain a value equal to the initial effective overburden pressure, then soil will loose all shear strength temporarily. Depending on the conditions such as density of soil, stratification, slope of the ground surface and nature of supported structures, this temporary loss of strength may result in serious engineering problems. The most common form of these problems, as far as artificial islands are concerned, are sand boils, excessive subsidence, slides and foundation failure. The second type of consequence arising from wave induced porewater pressures is somewhat less dramatic but still of major concern. Even if the wave induced porewater pressures do not reach level of liquefaction, they reduce the insitu effective stresses and shear resistance of the soil so that it becomes more susceptible to large scale deformation under a passing large wave or gravity stresses.

Another possible consequence of residual porewater pressure is the potential for settlement. The wave induced residual porewater pressure will eventually dissipate, at rates dictated by the drainage characteristics of the soil. This dissipation will be accompanied by a decrease in volume of the voids which may be reflected in corresponding settlements at the surface. The amount of settlement will depend on the level

of induced porewater pressure, the extent of affected zone and nature of overburden material.

At present, the analysis of instantaneous wave induced porewater pressure is best investigated throught the general computer program STAB-MAX (Siddharthan et al,1979). It is a coupled effective stress analysis taking into account the coupling of the sand skeleton and pore water in resisting the waves. The study of the response of seabed to wave loading by Yamamoto (1978) and Madsen(1978) provided the base for STAB-MAX. Yamamoto, in his study, assumed hydraulic isotropy and deposits of finite and infinite depth. On the other hand, Madsen assumed deposits of infinite depth but included hydraulic anisotropy. The computer program STAB-MAX is thus a generalisation of the Yamamoto-Madsen solutions to layered soils with hydraulic anisotropy and deposits of finite depth. A limited field verification of the capability of STAB-MAX has been reported by Finn et al (1982).

The computer programs available at present for predicting residual porewater pressure and estimating liquefaction potential under wave loading are OCEAN1 (Seed et al, 1977) and STABW (Siddharthan et al,1979). In this thesis, another computer program STABW3 is developed. This particular program is an extended version of STABW. A brief review of the analyses incorporated in these programs is presented in Section 2.5.

The analyses incorporated in the STAB-MAX, STABW, and STABW3 are all based on the assumption of level seafloor. Their application to gentle slopes may be acceptable for practical

purposes. But as the slope get steeper the prediction of porewater pressure based on these programs becomes increasingly conservative. The main sources that are responsible for the conservative predictions of porewater pressures are:

(i) greater drainage from a sloping seafloor than from a level one

(ii) the presence of static shear stresses in a sloping seafloor which tend to retard the rate of porewater pressure generation.

The stability of a sloping seafloor may be evaluated by limiting equilibrium methods of analysis. Henkel (1970) was the first to provide an analytical framework for the stability of sloping seafloor under a wave loading. His method is a total stress static method. The method considers the limiting equilibrium state of a circular slip surface for undrained conditions, taking into account wave pressures on the seafloor, gravity loads and the undrained strength of the soil. The main objection for this method is that it does not include the true cyclic nature of the wave loading and the porewater pressure associated with it which are so vital for the stability of seafloor slopes.

Finn and Lee (1979) proposed an effective stress stability analysis applicable to steeper slopes under wave loading. The method is a modification of Sarma's (1973) method of slices to include the wave pressures generated by the waves. The method considers an acting force system on the sliding mass consisting of gravity loads, wave pressure on seafloor, and instantaneous

and residual porewater pressures acting on the failure surface of the sliding mass. The main attraction of this method lies on the fact that it recognises the true cyclic nature of the wave loading and take into account of porewater pressures associated with the wave loading.

2.5 Review Of Analytical Methods

2.5.1 Seed And Rahman Method

Seed and Rahman (1977) were the first to propose an analytical procedure for evaluation of wave induced residual porewater pressure that takes into account both generation and dissipation effects. The procedure is quite similar to that developed for evaluating liquefaction potential under earthquake loading (Seed, et al 1971) except for the manner of determining the induced cyclic shear stresses.

Their method of analysis contains two separate phases. In the first phase, the wave induced shear stresses are computed using the computer program STR1. The program evaluates the shear stresses using the theory of elasticity, for the different wave components constituting the specified design storm. The shear stresses computed at the top of the soil deposit for each wave component are then used to establish the equivalent uniform storm using procedures proposed by Seed et al (1975). This enables the complex wave storm loading to be represented by an equivalent uniform wave storm loading consisting of an equivalent number of uniform cycles of a specified shear stress ratio.

In the second phase, the wave induced residual porewater pressures are computed through the finite element computer program OCEAN1. The cyclic shear stresses induced by the established equivalent wave loading are used in this program to estimate the residual porewater pressures. Some aspects of the theory involved, particularly the ones which are common to both the Seed-Rahman method of analysis and the method of analysis to be developed in this thesis are presented in Chapter 3.

The computation of cyclic shear stresses is accomplished by a finite element analysis of an idealized two dimensional problem, requiring two elastic constants, for convenience, chosen to be the shear modulus and bulk modulus. The shear and bulk moduli are functions of mean normal effective stresses and as the porewater pressure increases, the mean normal effective stress decreases, resulting in the degradation of shear and bulk moduli. This, in turn, affects the computed shear stresses. Therefore, in general, it is important to include degradation of shear and bulk moduli in computation of cyclic shear stresses and thereby to obtain reasonable estimates of the rate of porewater pressure generation.

Although the Seed-Rahman method of analysis takes into account of the variation in volume compressibility due to the effect of increasing porewater pressure, it never considers the degradation of the shear and bulk moduli in the computation of cyclic shear stresses. It is a known fact that in the case of deep uniform deposit, the maximum cyclic shear stress induced by wave loading is independent of the elastic constants. In

these cases, the degradation of moduli in the computation of shear stresses are not necessary. However, in the case of finite and non-uniform deposits, considered to be the general case, the shear stresses depend on the elastic constants and it is essential to modify the soil properties for the effect of increasing porewater pressure. In order to handle the most general case of non-uniform deposits a method of analysis which considers the degradation of soil properties along with variation of volume compressibility for the effect of increasing porewater pressure is needed. Such a method of analysis was first proposed by Siddharthan and Finn (1979) and it is outlined briefly in the next section.

2.5.2 Siddharthan and Finn Method

The method of analysis proposed by Siddharthan and Finn (1979, 1982) is basically a generalization of the Seed and Rahman method. In this method of analysis, the stress analysis phase is combined with the residual porewater pressure analysis phase into a single finite element computer program STABW. In this way, it is possible to modify elastic constants repeatedly to be comparable with the current value of porewater pressure and to re-evaluate cyclic shear stresses and thereby the rate of porewater pressure generation. The program has the option of carrying out analysis with or without soil property modifications for the effect of increasing porewater pressure.

Apart from this improvement, the other main difference in this approach from the Seed-Rahman approach is the manner by

which the equivalent uniform storm is established. Instead of the procedure adopted by Seed and Rahman which uses a simple weighting curve to determine equivalence, the more general procedure proposed by Lee and Chan (1972) is used. The details of the procedure are presented in Section 3.7.

CHAPTER 3

<u>GENERAL THEORY</u>

3.1 <u>Assumptions and Idealizations</u>

Most methods of analysis require that the problem
under consideration be idealized in some way so that a
convenient model may be formulated. The wave induced residual
porewater pressure analysis to be developed in this thesis is
no exception to this. The assumptions and idealizations implied
in defining storm characteristics, ocean and soil profiles are
described in this section. The assumptions involved in other
elements of the analysis, for example, in the development of
governing equations and in the computation of wave induced
shear stresses, are presented in sections where they are
developed.

3.1.1 <u>Storm Waves</u>

The offshore wave environment is a random process
dependent on wind speed, water depth, mudline characteristics
and various other factors. However, in practice, it is
customary to define the sea state at any time by two important
variables, namely, wave heights and periods existing at that
time. The common parameters that characterizes the sea state in
the statistical sense are the significant wave height H_s and
the significant wave period T_s. The significant wave height is
analytically defined as the average height of the highest third
of the waves and the significant wave period is the mean period

of the waves chosen for the determination of the significant wave height. The significant wave height and significant wave period can be estimated by wave hindcasting techniques which involve the application of wind data. These are determined directly in terms of wind speed U, fetch F and duration t over which the wind acts.

More direct information on wave characteristics can be determined from a continuous record of surface elevation obtained from a wave recorder. The important parameters required to define the overall wave characteristics are:

(i) the zero-crossing period, T_z, defined as the average period between sucessive zero up-crossing,

(ii) the crest period, T_c, defined as the average period between sucessive crests,

(iii) the vertical distance from the lowest trough to the highest crest.

In this thesis, the storm waves are described in terms of significant wave height and significant wave period.

The two approaches widely used for analysis involving wave loading are the discrete wave method of analysis and the spectral method of analysis. In this thesis, the discrete method of analysis is used. This approach makes no attempt to model wave loading process as a random excitation but assumes that the process can be split into discrete waves each of which has a specified period associated with it. The distribution of wave heights in a wave storm is assumed to be given by a Rayleigh density function and it is often specified in terms of

significant wave height in the form,

$$p(H) = 1 - \exp\{-2(H/H_s)^2\} \qquad (3-1)$$

where,

H = wave height

H_s = significant wave height

p(H) = probability density function

For a given significant wave height, the probability of occurence of a wave of height H, occurring between H_1 and H_2, where $H_1 < H < H_2$, is given by,

$$P(H) = p(H_1) - p(H_2) \qquad (3-2)$$

The probability of occurence P(H) given by equation (3-2) is assumed to be associated with a wave of height $(H_1 + H_2)/2$.

The maximum wave height H_m in the wave height distribution is assumed to be the breaking height associated with a still water depth d and for shallow water cases, it can be calculated using following equation suggested by McCowan (Sarpakaya et al, 1981),

$$H_m = 0.78 \ d \qquad (3-3)$$

For analysis, waves of height greater than H_m are assumed to be waves of height of H_m. In other words, the total number of waves of height greater than H_m in the distribution are added to the number associated with the wave of height H_m.

The Rayleigh distribution enables the storm to be represented by many waves, each of them differing in characteristics. It is assumed that these waves have characteristics in accordance with linear wave theory, which describes the wave by its period, wave height and water depth.

Some aspects of the linear wave theory are presented in Section 3.8. The waves are assumed to travel predominantly in one direction, that is, the effect of directional randomness is assumed to be negligible. Also, the shoaling effects, the wave scouring effects and the diffraction effects in modifying the responses are not taken into account.

3.1.2 Soil Profile and Ocean Floor

The entire soil profile is assumed to comprise of horizontally layered soils, each of them are of infinite lateral extent. The properties of soil deposits are assumed to vary only in the vertical direction and each deposit is divided into layers each with uniform properties. The ocean floor is assumed to be parallel to still water level.

3.2 Derivation Of Governing Equation

As discussed previously the governing equation of wave induced porewater pressure response in an offshore environment should incorporate the effect of both dissipation and generation. In developing the governing equation, it is assumed that Darcy's flow is valid. Hence from the one dimensional continuity equation in z direction,

$$\delta/\delta z \ \{ \ k_z/\gamma_w \cdot \delta u/\delta z \ \} \ = \ \delta\epsilon/\delta t \qquad (3-4)$$

where,

u = excess porewater pressure

k_z = coefficient of permeability in z(vertical) direction

γ_w = unit weight of water

ϵ = volumetric strain, reduction considered to be positive.

Consider an element of soil with excess porewater pressure u. Suppose it undergoes a change of Δu in excess porewater pressure during an interval of time Δt, then during that time interval, it will be subjected to a certain number of cycles of cyclic shear stress, which in turn, will cause an increase in porewater pressure given by $(\delta u_g/\delta t).\Delta t$, where $(\delta u_g/\delta t)$ is the rate of porewater pressure generation.

If the change in bulk stress is neglected then the volume change $\Delta\epsilon$ of the element in that interval of time is given by,

$$\Delta\epsilon = m_V(\Delta u - \delta u_g/\delta t .\Delta t) \qquad (3-5)$$

where,

m_V = coefficient of volume compressibility.

Now as $\Delta t \longrightarrow 0$,

$$\delta\epsilon/\delta t = m_V (\delta u/\delta t - \delta u_g/\delta t) \qquad (3-6)$$

From equations (3-4) and (3-6),

$$\delta/\delta z \{ k_z/\gamma_w . \delta u/\delta z \} = m_V (\delta u/\delta t - \delta u_g/\delta t) \qquad (3-7)$$

Equation (3-7) is the governing equation for porewater pressure response to storm waves. It has been used previously by Finn et al (1976) for the analysis of seismically induced porewater pressures.

3.3 Estimation Of Rate Of Porewater Pressure Generation

The rate of porewater pressure generation required in equation (3-7) can be determined by the procedure proposed by Seed and Rahman (1977). The basic steps involved are given

herein.

The rate of porewater pressure increase can be written in the form,

$$\delta u_g/\delta t = \delta u_g/\delta N \cdot \delta N/\delta t \qquad (3\text{-}8)$$

where N is the number of stress cycles during the storm.

The values of $\delta u_g/\delta N$ can be obtained from undrained tests. However, for practical purposes, the relationship between u_g and N can be expressed in terms of number of cycles N_L required for initial liquefaction in the following form,

$$u_g/\sigma'_{vo} = 2/\pi \ \text{arc Sin} \ (\ N/N_L\ )^{1/2\theta} \qquad (3\text{-}9)$$

where, σ'_{vo} = initial vertical effective stress

$\quad\theta$ = an empirical constant

The relationship in equation (3-9) is given in Figure 3.1 for different values of θ. The value of $\theta = 0.7$ is typical for clean medium sands.

Differentiation of equation (3-9) with respect to N and simplification yields,

$$\delta u_g/\delta N = \sigma'_{vo}/(\ \theta\pi N_L\ ) \cdot 1/f(r_u) \qquad (3\text{-}10)$$

where,

$$f(r_u) = \text{Sin}^{(2\theta-1)}(0.5\pi r_u) \cdot \text{Cos}(0.5\pi r_u)$$

$\quad r_u$ = porewater pressure ratio, u/σ'_{vo}

Also,

$$\delta N/\delta t = N_{eq}/T_D \qquad (3\text{-}11)$$

where N_{eq} = equivalent number of uniform stress cycles corresponding to the established equivalent uniform storm with duration T_D.

Therefore, from equations (3-8), (3-10) and (3-11)
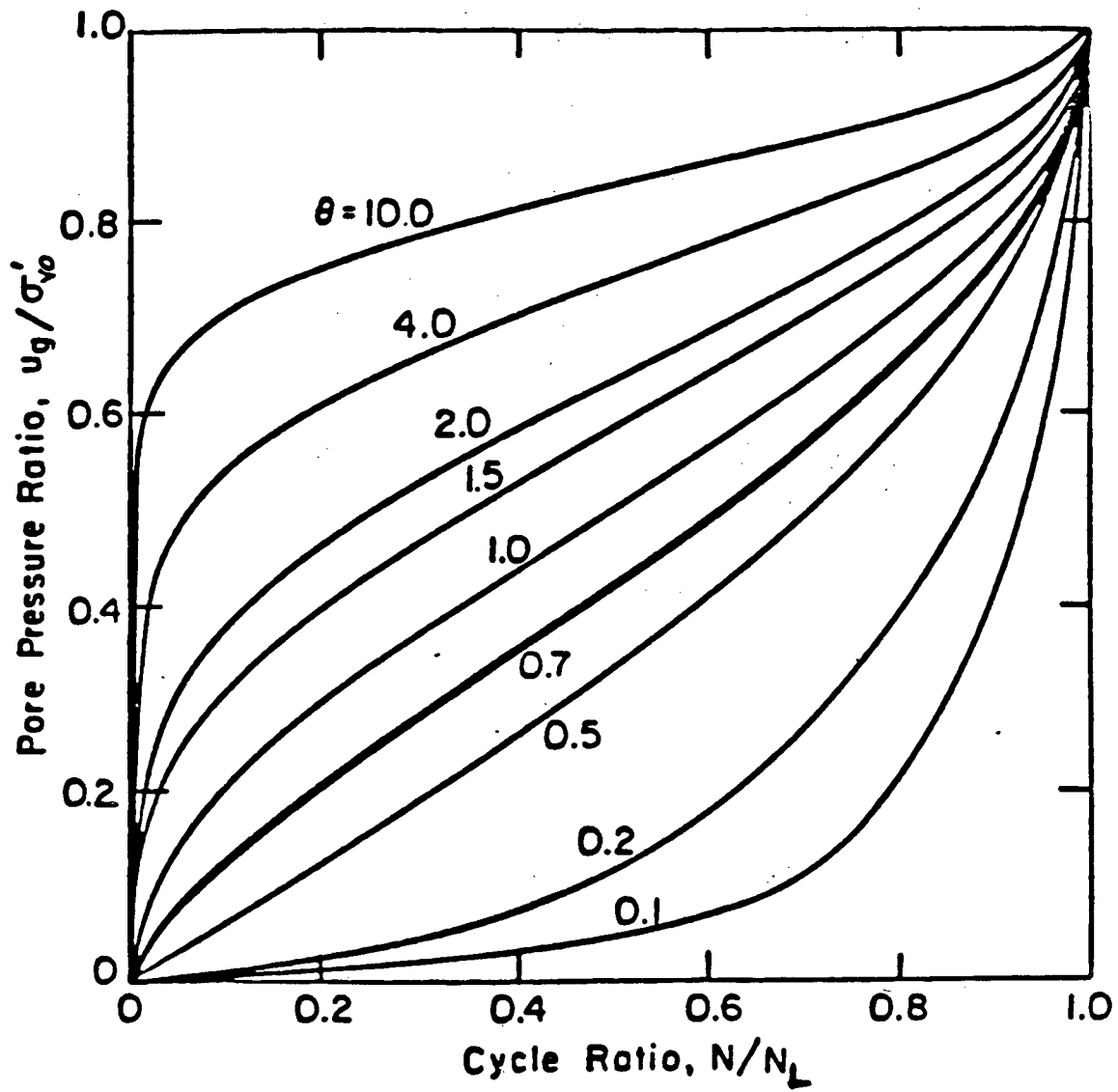
Figure 3.1; Rate of Porewater Pressure Generation

$$\delta u_g/\delta t \quad = \quad \sigma'_{vo}/(\theta \pi T_D) \; . \; (N_{eq}/N_L) \; . \; 1/f(r_u) \quad (3-12)$$

The rate of porewater pressure generation $\delta u_g/\delta t$, at any time, can be calculated from equation (3-12) knowing the value of porewater pressure at that time.

3.4 Solution Technique

With the rate of porewater pressure generation given by equation (3-12), it is now possible to solve equation (3-7) for the domain and boundary shown in Figure 3.2. The formulation of the proposed finite element method is outlined in detail in Section 4.2.

To compute the rate of porewater pressure generation from equation (3-12) at any location, one needs to know N_L, the number of cycles to cause initial wave induced liquefaction. N_L can be conveniently computed from a liquefaction strength curve such as the one shown in Figure 3.3. The shear stress ratio induced by the equivalent storm at the location of interest can be used to establish the appropriate N_L values. To establish a liquefaction strength curve, cyclic loading tests, usually the cyclic simple shear test or the cyclic triaxial test, can be performed on representative undisturbed samples.

In the case of tests performed in the triaxial apparatus, a correction factor has to be applied to the results to account for the two dimensional plane strain condition of ocean wave loading. A correction factor between 0.60 to 0.70 is considered reasonable. However, in the case of tests conducted in simple shear apparatus, the correction factor is not necessary, as it

u = O at z = O

x

z
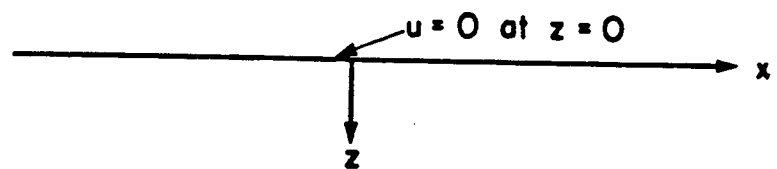
__Soil Deposit__

R

$$\frac{\partial}{\partial z}\left[\frac{Kz}{\gamma_w}\frac{\partial u}{\partial z}\right] = m_v\left[\frac{\partial u}{\partial t} - \frac{\partial u_g}{\partial t}\right]$$

$$\frac{\partial u}{\partial z} = O \ \text{at} \ z = D$$
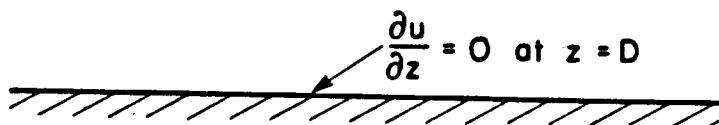
Figure 3.2; Basic Equation and Solution Domain
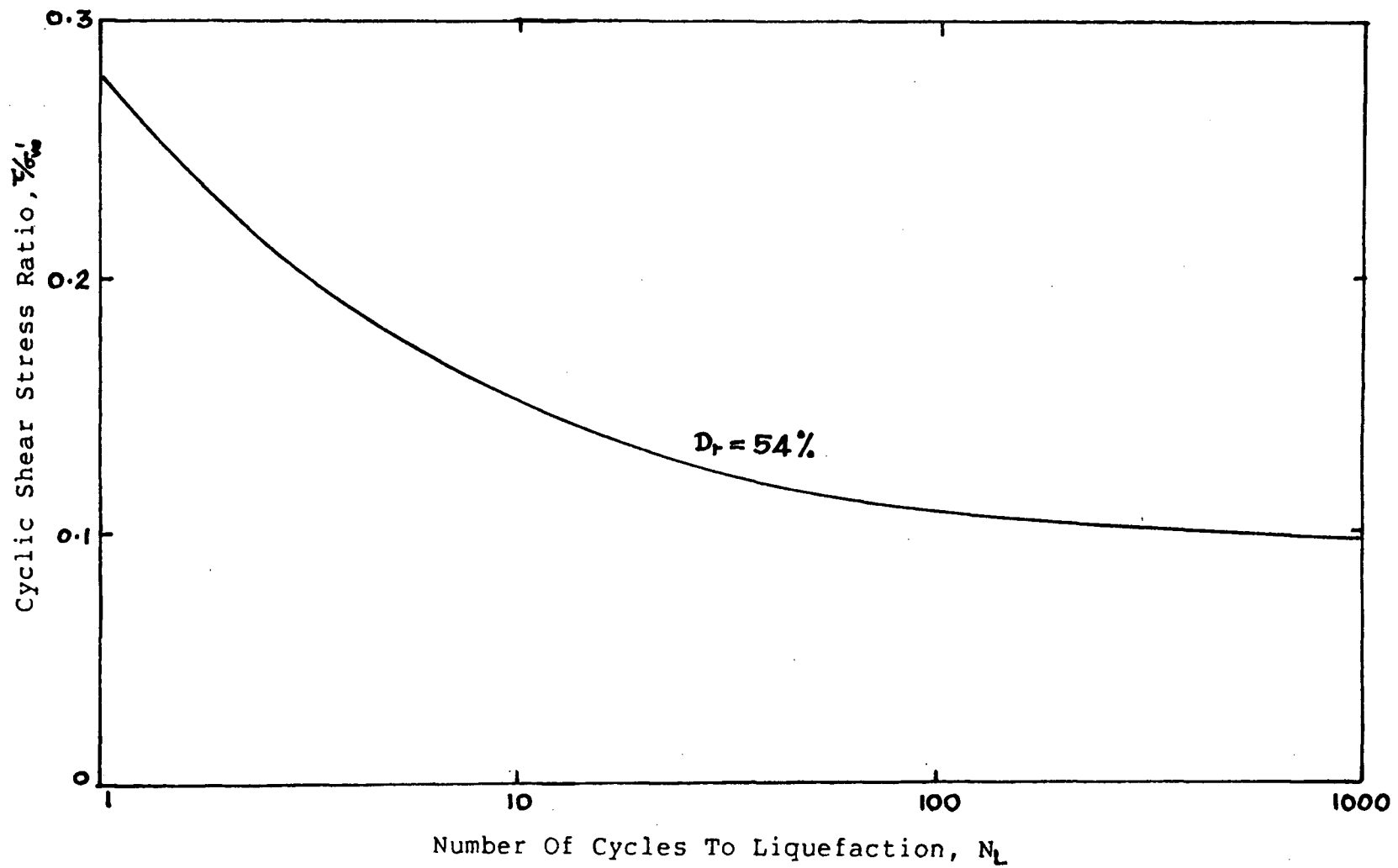
Figure 3.3; Liquefaction Strength Curve

(After Seed and Rahman, 1977)

provides the closest representation of field conditions (Seed, 1979).

3.5 Variation In Volume Compressibility

The volume compressibility of soil increases with increase in porewater pressure. The volume compressibility can be computed using the following equation proposed by Martin (1976).

$$m_v/m_{vo} = e^Y /(1 + y + 0.5y^2) \qquad (3-13)$$

where,

$y = A.r_u^B$

$A = 5(1.5 - D_r)$

$B = 3 \times 2^{-2D_r}$

$D_r =$ relative density

$r_u =$ porewater pressure ratio

$m_v =$ volume compressibility at porewater pressure ratio, u/σ_{vo}'

$m_{vo} =$ initial volume compressibility at zero porewater pressure ratio

Results from equation (3-13) for $D_r = 50\%$ is given in Figure 3.3.

3.6 Soil Moduli Variation

As discussed earlier in Section 2.5.1, the elastic constants used in the cyclic shear stress analysis have to be modified for the effect of porewater presssure. In the present
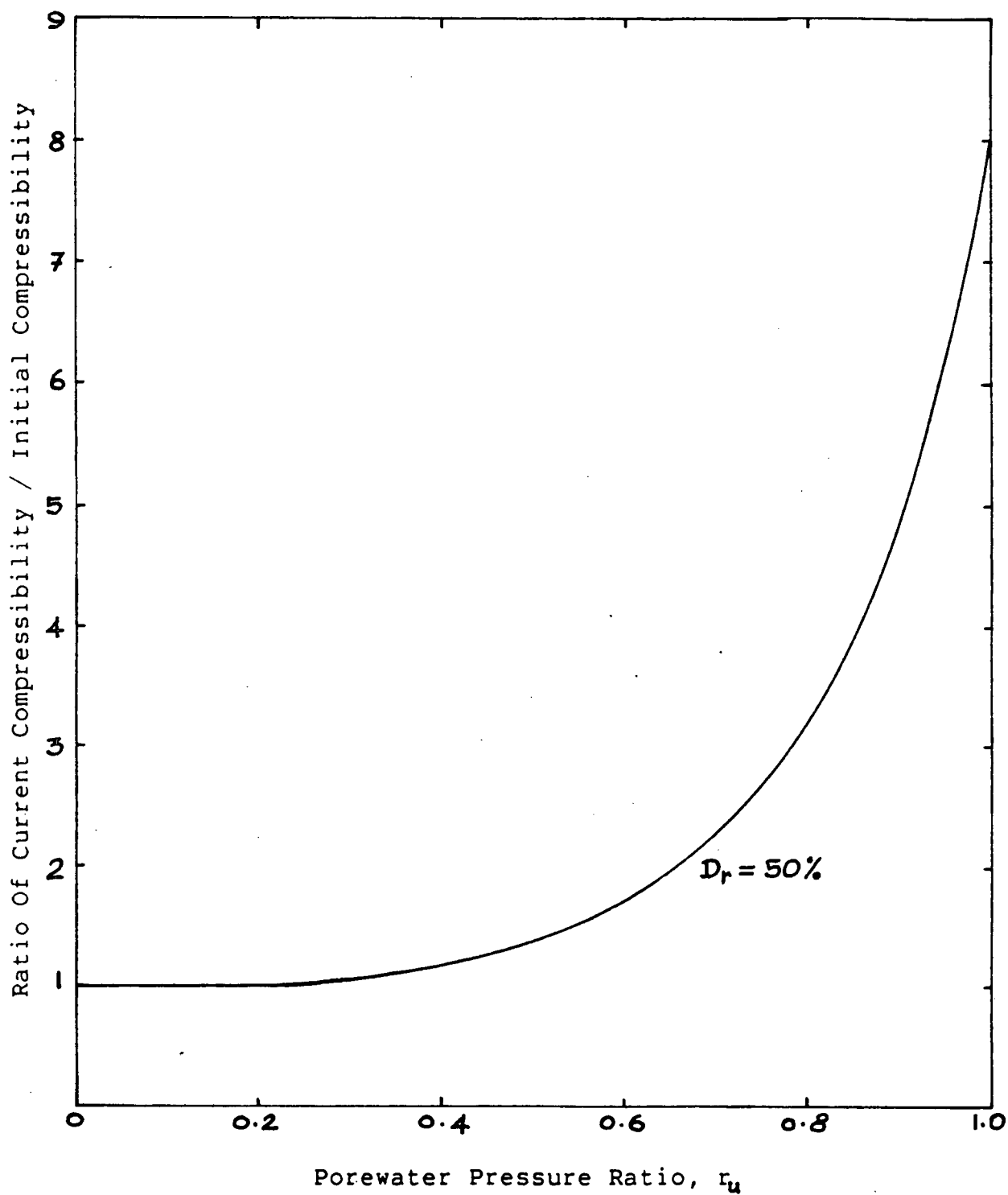
Figure 3.4; Variation of Volume Compressibility With
Porewater Pressure Ratio.

wave induecd residual porewater pressure analysis, the soil moduli are modified in the manner described below.

3.6.1 Modification Of Bulk Modulus

A comprehensive study by Duncan et al (1978) reveals that bulk modulus depends on minor principal effective stress and the variation can be approximated by an equation of the form,

$$B_m = K_b P_a (\sigma'_3 / P_a)^{1/2} \qquad (3-14)$$

where B_m = bulk modulus

K_b = bulk modulus constant

m = bulk modulus exponent

P_a = atmospheric pressure, expressed in the same units as σ'_3 and B_m.

σ'_3 = average effective minor principal stress, assumed to be $K_o \sigma'_{vo}$

With porewater pressure u, the minor principal effective stress is given by

$$\sigma'_3 = (K_o \sigma'_{vo} - u) \qquad (3-15)$$

Therefore, from equations (3-14) and (3-15), the compatible bulk modulus B_{mt} for the current level of porewater pressure is given by

$$B_{mt}/B_{mo} = \{ (K_o \sigma'_{vo} - u) / (K_o \sigma'_{vo})\}^m \qquad (3-16)$$

where B_{mo} is the initial bulk modulus at zero porewater pressure and K_o is the coefficient of earth pressure at rest.

Equation (3-16) represents the modification of bulk

modulus for the effect of porewater pressure adopted in this thesis.

3.6.2 Modification Of Shear Modulus

Seed and Idriss (1970) developed a relationship for the determination of maximum shear modulus G_{max} (at shear strains less than 10^{-4}%) in the form

$$G_{max} = 1000 \ k_{2max} \ (\sigma'_m)^{1/2} \qquad (3-17)$$

where,

σ'_m = mean normal effective stress in psf

k_{2max} = parameter which depends on soil type and relative density D_r

It is also suggested that k_{2max} for sands (Byrne, 1981) is as follows;

$$k_{2max} = (15 + 0.6 \ D_r) \qquad (3-18)$$

For gravels and silts, k_2 is given as

$$k_{2max} = (15 + 0.65 \ D_r) \ F \qquad (3-19)$$

The parameter F depends on soil type and typical values of F are,

$$F = 2.0 \quad \text{for gravels}$$

$$F = 0.6 \quad \text{for silts}$$

The empirical equation for the determination of values of maximum shear modulus, proposed by Hardin and Drnevich (1972) is of the form

$$G_{max} = 320.8 \ \{(2.973 - e)^2/(1 + e)\} \ (OCR)^k \ (\sigma'_m/P_a)^{1/2}$$

$$(3-20)$$

where,

e = void ratio

OCR = overconsolidation ratio

k = parameter that depends on the plasticity index of the soil.

The equations (3-17) and (3-20) imply that G_{max} depends on σ'_m and is proportional to $(\sigma'_m)^{1/2}$. This allows a modification of shear modulus for the effect of porewater pressure in the form,

$$G_{mt} = G_{mo} (\sigma'_{mt}/\sigma'_{mo})^{1/2} \qquad (3-21)$$

where,

G_{mt} = compatible shear modulus for the current level of porewater pressure u,

G_{mo} = initial value of shear modulus at zero porewater pressure,

σ'_{mt} = mean normal effective stress at current level of porewater pressure u,

σ'_{mo} = mean normal effective stress at zero porewater pressure.

σ'_{mo} and σ'_{mt} can be calculated using the following equations;

$$\sigma'_{mo} = (1 + 2 K_o)/3 \quad \sigma'_{vo} \qquad (3-22)$$

$$\sigma'_{mt} = (1 + 2 K_o)/3 \quad (\sigma'_{vo} - u) \qquad (3-23)$$

where σ'_{vo} = initial vertical effective stress.

In this thesis, the modification of shear modulus for the effect of porewater pressure, is taken into account in the form given by equation (3-21).

3.7 <u>Establishing Equivalent Uniform Storm</u>

As pointed out earlier in Section 2.5.2, the equivalent storm is established using the method proposed by Lee and Chan (1972). The very first step is to select a reference wave in the wave height distribution resulting from Rayleigh distribution (see Section 3.1.1). The maximum wave or a wave of height close to the maximum wave height is often chosen as the reference wave.

Now, the shear stress ratio τ/σ'_{vo} , at the top of the deposit (ie, $z \rightarrow 0$) is calculated for each of the wave components in the storm and also for the selected reference wave. Using these τ/σ'_{vo} values at z=0, for each of the waves involved, the number of cycles to cause initial liquefaction (N_L) is computed from an appropriate liquefaction strength curve, such as the one shown in the Figure 3.3.

The equivalent number of cycles, N_{eq}, for the selected reference wave can be calculated from the equation,

$$N_{eq} = \sum_{i=1}^{n_w} \left\{ \left(N_{Leq}/N_{Li} \right) \times N_i \right\} \qquad (3-24)$$

where,

N_{Leq} = number of cycles required to cause initial liquefaction obtained from appropriate liquefaction strength curve, corresponding to the shear stress ratio τ/σ'_{vo} at z=0 for the selected reference wave.

N_{Li} = number of cycles required to cause initial liquefaction obtained from liquefaction strength curve, corresponding to the shear stress ratio

τ/σ'_{vo} at z=0 for the ith wave component.

N_i = number of waves of the ith wave component in the wave storm.

n_w = total number of wave components representing the wave storm.

3.8 Linear Wave Theory

Linear wave theory has been used in this thesis for the purposes listed below:

(1) To describe each of the wave components in the storm.

(2) To compute the pressure wave loading on the seafloor required for the calculation of shear stresses due to each of the wave components.

The theory assumes that the seafloor to be rigid and impermeable. According to the theory, the equation of the wave profile of a wave of height H and period T is given by:

$$Y_s = H/2 \ \text{Cos} \ \{ \ 2\pi \ (x/L - t/T) \ \} \qquad (3-25)$$

and the wave length L can be obtained from the following implicit equation:

$$L = \left(0.5gT^2/\pi\right) \tanh \ (2\pi d/L) \qquad (3-26)$$

where,

d = still water depth

g = acceleration due to gravity

x = space coordinate in horizontal direction

t = time coordinate

The pressure wave loading Δp, imparted on the seafloor by

the wave is given by:

$$\Delta p = p_0 \; Cos \{ \; 2\pi \; (x/L - t/T) \; \}$$ (3-27)

where,

$p_0 = 0.5 \, \gamma_{\overline{w}} H \; / \; \{ \; Cosh \; (2\pi d/L) \; \}$

$\gamma_{\overline{w}}$ = density of sea water.

The definition of terms and other elements of linear wave theory are shown in Figure 3.5.
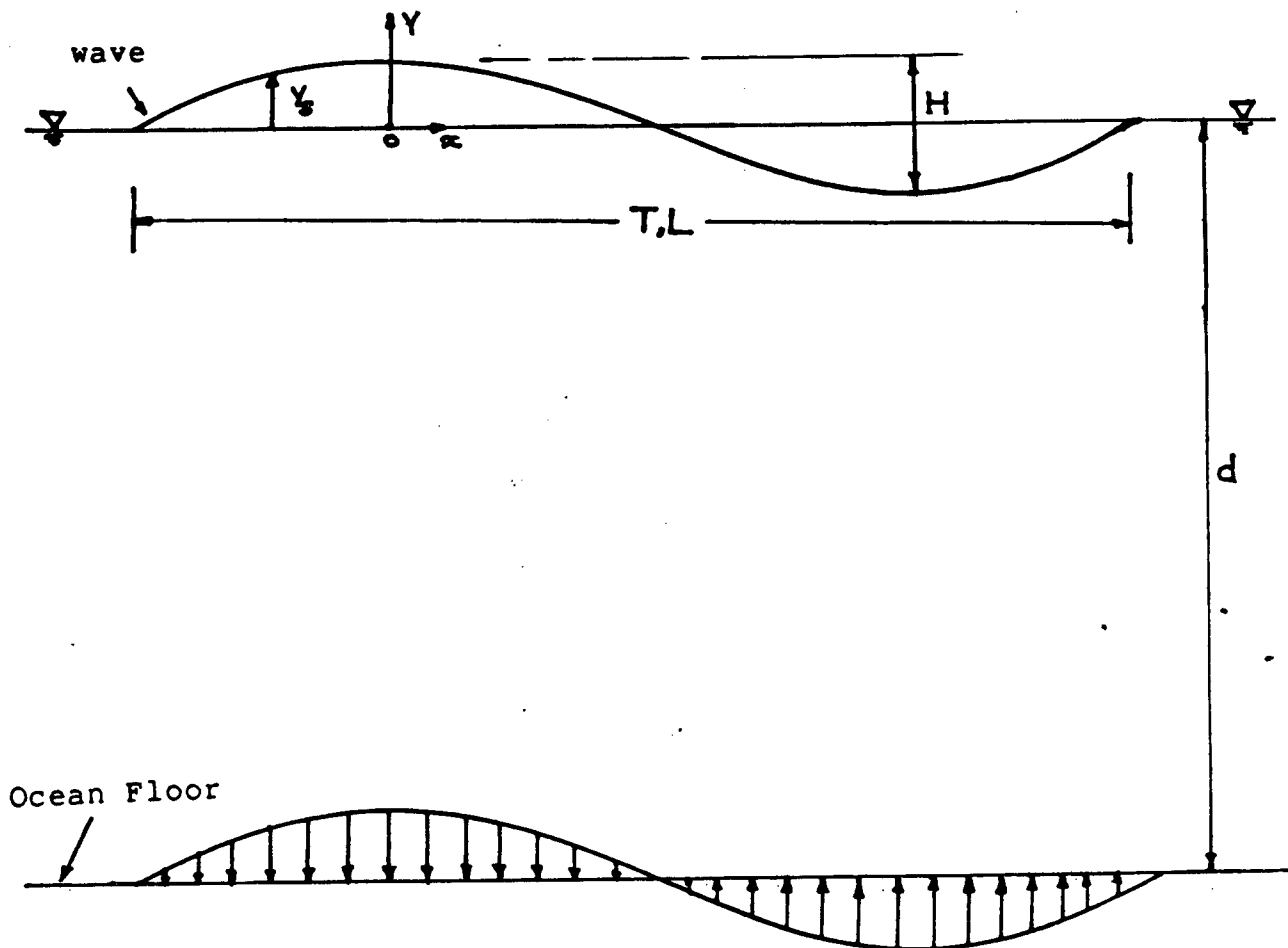
Figure 3.5; Wave Pressure and Definitions of
Terms - Linear Wave Theory.

CHAPTER 4

FINITE ELEMENT FORMULATION OF THE PROPOSED METHOD

4.1 Introduction

The method of analysis developed in this thesis for the evaluation of wave induced residual porewater pressures is an extended version of Siddharthan-Finn method with an apparent difference in the degree of the polynomial used in the interpolation for the porewater pressure field. The finite element computer program STABW3 uses a complete cubic polynomial interpolation function for the porewater pressure field, whereas STABW uses a linear interpolation function. The motivation for using a higher degree polynomial in the interpolation is for the reason stated below.

It has been observed that when a finite soil deposit is analysed for the wave induced residual porewater pressures, all existing analytical methods, which were briefly reviewed in the previous chapter, indicate higher residual porewater pressures at lower elevations for cases with soil having higher permeabilities than for cases with lower permeabilities, while all other potential variables remain the same. It is believed that this phenomenon is due to the increased downward flow of water associated with cases where the soil has a higher coefficient of consolidation, that is, higher permeability. In order to examine and verify the above phenomenon, it is neccessary to know the time history of flow through nodal points. This cannot be achieved through the existing methods

reviewed in Chapter 2 because of the fact that they use a linear interpolation function for the porewater pressure field. One requires a higher degree polynomial to include flow {in the form k_z (du/dz)} as a nodal variable.

A complete cubic interpolation function is chosen in the STABW3 finite element formulation. This requires two nodal variables per node to uniquely define the porewater pressure field. The porewater pressure u at the node and the flow through the nodal point in the form k_z (du/dz), are selected as the required nodal variables. The formulation allows the determination of the time history of residual porewater pressure response at any depth within the domain and also the flow through the interface at nodal points. Since a higher degree polynomial is used in the interpolation, it is apparent that higher accuracy and faster convergence may be achieved for the solution.

Though most of the important aspects are common for STABW and STABW3, the noticeable difference occurs in the formulation of the finite element equations as a result of differences in interpolation function. The other main difference in STABW3 finite element formulation comes from the fact that the terms in functional J {see equations (4-12) to (4-15)} are accounted for in a different manner than in STABW finite element formulation. The finite element formulation of STABW3 is given in the next section and the important aspects involved in the development of this method of analysis are already outlined in Chapter 3.

4.2 Formulation Of Finite Element Equations

The basic equation (see section 3.2) governing the residual porewater pressure response is,

$$\frac{\partial}{\partial z}\left(\frac{k_z}{\gamma_w}\frac{\partial u}{\partial z}\right) = m_v\left(\frac{\partial u}{\partial t} - \frac{\partial u_g}{\partial t}\right) \qquad (4\text{-}1)$$

At any instant of time, the right hand side of equation (4-1) may be considered to be a function of z only. Hence equation (4-1) reduces to,

$$\frac{\partial}{\partial z}\left(\frac{k_z}{\gamma_w}\frac{\partial u}{\partial z}\right) = Q(z) \qquad (4\text{-}2)$$

The functional J for a differential equation of the form, as in equation (4-2) is,

$$J = \int_0^D \left\{\frac{\partial}{\partial z}\left(\frac{k_z}{\gamma_w}\frac{\partial u}{\partial z}\right)u - 2\,Q(z)u\right\}dz$$

Expanding the above,

$$J = \left[\frac{k_z}{\gamma_w}\left(\frac{\partial u}{\partial z}\right)u\right]_0^D - \int_0^D \left[\frac{k_z}{\gamma_w}\left(\frac{\partial u}{\partial z}\right)^2 + 2\,Q(z)u\right]dz$$

with boundary conditions,

$$u = 0 \text{ at } z = 0$$

and $\quad \frac{\partial u}{\partial z} = 0 \text{ at } z = D,$

the boundary term in the functional vanishes. Hence,

$$J = -\int_0^D \left[\frac{k_z}{\gamma_w}\left(\frac{\partial u}{\partial z}\right)^2 + 2\,Q(z)u\right]dz \qquad (4\text{-}3)$$

Suppose the soil deposit is considered as an assemblage of finite number of elements, then

$$J = J_{total} = \sum_{elements} J_{element} \qquad (4\text{-}4)$$

4.2.1 Interpolation Function

In order to evaluate the functional, an interpolation function for u must be selected. Let us choose a cubic interpolation function for u. This would be more than enough to satisfy the completeness criterion.

Now,

$$u = a_1 + a_2\eta + a_3\eta^2 + a_4\eta^3 \qquad (4-5)$$

where,

η = local coordinate system, and

a_1 to a_4 = coefficients which need to be evaluated.

Each elememt has two nodes, therefore, two nodal variables per node is required to uniquely define u. Let us choose u and q as two nodal variables, where

$$q = k_z \left(\frac{\partial u}{\partial \eta}\right).$$

From equation (4-5)

$$\frac{\partial u}{\partial \eta} = a_2 + 2a_3\eta + 3a_4\eta^2$$

Then,

$$q = k_z(a_2 + 2a_3\eta + 3a_4\eta^2) \qquad (4-6)$$

Now, consider the ith element with nodes i and i+1 and thickness d_i.
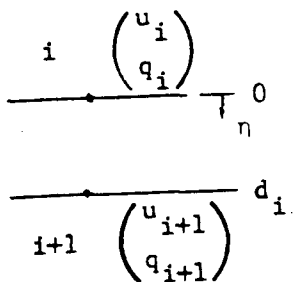
At $\eta = 0$, $u = u_i$ and $q = q_i$;

At $\eta = d_i$, $u = u_{i+1}$ and $q = q_{i+1}$.

Using these in equations (4-5) and (4-6) to get,

$$u_i = a_1 \tag{4-7}$$

$$q_i = k_z a_2 \tag{4-8}$$

$$u_{i+1} = a_1 + a_2 d_i + a_3 d_i^2 + a_4 d_i^3 \tag{4-9}$$

$$q_{i+1} = k_z (a_2 + 2a_3 d_i + 3a_4 d_i^2) \tag{4-10}$$

Solving for a_1 to a_4 from equations (4-7) to (4-10) and back substituting into equation (4-5) will yield,

$$u = \underline{N}^T \underline{u}_i^e = \sum_{j=1}^{4} N_j u_j \tag{4-11}$$

where

$$\underline{u}_i^e = \begin{Bmatrix} u_i \\ q_i \\ u_{i+1} \\ q_{i+1} \end{Bmatrix} \quad \begin{Bmatrix} u_1 \\ u_2 \\ u_3 \\ u_4 \end{Bmatrix} ; \qquad \underline{N}^T = (N_1, N_2, N_3, N_4)$$

and using $\lambda = \eta/d_i$

$$N_1 = (1 - 3\lambda^2 + 2\lambda^3)$$

$$N_2 = (d_i/k_z)(1 - 2\lambda^2 + \lambda^3)$$

$$N_3 = (3\lambda^2 - 2\lambda^3)$$

$$N_4 = (d_i/k_z)(-\lambda^2 + \lambda^3)$$

4.2.2 Element Matrix Equation

Consider $J_{element}$ from equation (4-3),

$$-J_{element} = \int_0^{d_i} [\frac{k_z}{\gamma_w} (\frac{\partial u}{\partial \eta})^2 + 2 \, Q(\eta)u] d\eta$$

$$= \int_0^{d_i} [\frac{k_z}{\gamma_w} (\frac{\partial u}{\partial \eta})^2 + 2 \, m_v(\frac{\partial u}{\partial t} - \frac{\partial u_g}{\partial t})u] d\eta$$

$$= I_1^e + I_2^e - I_3^e \qquad\qquad (4-12)$$

where

$$I_1^e = \int_0^{d_i} \frac{k_z}{\gamma_w} (\frac{\partial u}{\partial \eta})^2 \, d\eta$$

$$I_2^e = \int_0^{d_i} 2 \, m_v \, u(\frac{\partial u}{\partial t}) d\eta \qquad \text{and} \qquad I_3^e = \int_0^{d_i} 2 \, m_v \, u(\frac{\partial u_g}{\partial t}) d\eta$$

Now consider I_1^e

$$I_1^e = \int_0^{d_i} \frac{k_z}{\gamma_w} (\frac{\partial u}{\partial \eta})^2 \, d\eta$$

$$= \int_0^1 \frac{k_z d_i}{\gamma_w} (\frac{\partial u}{\partial \lambda})^2 \, d\lambda$$

From equation (4-11), $u = N_j u_j$, $j = 1,4$, , substituting this,

$$I_1^e = \int_0^1 \frac{k_z d_i}{\gamma_w} N_j' u_j \, N_k' u_k \, d\lambda, \quad i=1,4 \text{ and } j=1,4$$

$$\therefore \frac{\partial I_1^e}{\partial u_k} = \int_0^1 2 \frac{k_z}{\gamma_w} \cdot d_i \, N_j' N_k' \, u_j \, d\lambda$$

$$= [S_e] \{u_i^e\} \qquad (4\text{-}13)$$

where $[S_e] = 4 \times 4$ symmetric matrix with the general term given by,

$$S_{jk} = \int_0^1 2 \frac{k_z}{\gamma_w} \cdot d_i \, N_j' N_k' \, d\lambda$$

or

$$S_{11} = \frac{12}{5} \frac{k_z}{\gamma_w d_i}$$

$$S_{12} = S_{21} = \frac{1}{5} \cdot \frac{1}{\gamma_w}$$

$$S_{13} = S_{31} = -S_{11}$$

$$S_{14} = S_{41} = S_{12}$$

$$S_{22} = \frac{4}{15} \frac{d_i}{k_z \gamma_w}$$

$$S_{23} = S_{32} = -S_{21}$$

$$S_{24} = S_{42} = -\frac{1}{15} \frac{d_i}{k_z \gamma_w}$$

$$S_{33} = S_{11}$$

$$S_{34} = -S_{12}$$

$$S_{44} = S_{22}$$

Now consider I_2^e

$$I_2^e = \int_0^{d_i} 2 m_v u(\tfrac{\partial u}{\partial t}) d\eta = \int_0^1 2 m_v d_i u(\tfrac{\partial u}{\partial t}) d\lambda$$

$$= \int_0^1 2 m_v d_i N_k u_k N_j \dot{U} \, d\lambda$$

$$\therefore \quad \frac{\partial I_2^e}{\partial u_k} = \int_0^1 2 m_v d_i N_k N_j \dot{U} \, d\lambda$$

$$= [D_e] \{\dot{U}_e\} \qquad (4-14)$$

where $[D_e] = 4 \times 4$ symmetric matrix with the general term given by,

$$D_{jk} = \int_0^1 2 \, m_v d_i \, N_k N_j \, d\lambda$$

or

$$D_{11} = \frac{26}{35} \, m_v d_i$$

$$D_{12} = D_{21} = \frac{11}{105} \, \frac{m_v d_i^2}{k_z}$$

$$D_{13} = D_{31} = \frac{9}{35} \, m_v d_i$$

$$D_{14} = D_{41} = -\frac{13}{210} \, \frac{m_v d_i^2}{k_z}$$

$$D_{22} = \frac{2}{105} \, \frac{m_v d_i^2}{k_z^2}$$

$$D_{23} = D_{32} = -D_{14}$$

$$D_{24} = D_{42} = -\frac{1}{70} \, m_v \frac{d_i^3}{k_z^2}$$

$$D_{33} = D_{11}$$

$$D_{34} = D_{43} = -D_{12}$$

$$D_{44} = D_{22}$$

Now consider I_3^e

$$I_3^e = \int_0^{d_i} 2 \, m_v \, u \left(\frac{du_g}{dt}\right) d\eta$$

Let us assume a simple linear variation for $(\partial u_g/\partial t)$ as,

$$\frac{\partial u_g}{\partial t} = (1-\lambda) \left(\frac{\partial u_g}{\partial t}\right)_i + \left(\frac{\partial u_g}{\partial t}\right)_{i+1}$$

To accomadate this into the finite element formulation, let $(\partial u_g /\partial t)$ as

$$(\frac{\partial u_g}{\partial t}) = (M_1 \; M_2 \; M_3 \; M_4) \begin{Bmatrix} (\frac{\partial u_g}{\partial t})_i \\ 0 \\ (\frac{\partial u_g}{\partial t})_{i+1} \\ 0 \end{Bmatrix}$$

where

$$M_1 = (1-\lambda)$$

$$M_2 = M_4 = 0$$

$$M_3 = \lambda$$

Using this technique,

$$I_3^e = \int_0^1 2 \, m_v d_i \, N_k u_k \, M_j \{\frac{\partial u_g}{\partial t}\} d\lambda$$

$$\therefore \quad \frac{\partial I_3^e}{\partial u_k} = \int_0^1 2 \, m_v d_i \, N_k M_j \{\frac{\partial u_g}{\partial t}\} d\lambda$$

$$= [R_e] \{(\frac{\partial u_g}{\partial t})_e\} \tag{4-15}$$

where $[R_e] = 4 \times 4$ symmetric matrix with the general term given by,

$$R_{jk} = \int_0^1 2 \, m_v d_i \, N_k M_j \, d\lambda$$

or

$$R_{13} = R_{31} = \frac{3}{10} \, m_v d_i \qquad\qquad R_{33} = R_{11} = \frac{7}{10} \, m_v d_i$$

$$-R_{23} = R_{41} = -\frac{1}{15} \frac{m_v d_i^2}{k_z} \qquad\qquad -R_{43} = R_{21} = \frac{1}{10} \frac{m_v d_i^2}{k_z}$$

All other terms are zero.

4.2.3 Global Matrix Equations

Now,

$$\frac{\partial J_{element}}{\partial \{u_i^{\ e}\}} = \frac{\partial I_1^{\ e}}{\partial \{u_i^{\ e}\}} + \frac{\partial I_2^{\ e}}{\partial \{u_i^{\ e}\}} + \frac{\partial I_3^{\ e}}{\partial \{u_i^{\ e}\}}$$

From equations (4-13), (4-14) and (4-15)

$$\frac{\partial J_{element}}{\partial \{u_i^{\ e}\}} = [S_e]\{u_i^{\ e}\} + [D_e]\{\dot{U}_e\} + [R_e]\{(\frac{\partial u_g}{\partial t})_e\}$$

Using variational principles,

$$\frac{\partial J}{\partial \{u\}} = 0$$

That is,

$$\sum_{elements} \frac{\partial J_{element}}{\partial \{u_i^{\ e}\}} = \{0\}$$

$$\therefore \quad \sum_{elements} [S_e]\{u_i^{\ e}\} + [D_e]\{\dot{U}_e\} + [R_e]\{(\frac{\partial u_g}{\partial t})_e\} = \{0\}$$

Summing up would yield the global matrix equation as

$$[S]\{u\} + [D]\{\frac{\partial u}{\partial t}\} + [R]\{\frac{\partial u_g}{\partial t}\} = \{0\} \qquad (4-16)$$

The global matrices $[D]$ and $[R]$ are functions of compressibility m_v and, hence, vary with porewater pressure ratio. The global matrix $[S]$ is constant for a given problem.

The matrix equation (4-16) can be treated as an ordinary differential equation and be integrated over the time interval

t, t+Δt to get

$$[S]\beta\{u_{t+\Delta t}\} + \alpha\{u_t\}]\Delta t + [\bar{D}][\{u_{t+\Delta t}\} - \{u_t\}] - [\bar{R}]\{\frac{\partial u_g}{\partial t}\}\Delta t = \{0\}$$

(4-17)

where $\alpha+\beta = 1$ and subscripts t and t+Δt correspond to values at time t and t+Δt respectively. Matrices $[\bar{D}]$ and $[\bar{R}]$ are constructed using average values of variables between time t and t+Δt. β values greater than or equal to 0.5 corresponds to different approximations. However, in this program a value of $\beta = 0.5$ is used.

Equation (4-17) can be grouped together to form,

$$[AQ]\{u_{t+\Delta t}\} = \{BQ1\} + \{BQ2\}$$

(4-18)

where

$$[AQ] = [S]\beta\Delta t = [\bar{D}]$$

$$\{BQ1\} = (-[S]\alpha\Delta t + [\bar{D}])\{u_t\}$$

$$\{BQ2\} = [R]\{(\frac{\partial u_g}{\partial t})\} \cdot \Delta t$$

With specification of boundary conditions, appropriate columns and rows of $[AQ]$ are struck out to form a net global matrix $[AQ^*]$. So are corresponding rows of $\{BQ1\}$ and $\{BQ2\}$ to form net vectors $\{BQ1^*\}$ and $\{BQ2^*\}$.

Hence,

$$[AQ^*]\{u_{t+\Delta t}\} = \{BQ1^*\} + \{BQ2^*\} = \{BQ^*\}$$

(4-19)

The program has the option of compressibility, either varying or remains constant. In the event of constant

compressibility, equation (4-19) is solved instantly for every time step. However, in the event of varying compressibility, equation (4-19) is solved iteratively. Each time variable matrices $[\bar{D}]$ and $[\bar{R}]$ are calculated using the best current estimate of nodal variables. The iterative procedure is repeated until a specified accuracy or a specified maximum number of iterations is obtained, whichever occurs first.

CHAPTER 5

ISLAND GEOMETRIES AND SOIL PROPERTIES FOR WAVE ANALYSES

5.1 Island Configuration

Wave induced residual porewater pressure analyses using STABW3 were conducted for three different islands at water depths 12m, 21m and 31m respectively. The other detail of the islands are presented in Table 5.1.

The berm configuration and the vertical sections selected for the analyses are shown in Figure 5.1 to Figure 5.3. Since only vertical sections are considered in the analyses, the slope of the berm does not directly affect the method of analysis except for defining variations in water depth. However, the slopes play a major role in the structural stability of the islands and also in containing the flow of liquefied soil in cases of liquefaction.

To be able to analyse an island for wave induced porewater pressure, the vertical sections considered has to be of infinite lateral extent and moreover the top profile has to be parallel to still water surface. But in reality, the sections, for example AA to GG of island 1, are not of infinite lateral extent and also they are not parallel to still water surface. The actual lateral length and the top profile of those sections depend on the shape and slope of the berm. In the analyses conducted in this thesis, all such sections are assumed to be of infinite lateral extent and the top profile to be parallel to the still water surface.

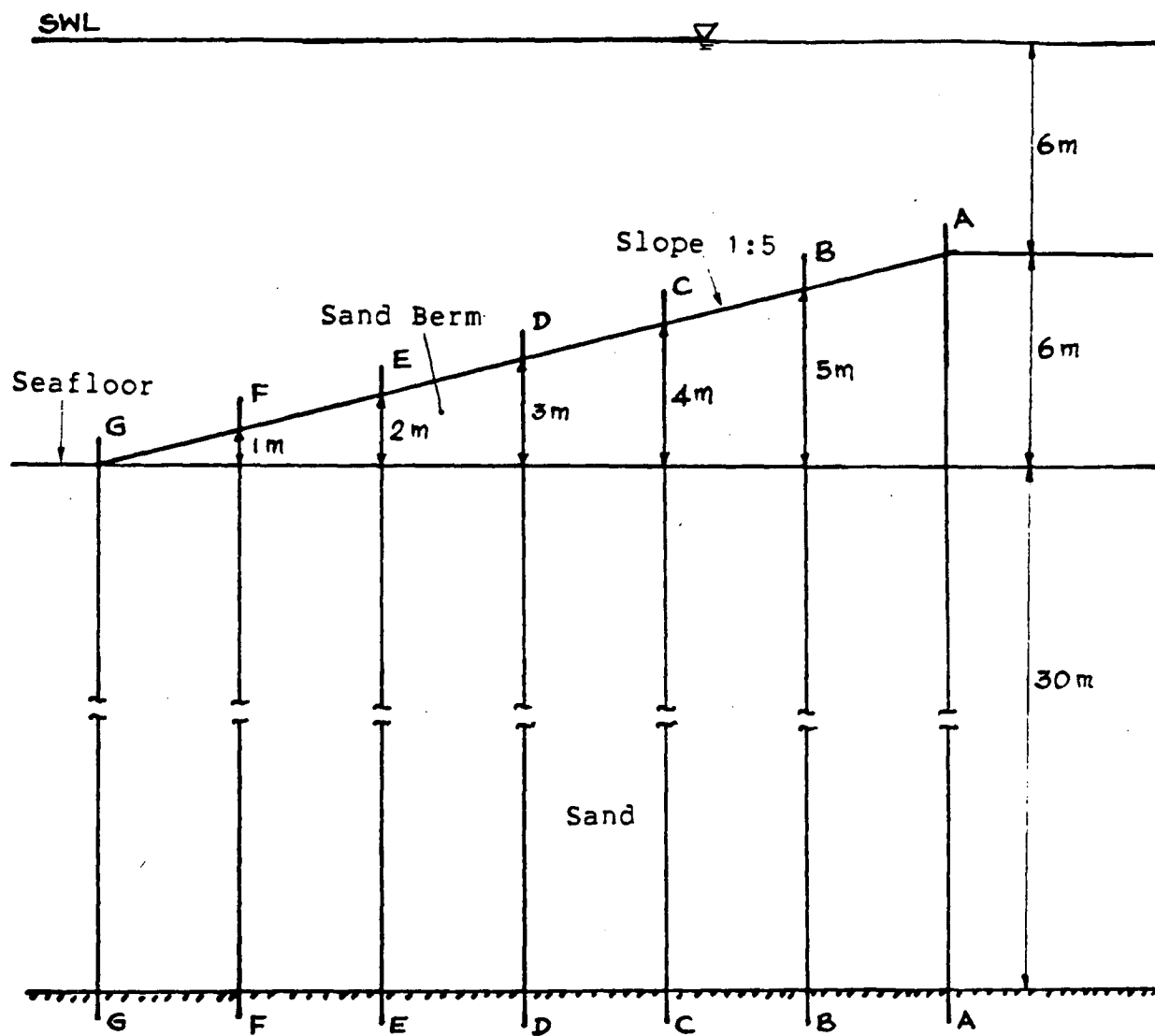| Island No.	Berm height(m)	Still Water depth(m)	Set down depth(m)
1	6.0	12.0	6.0
2	15.0	21.0	6.0
3	25.0	31.0	6.0

Table 5.1 ; Details Of Islands

Figure 5.1; Sections of Island 1 for Wave Induced Residual
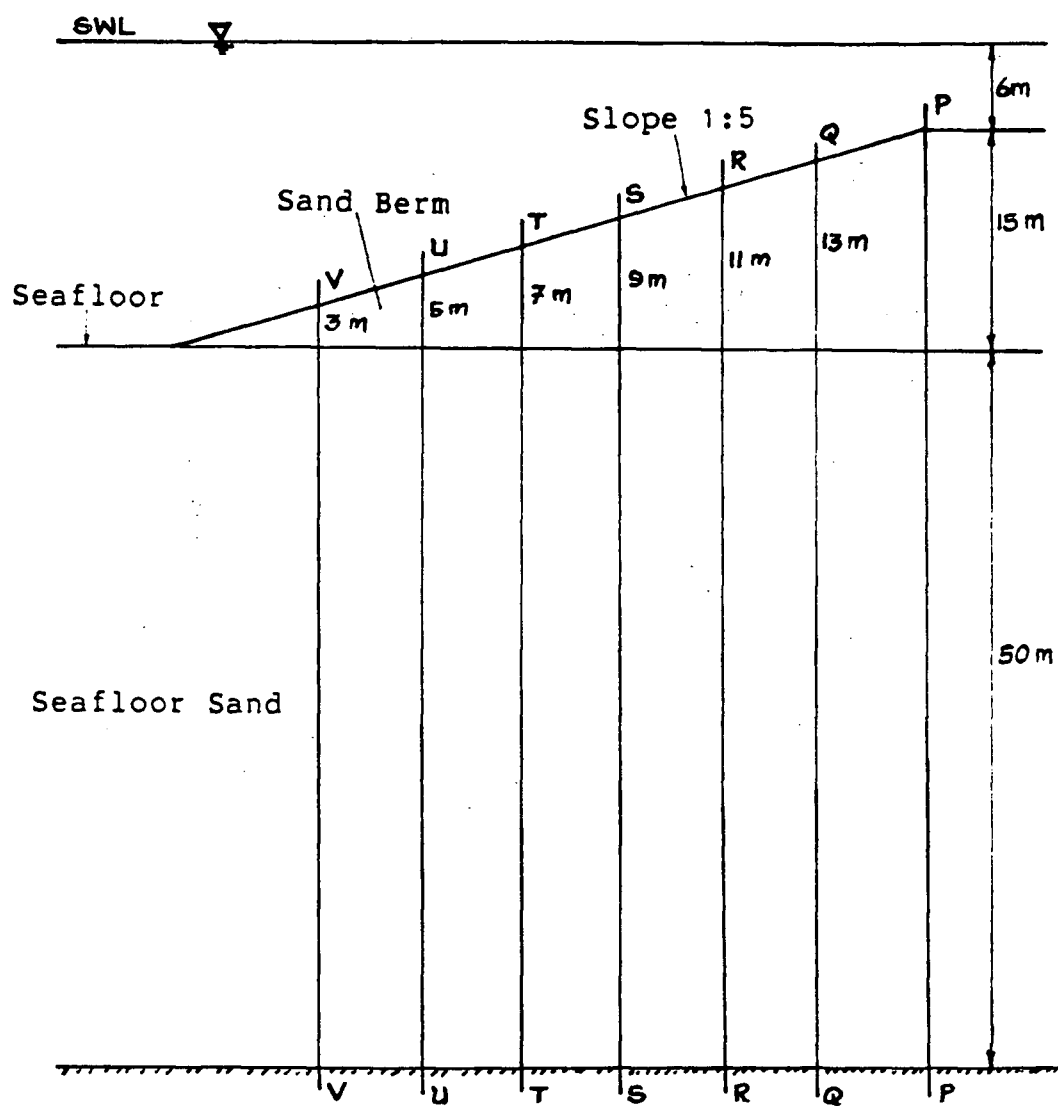Porewater Pressure Analysis.

Figure 5.2; Sections of Island 2 for Wave Induced Residual
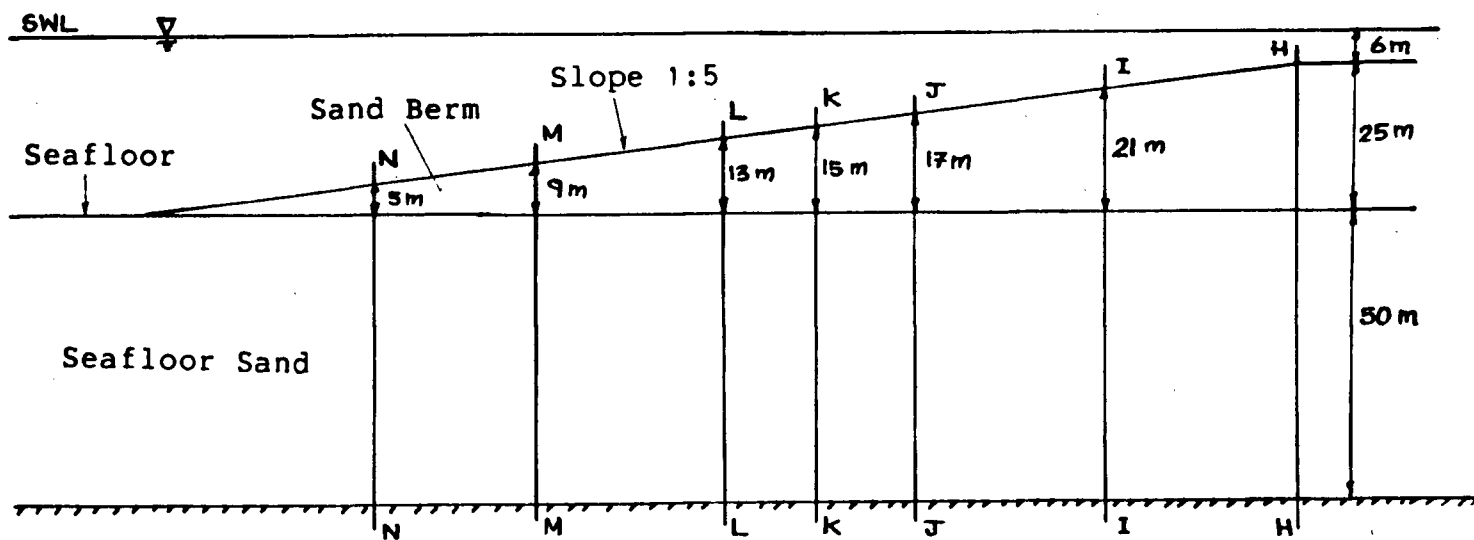Porewater Pressure Analysis.

Figure 5.3; Sections of Island 3 for Wave Induced Residual

Porewater Pressure Analysis.

The above assumption is justifiable in the cases of berms of very gentle slopes. For berms of sharp slopes, it is believed that the above assumption would lead to conservative estimates of wave induced residual porewater pressures because of the effect of static shear stresses. The presence of static shear stresses is to retard the rate of porewater pressure generation and hence the resulting porewater pressure response with the above assumptions would be higher than as it actually would be. The conservative nature is also due to fact that drainage would be faster in a slope than in horizontal ground.

The effects of static shear stresses and the slope of berms can be taken into account by various ways as briefly described below.

1. By using a porewater pressure generation model that takes into account of the influence of static shear stresses in the development of porewater pressure during cyclic loading. An example would be the model proposed by Finn et al (1978).

2. By using a modified equivalent permeability to cater for the increase in the drainage resulting from sloping ground.

3. By using a modified strength curve to cater for preshearing and preconsolidation.

However, these types of refinements are rarely required because of the uncertainity associated with the information gathered from an offshore site.

5.2 Specified Storm Waves

Storm waves are described by three parameters. They

are the significant wave height, the significant wave period and the duration. Each of these parameters depends on the location of the site and several other factors related to the site. For the purpose of the analyses, storms are specified for each of the island and the details are given in Table 5.2. The number of cycles in each case, is given by (6 x 3600)/8, which is equal to 2700.

5.3 Soil Properties

5.3.1 Basic Soil Properties

The basic soil properties such as densities, relative density, void ratio, specific gravity of solid etc used in the analyses are shown in Table 5.3.

5.3.2 Derived Soil Properties

Initial Shear Modulus

For sands and gravels;

The initial value of shear modulus for sand and gravel were computed using the equations (4-17), (4-18) and (4-19). For sand of D_r = 50%, from equation (4-18),

k_{2max} = 45.

For gravel and rockfill of D = 50%, from equation (4-19),

k_{2max} = 95.

σ'_m required for shear modulus G_{max} calculation in equation (4-17) was calculated using the following equation,

$$\sigma'_m = (1 + 2K_o)/3 . \sigma'_{vo} \qquad (5-1)$$

Island No.	H_S (m)	T_S (sec)	T_D (hrs)
1	4.0 } 6.0	8.0	6.0
2	9.0	8.0	6.0
3	12.0	8.0	6.0

Table 5.2; Specified Storms Of the Islands

Property	Soil Type		
	Sand	Gravel	Clay
Total Unit Weight(kN/m^3)	19.0	19.5	18.0
Sub. Unit Weight(kN/m^3)	9.0	9.4	8.0
Specific Gravity	2.65	2.67	2.67
Void Ratio	0.85	0.65	0.90
Relative Density (%)	50.0	50.	-
Angle of Internal Friction (deg)	33.	37.	22.
Initial Compressibility (m^2/kN)	3×10^{-5}	1.9×10^{-5}	10^{-4}
Vertical permeability (cm/sec)	$10^{-3}-10^{-4}$	10.0	10^{-7}
Empirical Constant	0.70	0.10	0.10
Bulk Modulus exponent	0.50	0.50	0.0
Poisson Ratio	0.35	0.25	0.45

Table 5.3; Soil Properties Selected For Wave Analyses

K_o was calculated using the equation,

$$K_o = 1 - \sin \phi' \qquad (5-2)$$

where ϕ' = angle of internal friction.

For clays;

The initial shear modulus G_{max} for clays was computed from the following equation,

$$G_{max} = 1000 \; S_u \qquad (5-3)$$

where S_u = undrained strength of clay.

Initial Bulk Modulus

The bulk modulus, B, for sand, gravel and clay were computed using the elastic relationship,

$$B/G = 2(1 + \nu)/3(1 - 2\nu) \qquad (5-4)$$

where ν = initial Poisson ratio,

G = shear modulus.

5.3.3 Selection Of Initial Volume Compressibility

A close examination of the governing equation for the wave induced porewater pressure in Section 3.2 reveals that the parameter that plays the most crucial role in determining the levels of porewater pressure that may develop in the berm is the coefficient of consolidation defined as $k_z/m_v \gamma_w$. For this reason, both k_z and m_v are equally important and should be determined experimentally in order to obtain the most realistic estimates of wave induced porewater pressures. Unfortunately, no experimental data on compressibility are available on

potential sand fill. A brief review on selected compressibility data on sand is presented herein.

The compressibility of sand is usually determined in an oedometer test. The sand is confined in a stiff stainless steel ring and vertical settlements under increasing vertical effective stress are recorded. A typical oedometer test result is shown in Figure 5.4, where the volumetric strain, ϵ_v%, is plotted against vertical effective stress, σ_v' .

The coefficient of volume compressibility m_v is defined as,

$$m_v = d\epsilon_v/d\sigma_v' \qquad\qquad (5-5)$$

where $d\epsilon_v$ = change in volumetric strain corresponding to a small change in effective vertical stress, $d\sigma_v'$.

Therefore, the slope of the experimental curve plotted in the form shown in Figure 5.4, is the coefficient of volume compressibility.

Two different phases of loading can be identified in Figure 5.4. The first one corresponds to virgin loading where the effective stress is always increased. The other phase corresponds to rebounding where the effective stress is reduced. It is noticeable that the compressibilies (slope of the curve) under these two loading phases are quite different and the compressibility being higher under virgin loading. It is also seen from the Figure 5.4 that during unloading the rebound compressibility increases and further the amount of increase depends on the level of unloading.

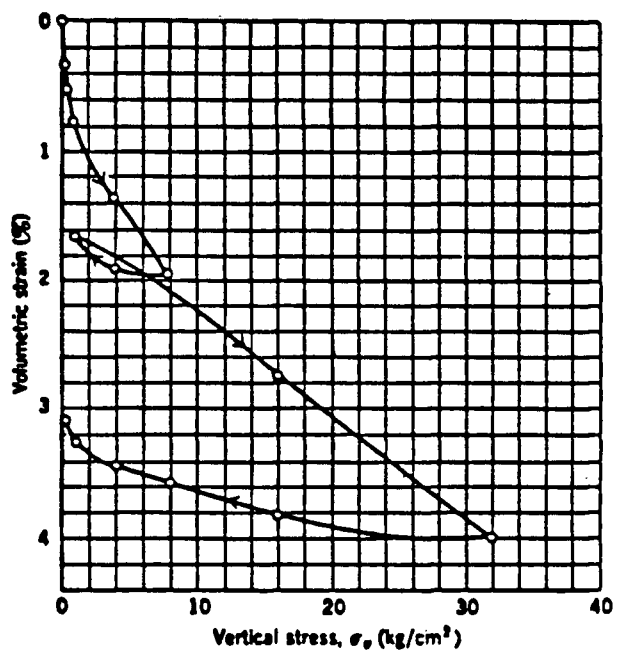During wave loading, residual porewater pressures are

Figure 5.4; Oedometer Test Results For a Libyan Sand
(After Lambe and Whitman, 1969)

generated. As a result of this, the effective stress regime is changed. That is, the initial effective stress, σ'_{vo} , is reduced by the increase in porewater pressure to result in a new current effective stress of $(\sigma'_{vo} -u)$ while σ'_{vo} itself remain constant. Therefore, in effect the sand is rebounding during cyclic loading which means appropriate m_v values have to be obtained from rebound portions of experimental curves. The rebound compressibility values have to be also adjusted depending on the level of residual porewater pressures.

The data on compressibility of sand due to rebounding is very limited. The major contribution in this area is the experimental data by Lee and Albaisa (1974). Based on their comprehensive study, Seed et al (1976) proposed variations of rebound compressibility with increasing porewater pressure at constant total stress for sands at various relative densities. The important conclusion emerged from the study of Seed et al (1976) regarding the variation of compressibility ratio, expressed as the ratio of current compressibility to the compressibility at low excess porewater pressure, is that for values of porewater pressure ratio upto 60%, neither the grain size nor the relative density have a marked influence on the compressibility ratios. The rebound compressibility of sandy soils can be determined from Figure 5.5. For the analysis conducted in this thesis, the selected rebound compressibility of sand fill (D_r = 50%) is 3.0 x 10^{-5} m²/kN (0.15 x 10^{-5} ft²/lb), which agrees quite well with the corresponding value from the Figure 5.5.
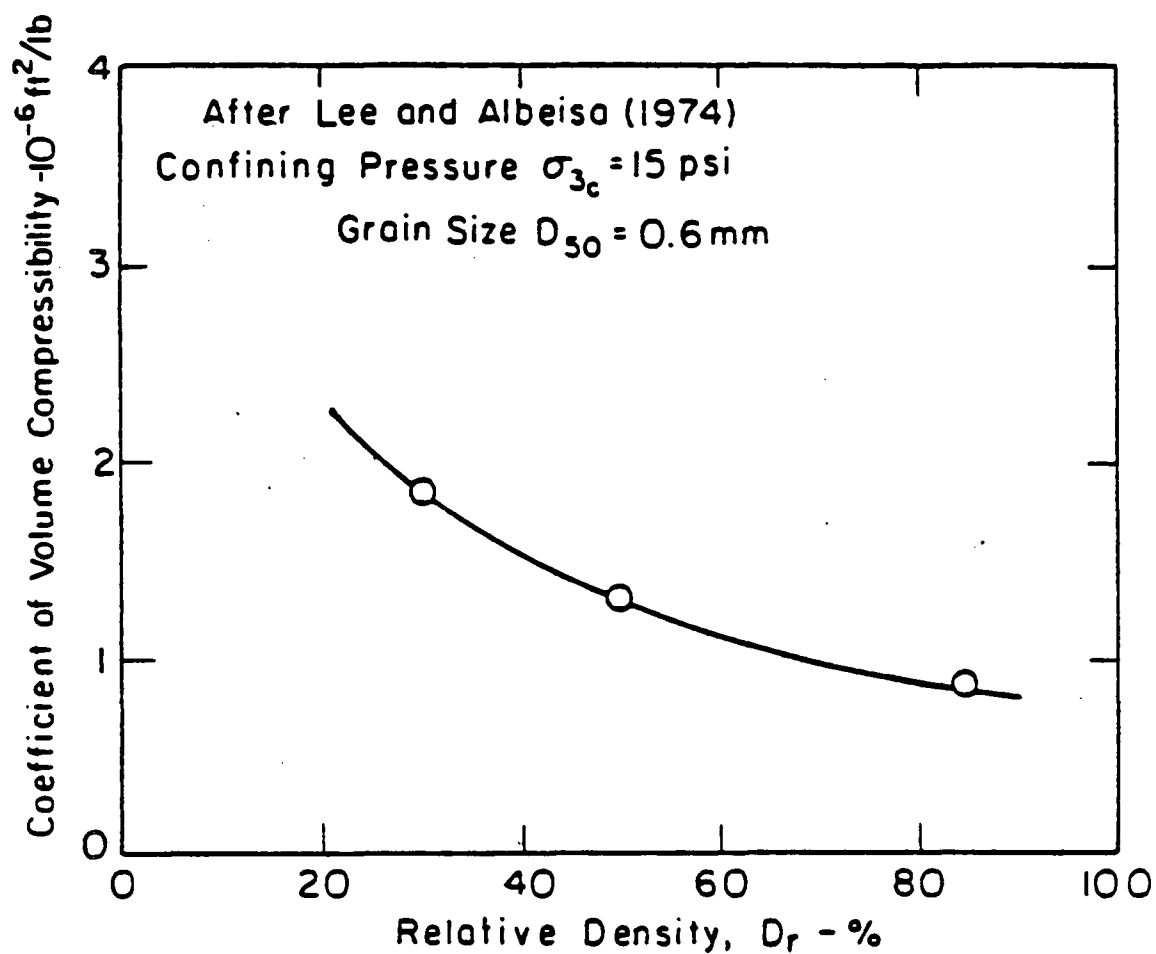
Figure 5.5; Effect Of Density On Compressibility At

Low Excess Porewater Pressure.

(After Martin and Seed, 1978)

Rebound compressibility of sand can also be computed from rebound modulus, $\bar{E}_r$, given by $d\sigma_v'/d\epsilon_v$. The rebound compressibility is thus the reciprocal of the rebound modulus. Based on the experimental study, Martin et al (1976) developed an expression for $\bar{E}_r$ at any current effective stress σ_v', in terms of initial effective vertical stress σ_{vo}', as

$$E = (\sigma_v')^{1-m}/mk_2(\sigma_{vo}')^{n-m} \tag{5-6}$$

With appropriate values of m, n and k_2 for the sand, E and thereby rebound compressibility can be computed.

Rebound compressibility can also be determined from the compressibility under virgin loading. The factor by which the compressibility value for virgin loading be divided in order to obtain rebound compressibility is often recommended to be atleast 2. Table 5.4 presents the compressibility data quoted by Lambe and Whitman (1979) for virgin loading for different soils under two different stress ranges. In the low stress range, the rebound compressibility computed from above data is about 1.0×10^{-5} m²/kN for dense sand and 3.6×10^{-5} m²/kN for loose sand. Therefore, for medium dense sand, rebound compressibility in the range 1.0×10^{-5} m²/kN and 3.6×10^{-5} m²/kN may be expected. It is observed that the selected rebound compressibility of 3×10^{-5} m²/kN for the medium dense sand fill in the analyses reported in this thesis falls within this range.

The oedometer measurements of compressibility are often found to be unreliable because of the errors involved in the standard oedometer equipment. The primary sources of errors are

Soil	Relative Density	Virgin Compressibility m_v (10^{-5}) m^2/kN	
		For 62 - 103 kN/m²	For 200 - 510 kN/m²
Uniform Gravel 1 mm< D < 5 mm	0 100	3.30 0.85	1.67 0.56
Well Graded Sand 0.02mm< D < 1 mm	0 100	7.24 1.93	3.92 0.82
Uniform Fine Sand 0.07mm< D <0.3mm	0 100	6.81 1.96	2.84 0.83
Uniform Silt 0.02mm< D <0.07mm	0 100	35.71 2.84	5.81 1.32

Table 5.4: Compressibilities of Cohesionless Material
in Given Stress Range For Relative Densities
0% and 100%. (After Lambe and Whitman, 1979)

Note; For Rebound Compressibilities, the above values have
to be divided by atleast 2.

due to;

1. Compressibility of the oedometer system. This is found to be comparable with that of sand and thus very difficult to correct,

2. Side friction,

3. High void spaces at the contact of the consolidation ring,

4. Improper contacts with the top and bottom porous stones,

5. Inaccurate relative density measurements resulting from small specimen size.

Because of these errors, the compressibility of sand is often overestimated. For this reason, Cornforth (1974) studied the compressibility of sand in the triaxial apparatus. The tests were conducted on Brasted sand under K_o conditions. He observed that the consolidation curves were parabolic and there is a linear relation between volumetric strain and root vertical effective stress as,

$$\epsilon_v\% = X (\sigma'_v)^{1/2} \tag{5-7}$$

X is dependent on the dry relative density, RDD, of the sand. The results from his study are presented in Figure 5.6.

For $D_r = 50\%$,

$$X = 0.026$$

From equation (5-7),

$$m_v = d\epsilon_v/d\sigma'_v = 0.005 \ X \ (\sigma'_v)^{-1/2} \tag{5-8}$$

Therefore, for $D_r = 50\%$,

$$m_v = 0.00013 \ (\sigma'_v)^{-1/2} \tag{5-9}$$

For mean effective vertical stress of 10 kN/m²,
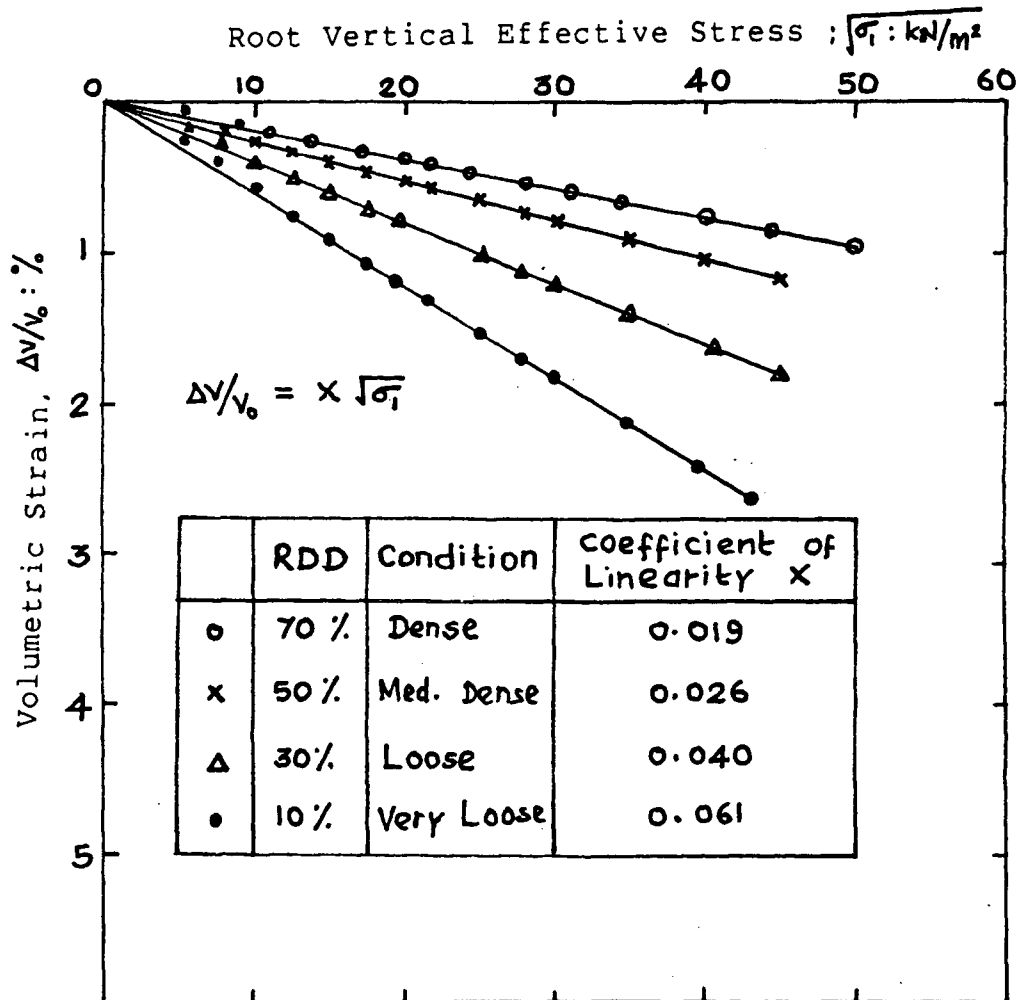
$$m_v = 4 \times 10^{-5} \ m^2/kN$$

Figure 5·6; Volumetric Strain Vs Root Vertical Effective Stress
(After Cornforth, 1974)

Since this value is for virgin loading, it should be divided by a factor of 2.

Therefore, the rebound compressibility is,

$$m_v = 2.0 \times 10^{-5} \ m^2/kN$$

Hence, for the stress range of interest, the selected value of rebound compressibility compares well with the value calculated above.

5.4 Liquefaction Strength Curve

The liquefaction strength curve for sand of $D_r = 50\%$ used in the analyses is given in Figure 5.7. The curve was deduced from the strength curve for sand of $D_r = 54\%$ presented in Figure 3.3, by reducing the cyclic shear stress ratio by a factor 50/54.
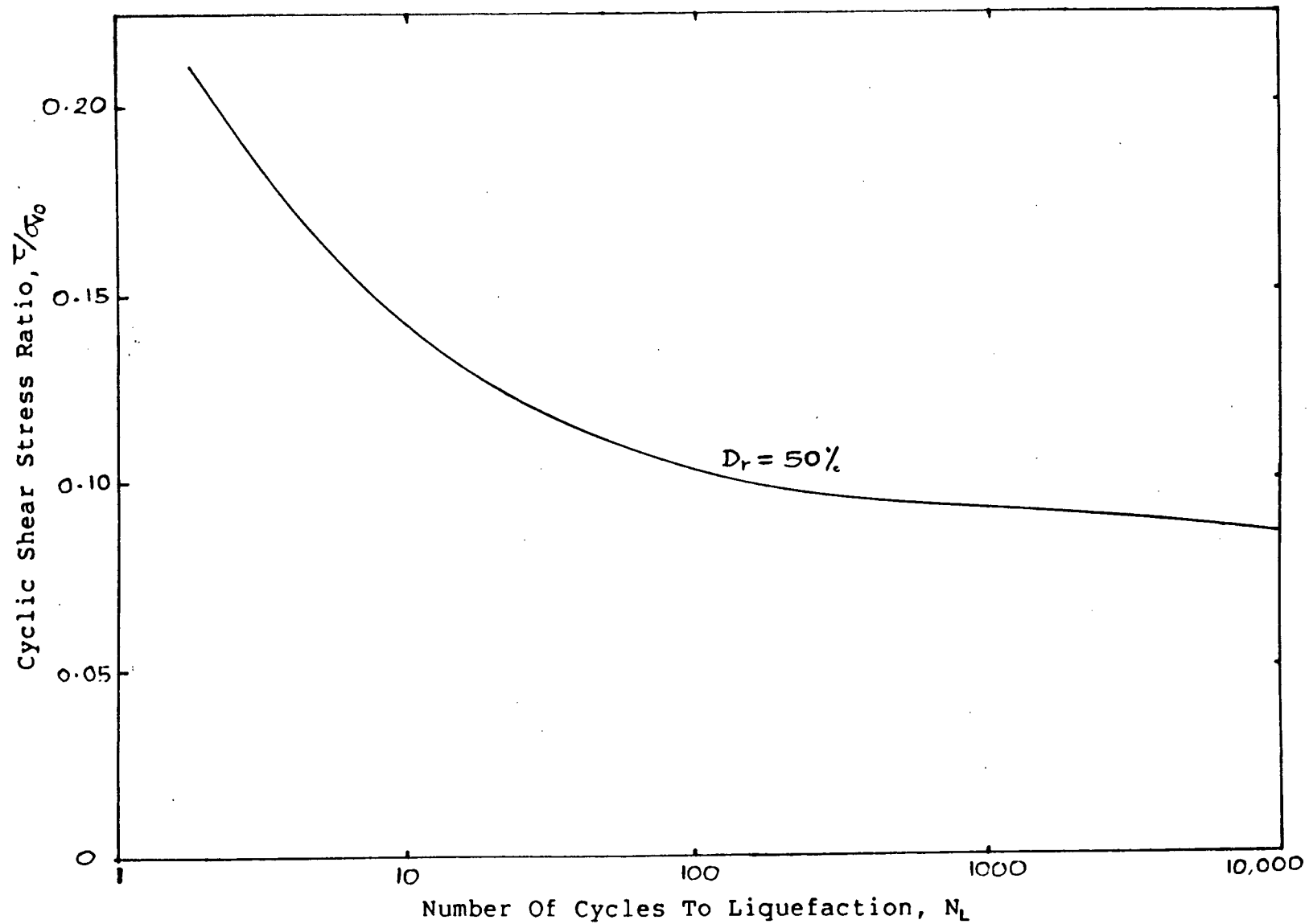
Figure 5·7; Liquefaction Strength Curve of Sand

CHAPTER 6

WAVE INDUCED RESIDUAL POREWATER PRESSURE ANALYSIS

6.1 General

The wave induced residual porewater pressure analyses reported herein were conducted using computer program STABW3. In all cases, modifications of soil properties for the effect of porewater pressure was taken into account in the manner discussed in Section 3.6. The importance of incorporating soil property modification for the effect of increasing porewater pressure has been discussed already in Section 2.5.

The porewater pressure responses established in the analyses are all free field responses. The distortion of porewater pressure response due to the presence of any structures were not considered in the analyses. Hence, considerable caution should be exercised in interpreting the responses in the vicinity of any structures placed on the berm.

6.2 Response of Islands on Sand Foundation

The first series of analyses on islands 1, 2 and 3 sitting on a sand foundation susceptible to liquefaction were conducted for different drainage characteristics of the sand fill. The initial compressibility of the sand fill for this particular series of analyses is taken as 3.0×10^{-5} m^2/kN. The other properties of the sand fill and seafloor sand are given

in Table 5.3.

The effect of dissipation on the porewater pressure response is controlled by the value $k_z/m_v \gamma_w$. Having selected the same compressibility value for all the analyses, it is now possible to compare the effect of drainage characteristics, that is, the effect of variation in k_z on the porewater pressure response.

6.3 Wave Induced Porewater Pressure Response Of Island 1 to 6m, 6 hour Storm

Figure 6.1 to 6.7 show the residual porewater pressures induced at the end of a 6 hour storm with significant wave height of 6m at selected sections AA to GG of island 1 for the different permeability values of $k_z = 10^{-3}$ cm/s and $k_z = 10^{-4}$ cm/s. For the permeability value of 10^{-3} cm/s, the results indicate that there is no liquefaction at any of the sections considered in the analyses in constrast to results with $k_z = 10^{-4}$ cm/s, where liquefaction occurs to substantial depth at all sections. This clearly shows the significance of drainage on the wave induced porewater pressure response. For the case with $k_z = 10^{-3}$ cm/s, the initial drainage is much greater than in the case with $k_z = 10^{-4}$ cm/s, and as a result the porewater pressures developed in the former case are much lower. It is interesting to note, at this point, that the analyses assuming undrained conditions would have predicted liquefaction to depths as much as 9 to 10 m in all the sections of the island.
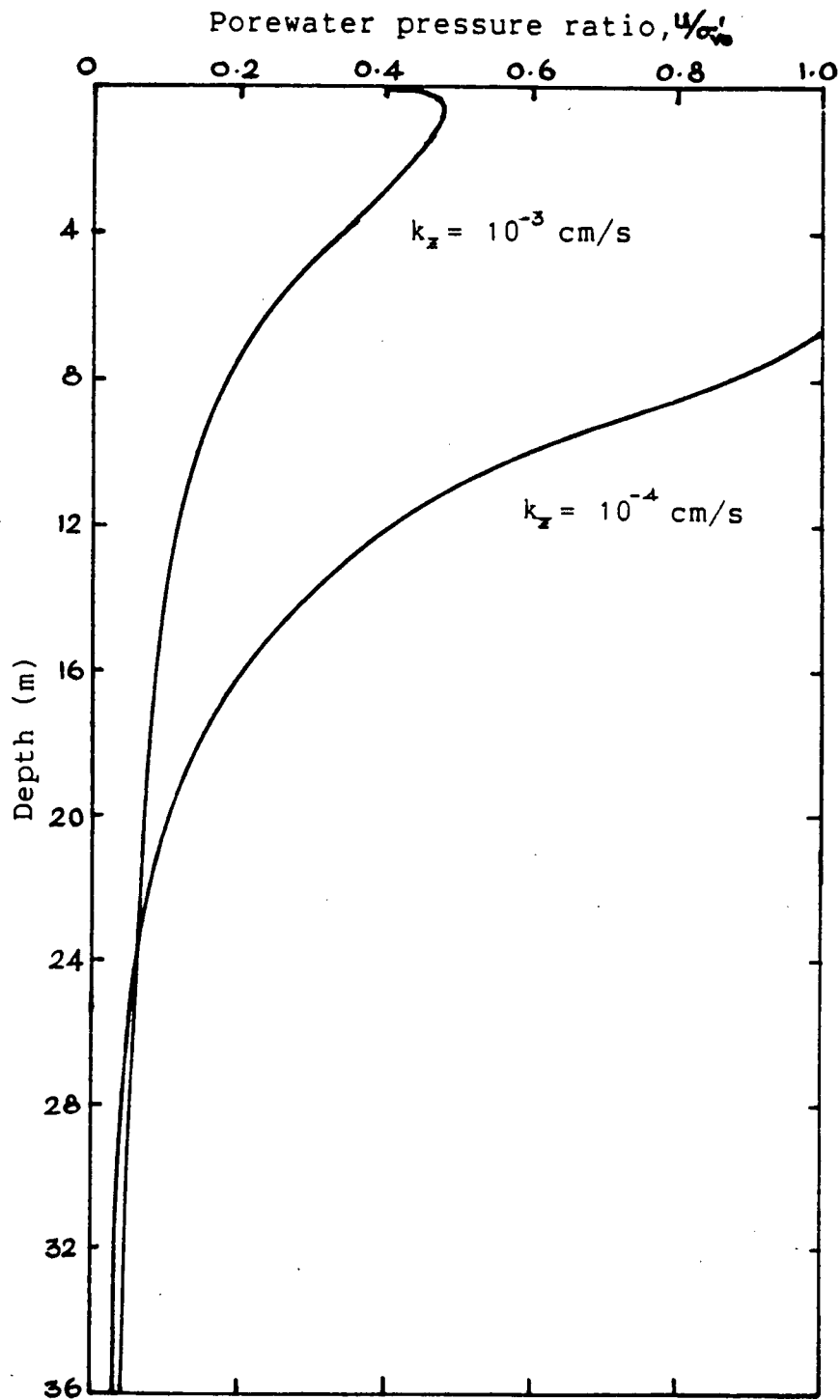
Figure 6.1; Section-AA; Residual Porewater Pressure Response
At the end of 6m 6 hour Storm.

Figure 6.2; Section-BB; Residual Porewater Pressure Response
At the end of 6m 6 hour Storm.

Figure 6.3; Section-CC; Residual Porewater Pressure Response
At the end of 6m 6 hour Storm.

Figure 6.4; Section-DD; Residual Porewater Pressure Response
At the end of 6m 6 hour Storm.

Figure **6**.5; Section-EE; Residual Porewater Pressure Response
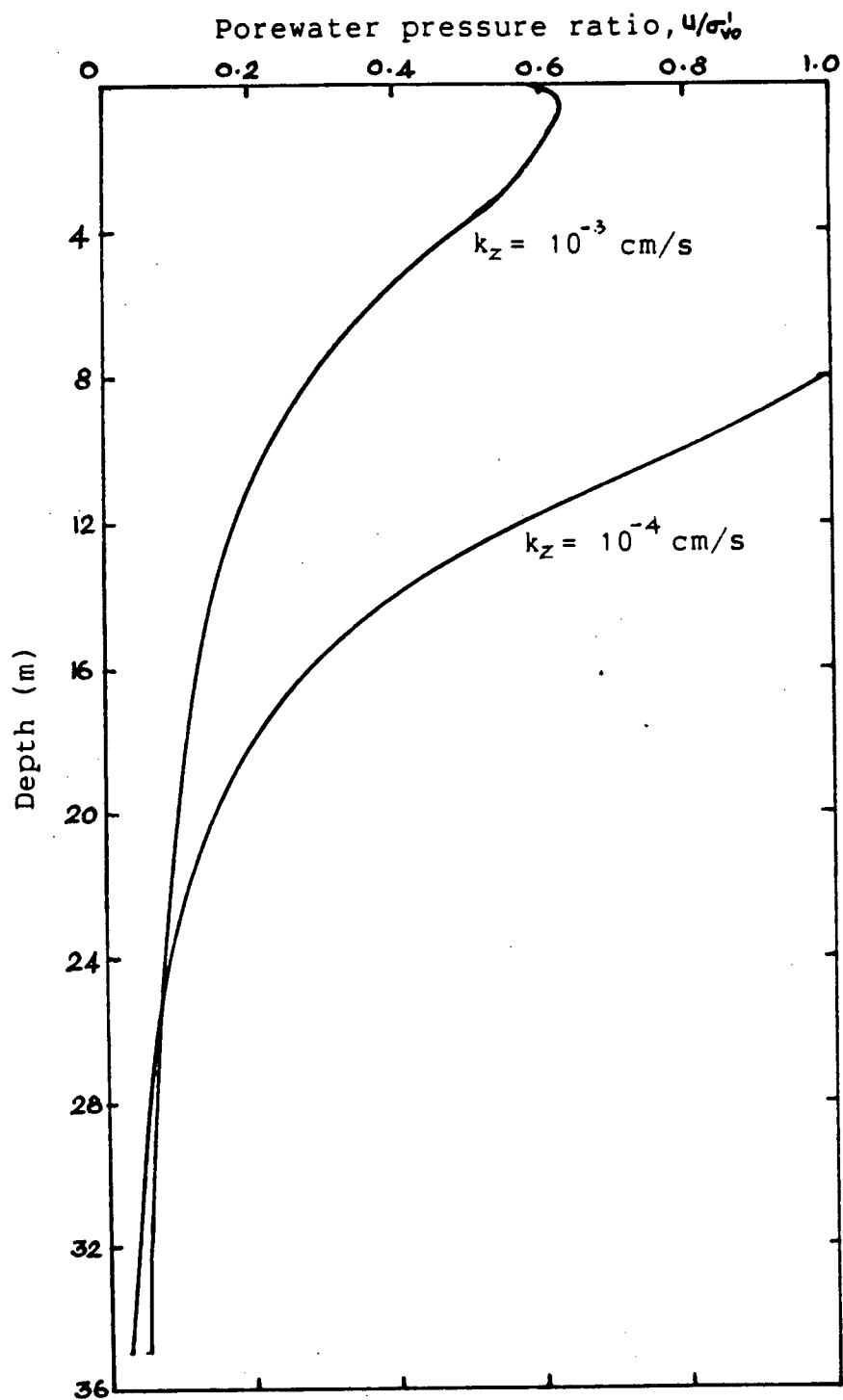At the end of 6m 6 hour Storm.

Figure 6.6; Section-FF; Residual Porewater Pressure Response
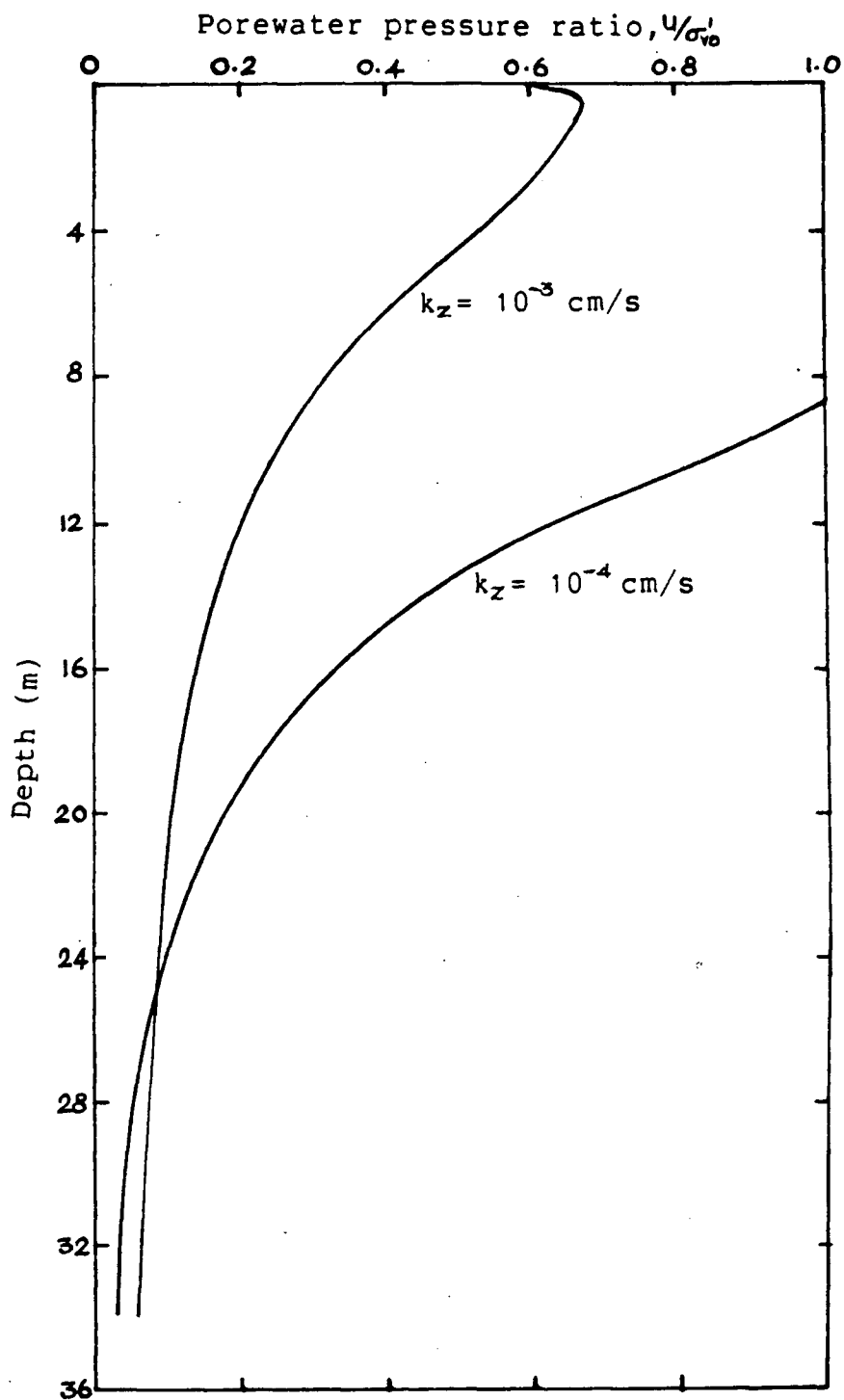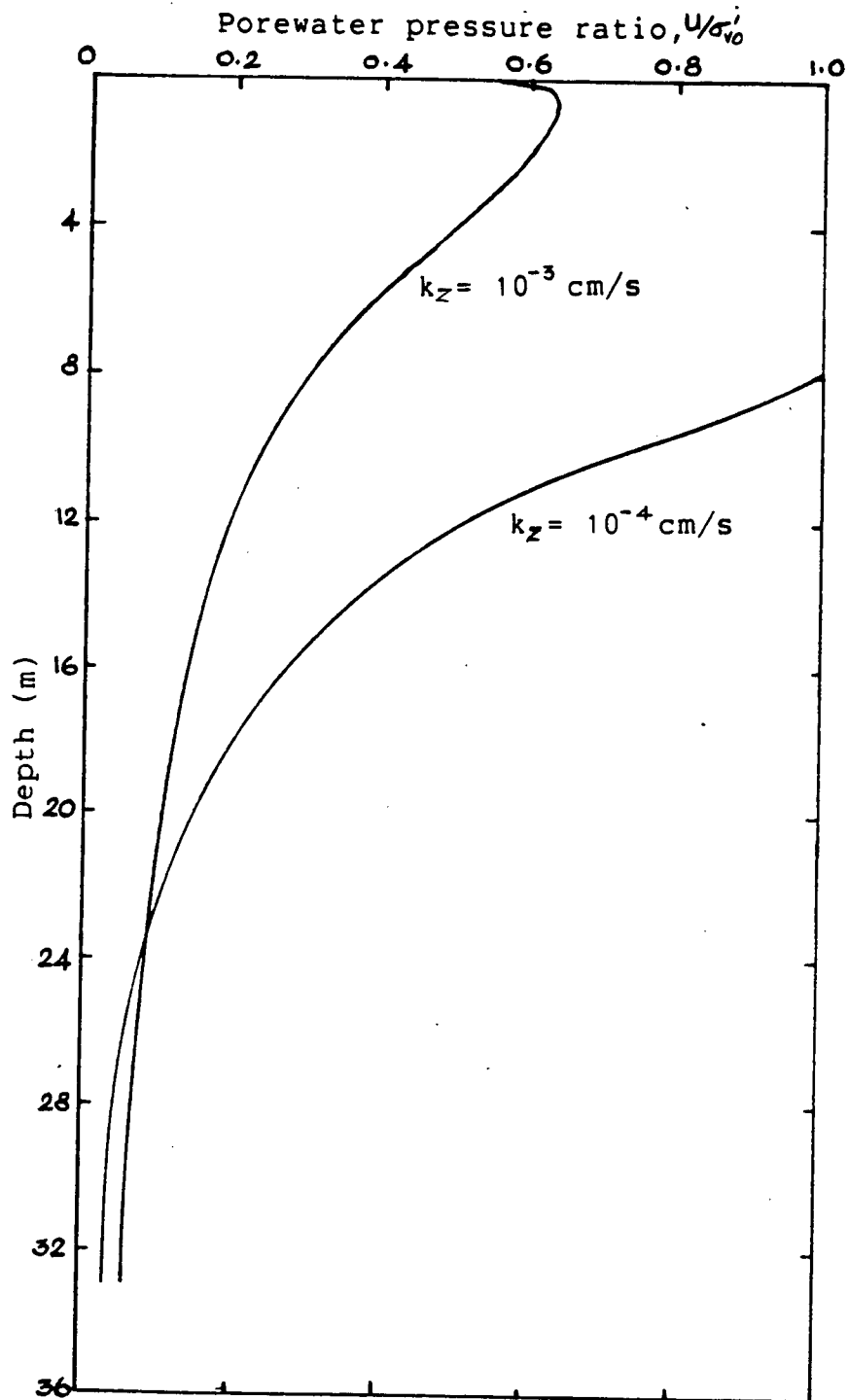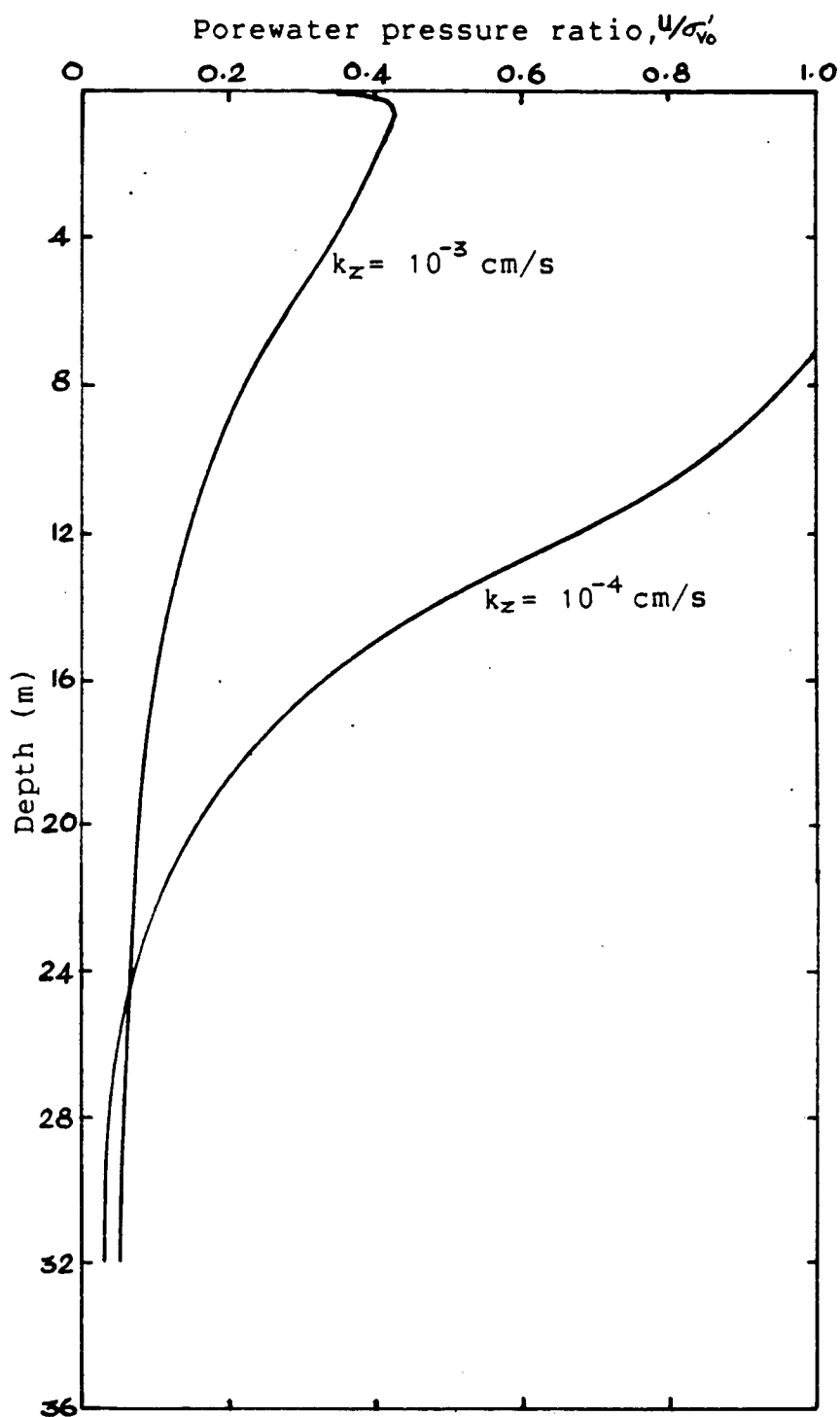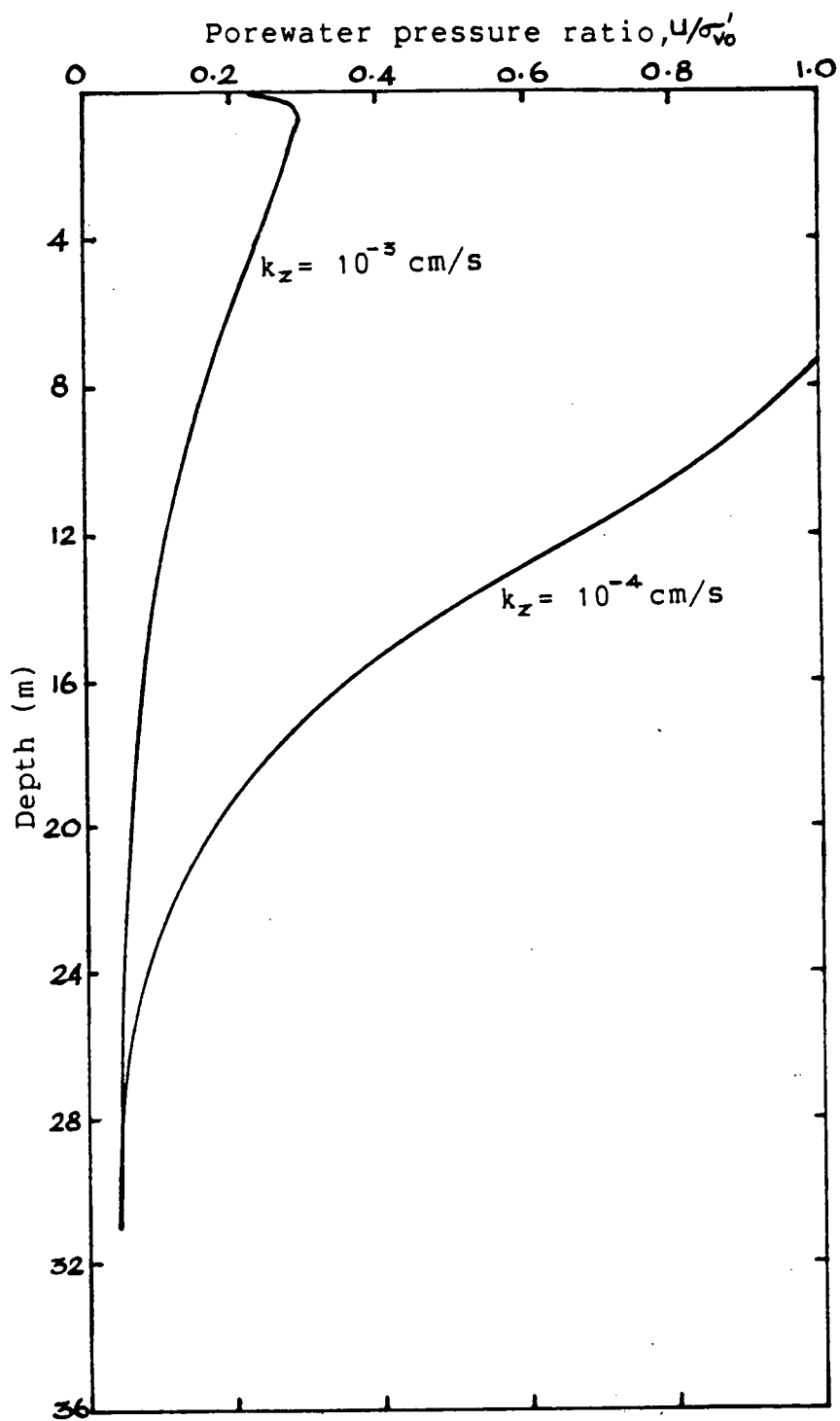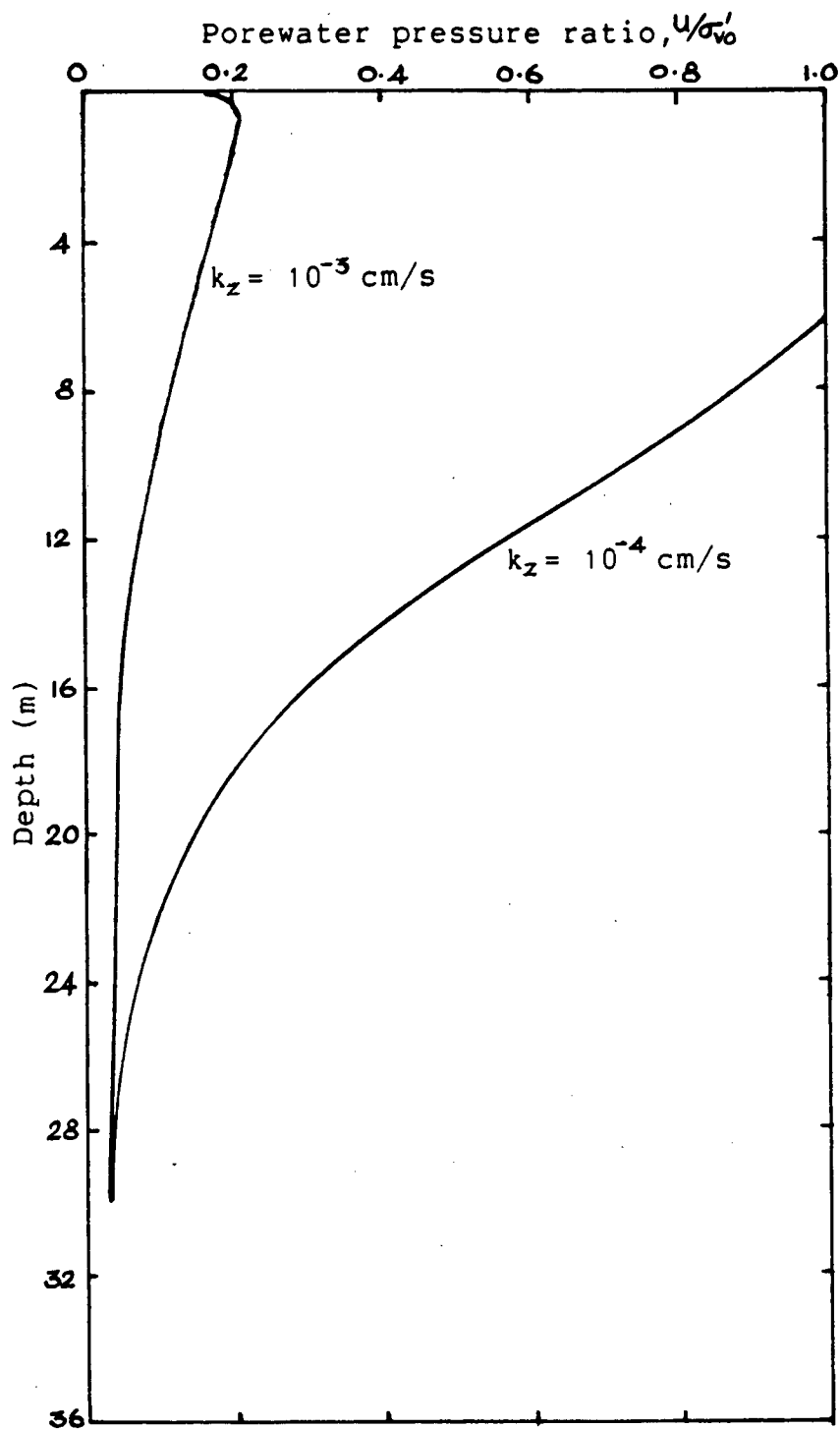At the end of 6m 6 hour Storm.

Figure 6.7; Section-GG; Residual Porewater Pressure Response
At the end of 6m 6 hour Storm.

The residual porewater pressure distributions presented in Figures 6.1 to 6.7 show the same trend; the maximum porewater pressure ratio, u/σ'_{vo} , occurs very near the top and decays rather steadily as the depth increases. In the case with $k_z = 10^{-4}$ cm/s, the decay starts to occur beneath the zone of liquefaction. This decaying trend is similar to the typical shear stress ratio distribution, such as the one shown in Figure 6.8. This is as expected because as the shear stress ratio decreases, the number of cycles required to cause initial liquefaction, N_L, increases. Now from equation (3-12), the porewater pressure generation is inversely proportional to N_L. Hence, the porewater pressure generated would be higher at the top and decrease as the depth increases.

It is also seen that as the depth of water increases, for example, 6 m at section AA to 12 m at secton GG, the porewater pressure response increases up to a certain critical location and then starts to decrease. The above trend is apparent for both values of k_z. For analyses with $k_z = 10^{-3}$ cm/s, the maximum porewater pressure ratio developed at sections AA to GG are such that it increases from 47% at section AA to 66% at section CC and decreases to 22% at section GG. On the other hand, for analyses with $k_z = 10^{-4}$ cm/s, the maximum depth of liquefaction increases from 6.5m at section AA to 9m at section CC and then decreases to 6m at section GG.

Table 6.1 shows the maximum porewater pressure response in terms of porewater pressure ratio, u/σ'_{vo} , for the case with $k_z = 10^{-3}$ cm/s and in terms of depth of liquefaction for the case
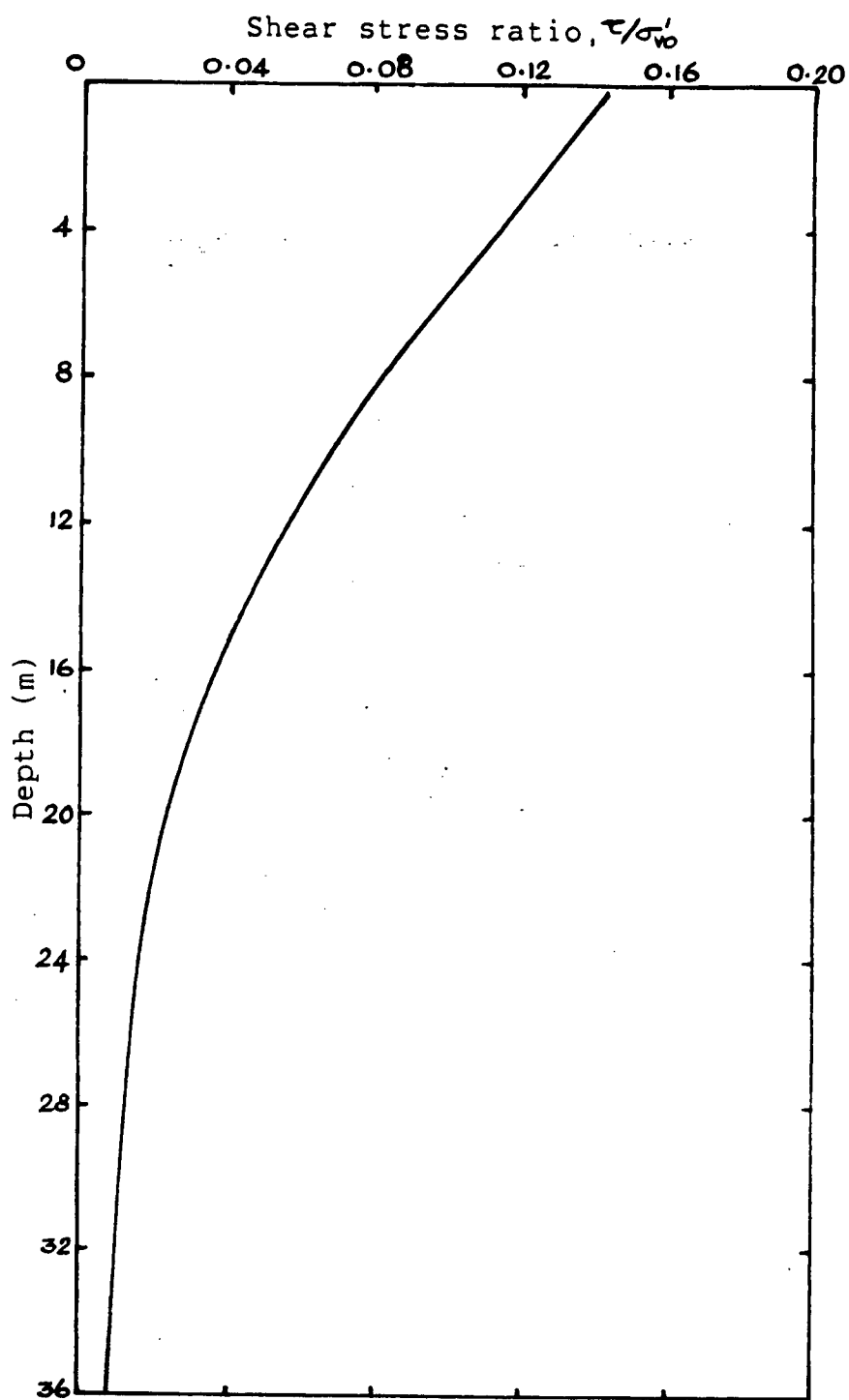
Figure 6.8; Section-AA; Shear Stress Ratio Distribution
At the start of the Storm.

Section	Water depth(m)	(d/H_S)	Maximum pwp Response	
			pwp Ratio (%) $k = 10^{-3}$ cm/s	Liquefaction depth(m) $k = 10^{-4}$ cm/s
AA	6	1.00	47	6.5
BB	7	1.17	62	8.0
CC	8	1.33	67	9.0
DD	9	1.50	65	8.5
EE	10	1.67	43	7.0
FF	11	1.83	29	6.5
GG	12	2.00	22	6.0

Table 6.1 ; Maximum Porewater Pressure Response At Sections
of Island 1 At the End of the 6m 6 hour Storm

with $k_z = 10^{-4}$ cm/s at the selected sections of the island 1. The above results are presented in Figure 6.9 and 6.10 respectively. From these figures, it can be concluded that the effect of the storm is severe at one particular section and the location of this critical section in terms of its water depth is given approximately by 1.4 to 1.5 times the significant wave height of the storm, regardless of the k_z values.

Results from Figures 6.1 to 6.7 also indicate that for a particular location, there exists a critical value of permeability that would prevent any liquefaction at that location during storm activity. If the permeability is greater than this critical value then there would not be any liquefaction and if the permeability is less than this critical value then liquefaction would occur at this particular section. The level of porewater pressure ratio induced or the extent of the liquefaction zone depends on by how much the permeability is greater or lesser than the critical value.

Having recognised that section CC is the closest to the critical location, where the effect of the 6m, 6 hour storm is felt severely, analyses were conducted at section CC, to determine the critical value of permeability that would prevent liquefaction or in other words, that would limit the porewater pressure ratio to within 95 to 100%. This critical value of permeability would serve as the minimum permeability required to prevent liquefaction within the entire island for the specified 6m, 6 hour storm.
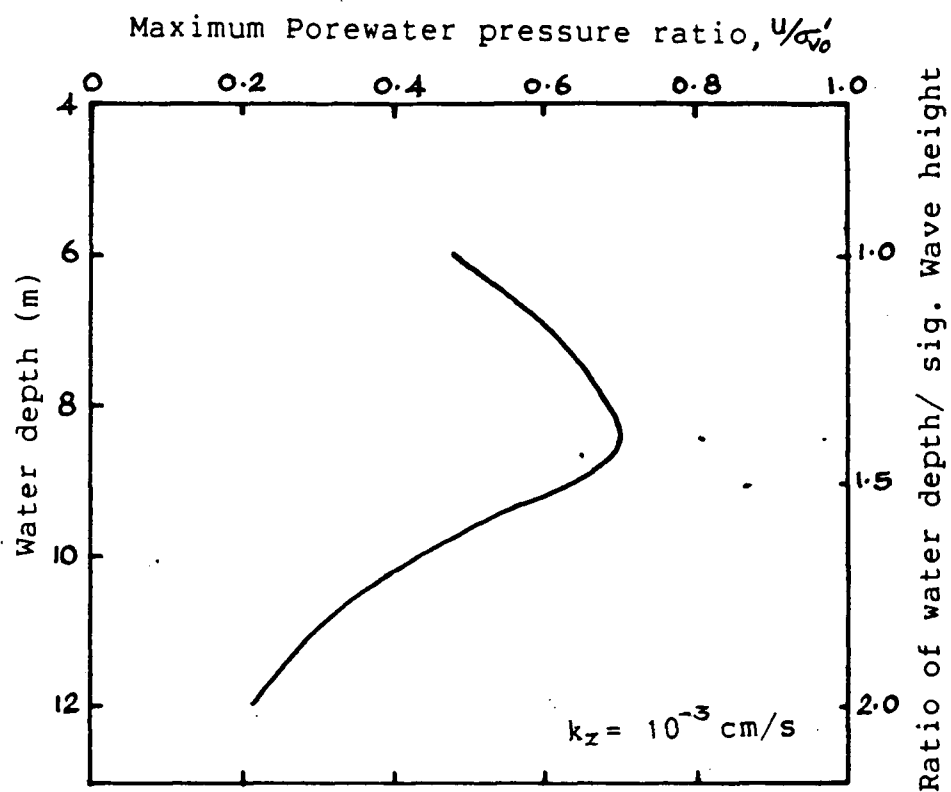
Figure 6.9; Maximum Porewater Pressure Response of Island 1 At the end of 6m 6 hour Storm.
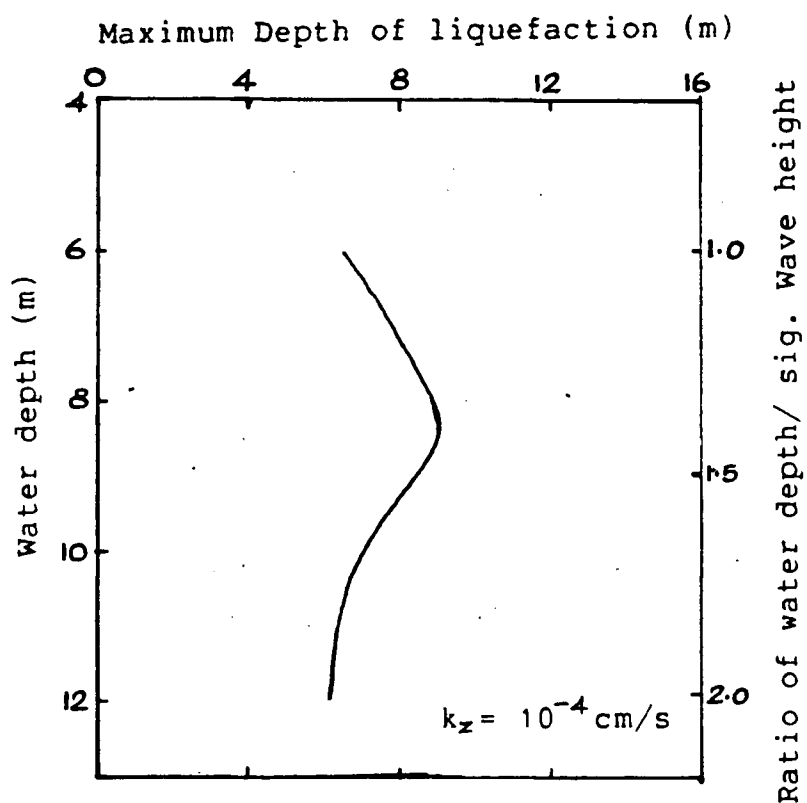
Figure **6**.10; Maximum Porewater Pressure Response of Island 1
At the end of 6m 6 hour Storm.

Figure 6.11 shows the residual porewater pressure distribution at section CC for the different values of k_z between 10^{-3} and 10^{-4} cm/s with the initial compressibility in each of these cases kept as 3.0×10^{-5} m²/kN. It is seen from the figure that the critical value of permeability that is required to limit porewater pressure development below 95 to 100% of the initial effective stress for the specified 6m, 6 hour storm is around 8.0×10^{-4} cm/s. It is interesting to note that the permeability required to limit porewater pressure ratio to 65% or less within the entire island for the specified storm is 10^{-3} cm/s. It is often convenient to interpret these results in terms of coefficient of consolidation. The initial coefficient of consolidation, C_{vo}, required to meet the above mentioned criteria are 2.7×10^{-2} m²/s and 3.4×10^{-2} m²/s respectively.

6.3.1 Wave Induced Porewater Pressure Response of Island 1 to 4m, 6 hour Storm

Figures 6.12 to 6.14 show the residual porewater pressure induced at the end of the 4m, 6 hour storm at section AA, CC and DD of island 1 for different k_z values of 10^{-3} and 10^{-4} cm/s. It is evident from these figures that the porewater pressure response show the same kind of steady decaying trend as the earlier response with the 6m storm. The apparent difference being that the porewater pressure response shows a steady decrease as the water depth increases from 6m at section
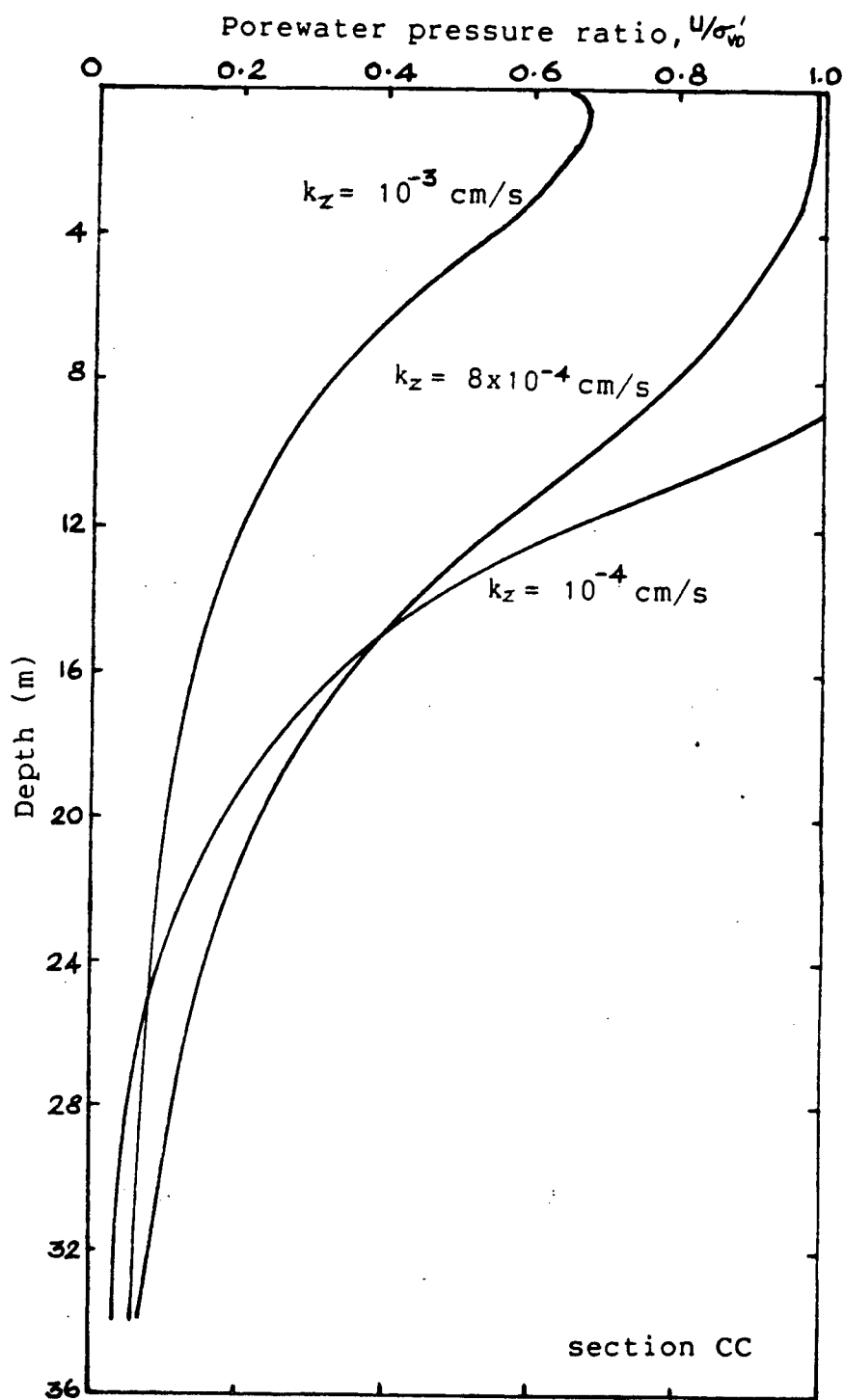
Figure 6.11; Porewater Pressure Response At the end of
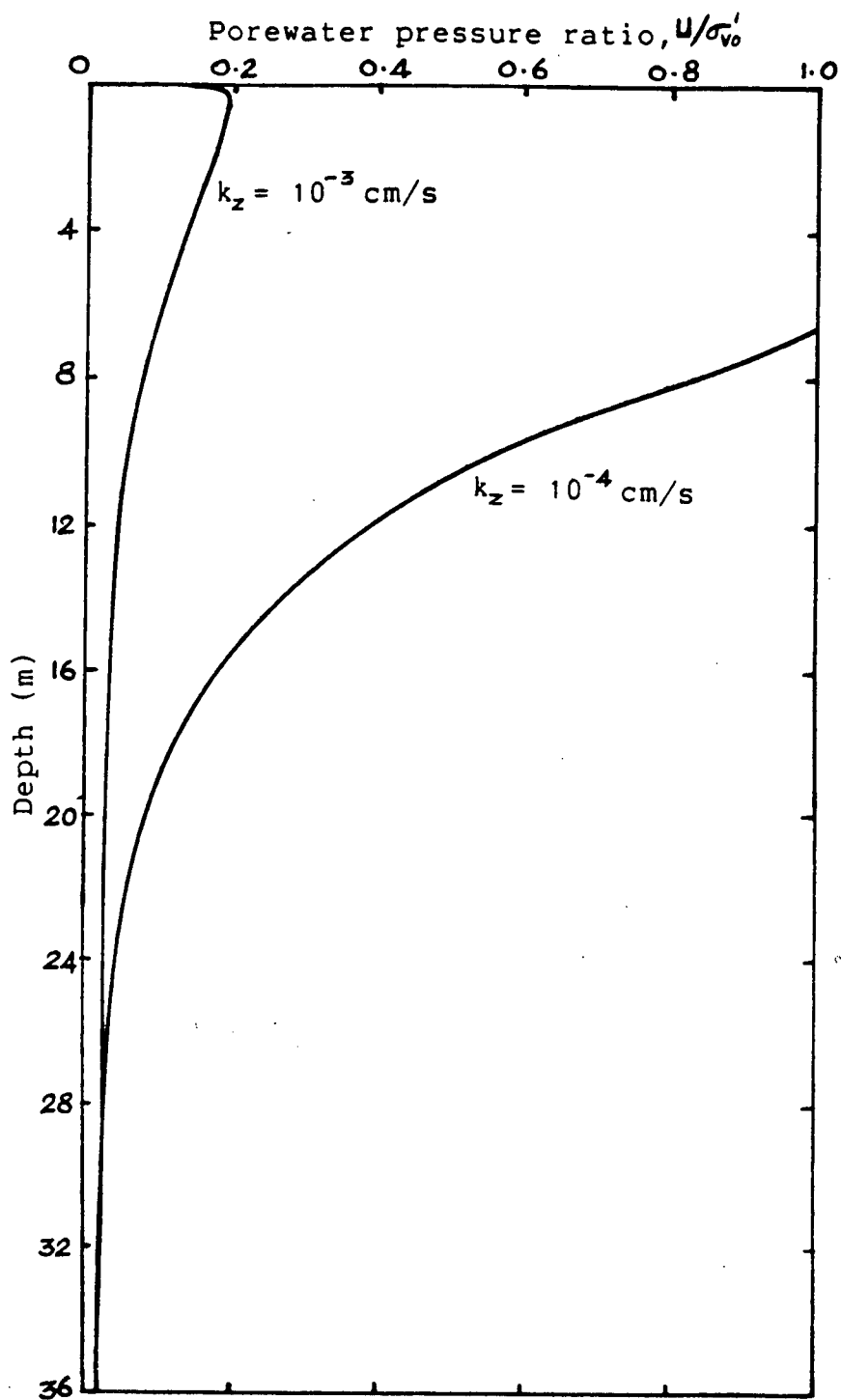6m 6 hour Storm for Different Permeabilities.

Figure 6.12; Section-AA; Residual Porewater Pressure Response
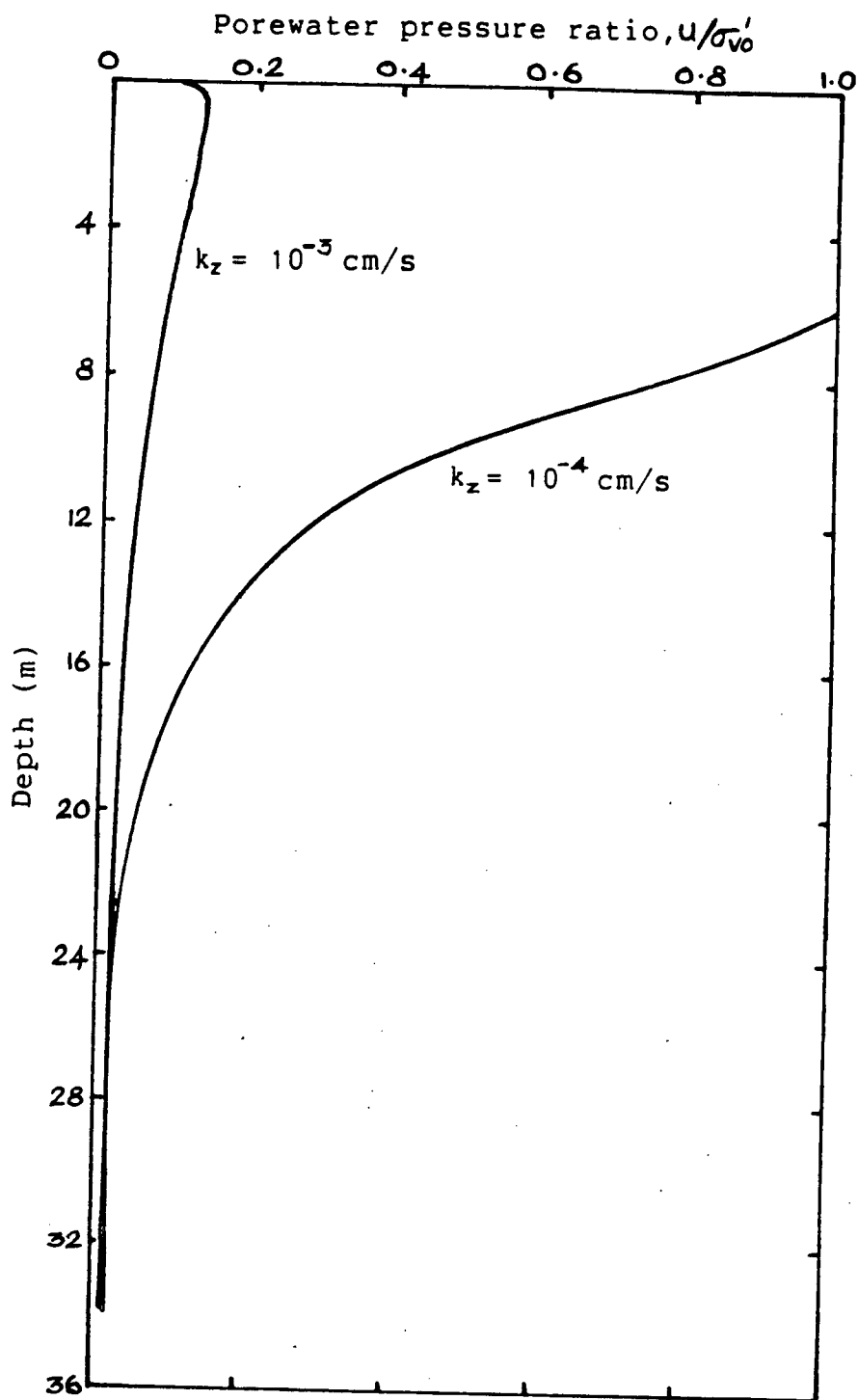At the end of 4m 6 hour Storm.

Figure **6**.13; Section-CC; Residual Porewater Pressure Response At the end of 4m 6 hour Storm.
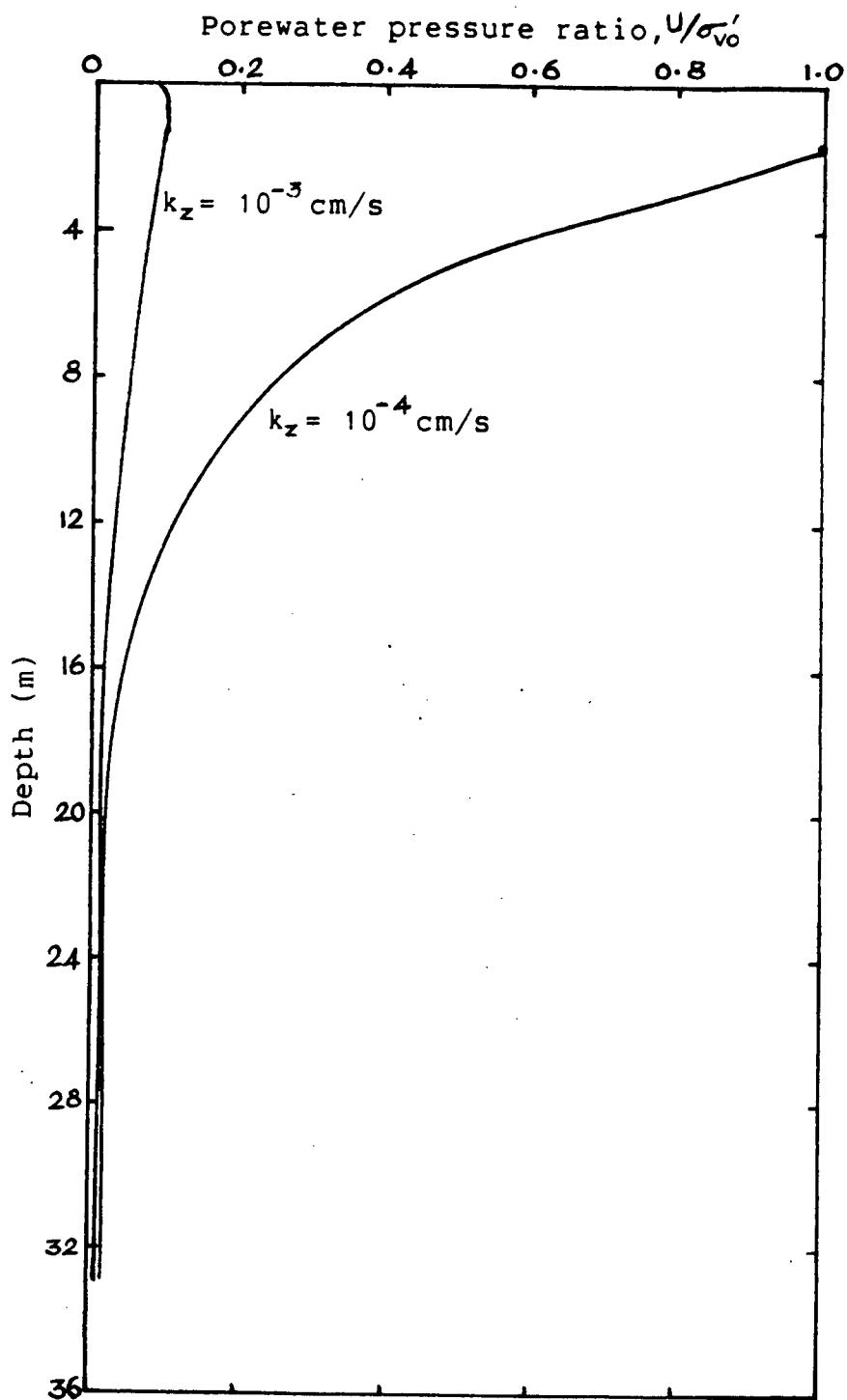
Figure 6.14; Section-DD; Residual Porewater Pressure Response
At the end of 4m 6 hour Storm.

AA to 9m at section DD.

For analyses with $k_z = 10^{-3}$ cm/s, the maximum porewater pressure ratio developed at section AA is 19% and at section DD is 10%. Further, for the case with $k_z = 10^{-4}$ cm/s the results indicate that the depth of liquefaction at section AA is 6.5m and it reduces to 2m at section DD.

The maximum porewater pressure response for the two cases of k_z values are presented in Table 6.2 and the results are plotted in Figures 6.15 and 6.16. Both figures show that the maximum porewater pressure occurs at section AA, where the water depth is 1.5 times significant wave height.

Section AA could not be guaranteed directly as the critical location for the 4m storm since there can be a critical location at water depths less than 6m. However, as far as the island is concerned, the minimum water depth to island surface is 6m and accordingly section AA can be treated as the critical location for the 4m storm.

Figure 6.16 also indicates that during the 4m storm, the depth of water beyound which liquefaction would not occur for the k_z value of 10^{-4} cm/s is approximately given by 2.42 times the significant wave height.

Additional analyses were conducted at section AA, the critical section for the 4m, 6 hour storm for different permeability values between 10^{-3} and 10^{-4} cm/s to determine the critical permeability value that would prevent liquefaction within the entire island during the storm activity. The results of these analyses are presented in Figure 6.17. It is evident

Section	Water depth(m)	(d/H_s)	Maximum pwp Response	
			pwp Ratio (%) $k = 10^{-3}$ cm/s	Liquefaction depth(m) $k = 10^{-4}$ cm/s
AA	6	1.50	19	6.5
CC	8	2.00	13	5.0
DD	9	2.25	10	2.0

Table 6.2; Maximum Porewater Pressure Response At Sections of Island 1 At the End of the 4m 6 hour Storm
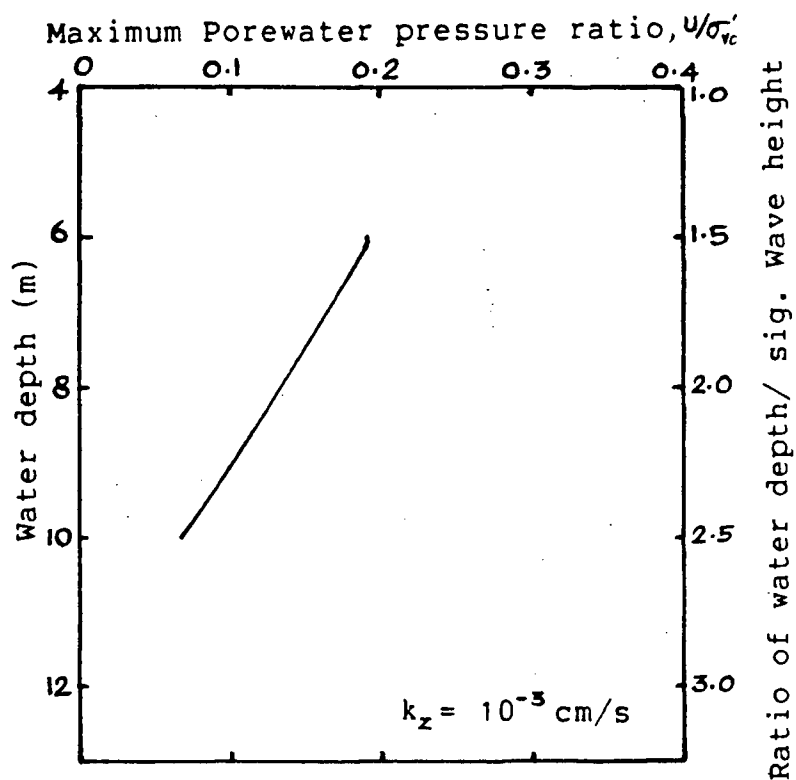
Figure 6.15; Maximum Porewater Pressure Response of Island 1
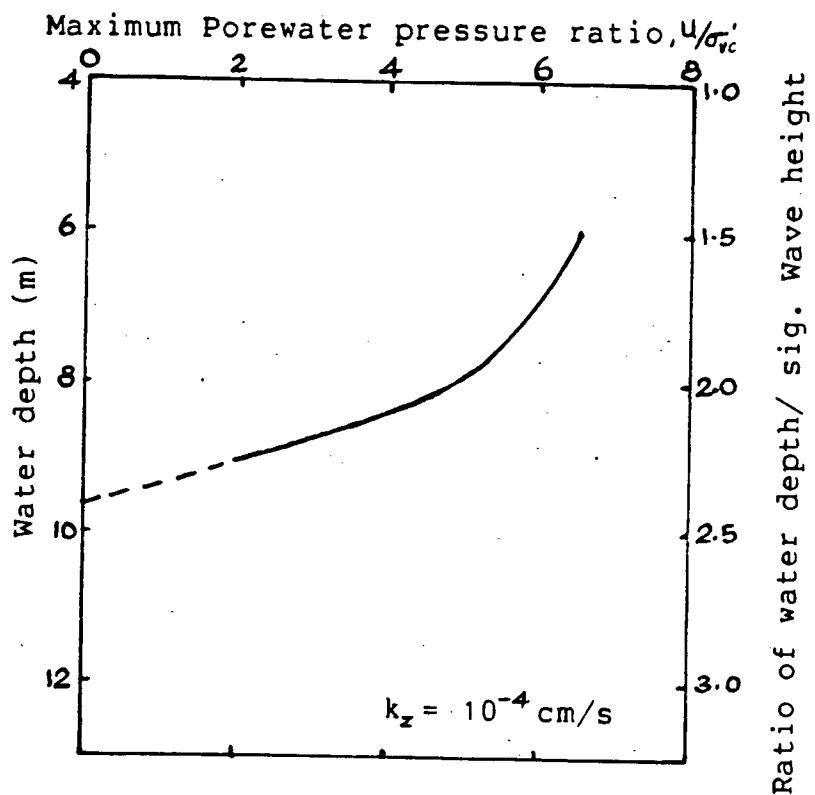At the end of 4m 6 hour Storm.

Figure **6**.16; Maximum Porewater Pressure Response of Island 1
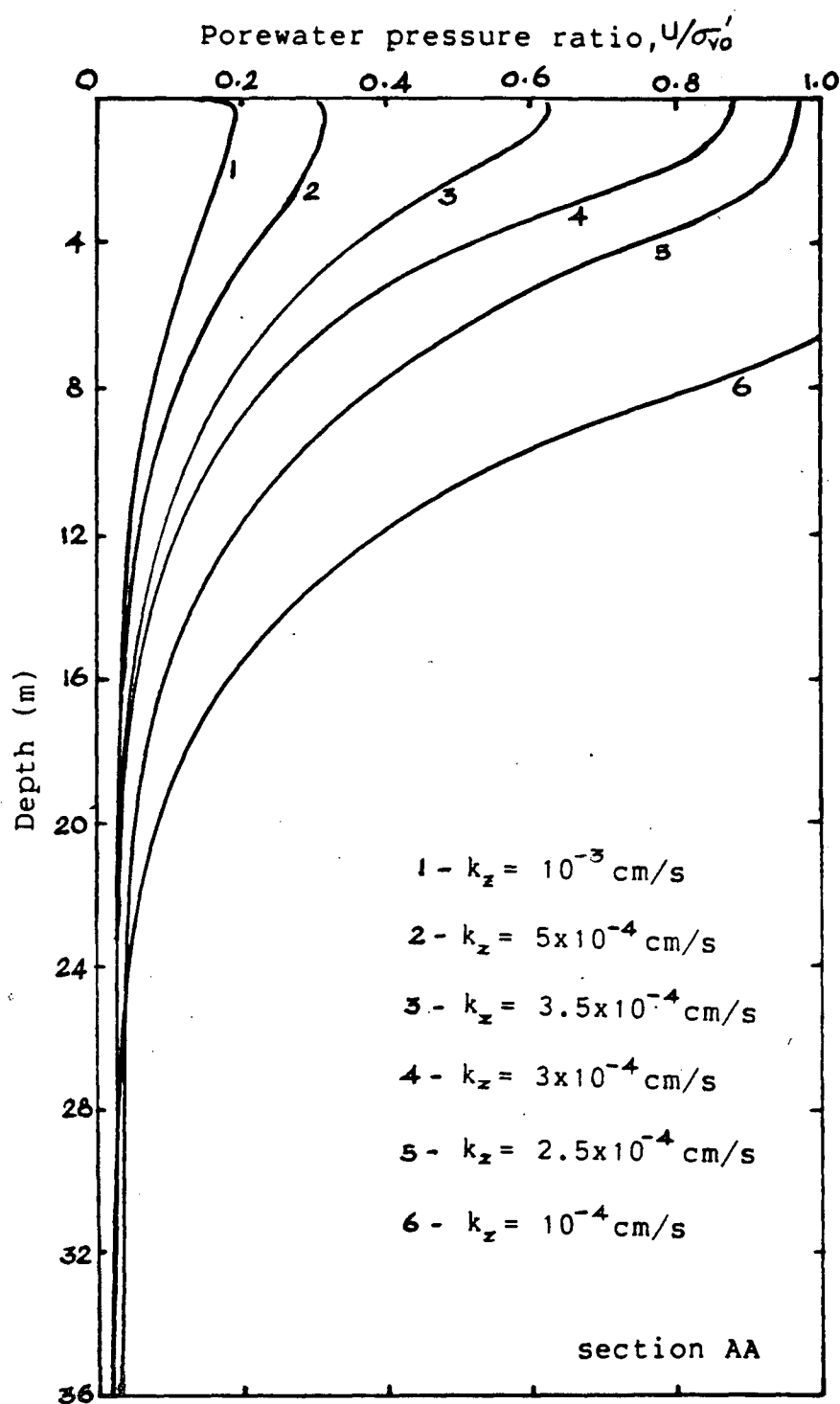At the end of 4m 6 hour Storm.

Figure 6.17; Porewater Pressure Response At the end of 4m 6 hour Storm for Different Permeabilities.

that the critical value of permeability that limits the porewater pressure ratio to within 95 to 100% is 2.5 x 10^{-4} cm/s while a value of 3.5 x 10^{-4} cm/s is sufficient to limit porewater pressure ratio to 65% or less. The corresponding values of initial coefficient of consolidation are 8.5 x 10^{-3} m^2/s and 1.19 x 10^{-2} m^2/s respectively.

6.3.2 Comparison of Performance to the Two Different Storms

Table 6.3 provides the opportunity to compare the effect of storm characteristics on the induced porewater pressure response at the selected sections AA, CC and DD. The results clearly indicate that the more severe the intensity of the storm, the higher the maximum porewater pressure response will be. For example, the maximum porewater pressure ratio developed for the case k_z = 10^{-3} cm/s is 19% (at section AA) due to 4m storm, while it is 67% (at section CC) due to 6m storm.

The effect of storm intensity is also clearly seen in the permeability requirement for the criteria discussed earlier. The permeability required to limit porewater pressure ratio to within 95 to 100% is 2.5 x 10^{-4} cm/s and 8.0 x 10^{-4} cm/s for the 4m and 6m storm respectively. This indicates that the requirement is more stringent in the case of severe storms. The same trend is apparent in the requirement to limit porewater pressure ratio to 65% or less.

To understand the effect of the storm intensity more

Section	Water depth (m)	pwp ratio (%) $k_z = 10^{-3}$cm/s		Liquefaction depth(m) $k_z = 10^{-4}$cm/s	
		$H_s = 4$m	$H_s = 6$m	$H_s = 4$m	$H_s = 6$m
AA	6	19	47	6.5	6.5
CC	8	13	67	5.0	9.0
DD	9	10	65	2.0	8.5

Table 6·3 ; Comparison of Maximum Porewater Pressure Response to Two Different Storms

clearly, it is perhaps important to compare the time history of the porewater response during the storms. Such a comparison at a particular depth 3m below the island top surface at section CC is highlighted in Figure 6.18.

As can be seen from the figure, the residual porewater pressure builds up steadily in the case with $k_z = 10^{-3}$ cm/s until the end of the storm and dissipates fairly rapidly after the storm activity. In contrast to this, the porewater pressure in the case with $k_z = 10^{-4}$ cm/s builds up fairly rapidly, attains liquefaction level and dissipates rather slowly after the storm. The constrasting behavior can be attributed to the differences in drainage characrteristics.

For both values of k_z, the rate of residual porewater pressure build up is found to be higher during the 6m storm than the 4m storm. It is also noticeable that for the case with $k_z = 10^{-4}$ cm/s, liquefaction level is attained within first half an hour of the 6m storm, whereas for the 4m storm, 3 hours is required to attain liquefaction level. The dissipation after the end of storms is faster for 4m storm than the 6m storm.

The difference in the rate of residual porewater pressure build up can be attributed to the difference in N_{eq}, the equivalent number of cycles of the reference wave, since all other potential variables remain the same initially for the two storms. The major contributing factor to the residual porewater pressure is the porewater pressure generated due to the action of cyclic shear stresses. It can be seen from equation (3-12) that u_g is directly proportional to (N_{eq}/N_L) for a given
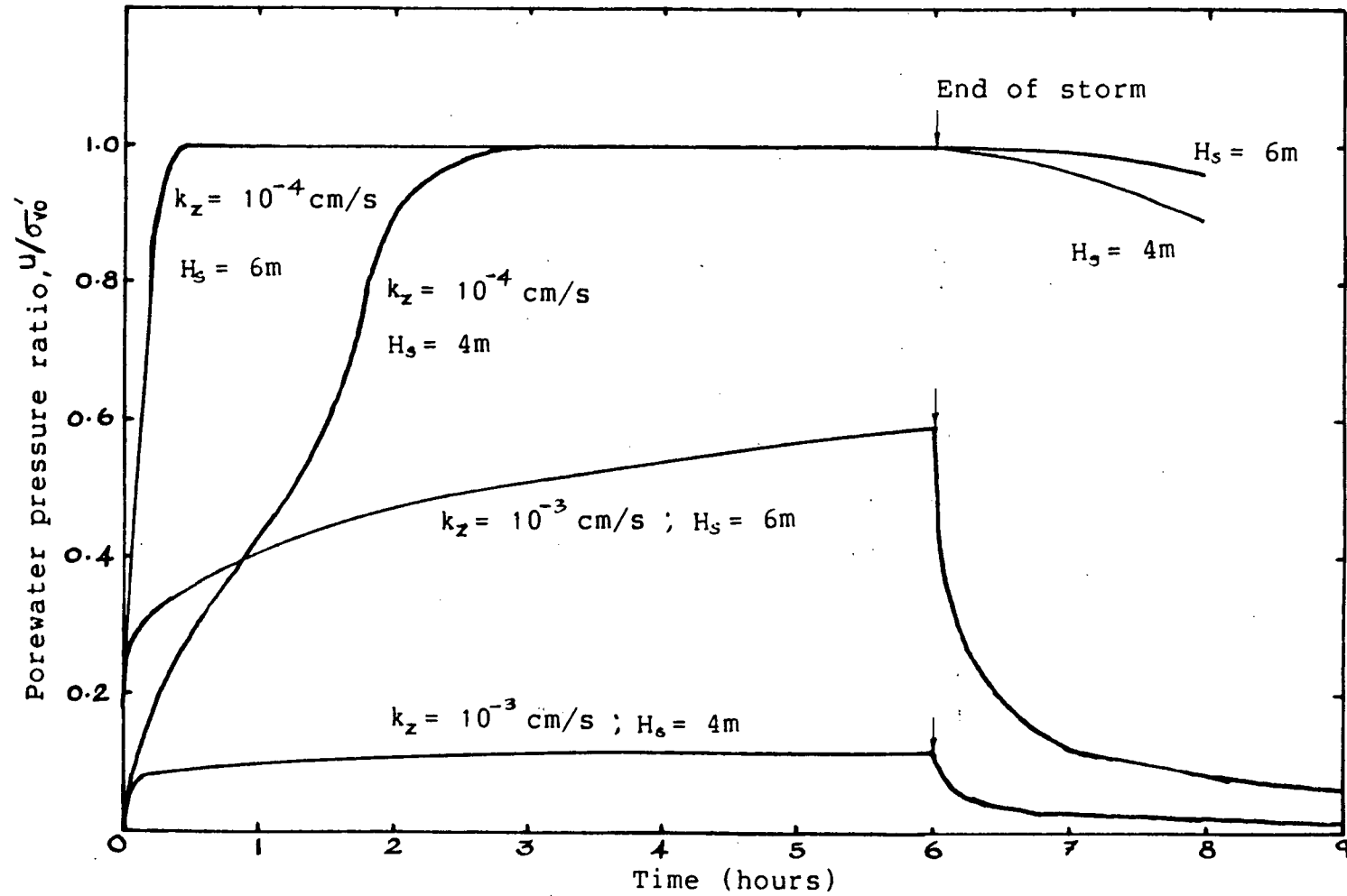
Figure 6.18; Time History Of Porewater Pressure At 3m

Below Island Surface At Section CC.

porewater pressure ratio. Since the difference in N_L is marginal at the start of the storms, the dominating parameter becomes N_{eq}. The values of N_{eq} for the 4m and 6m storm at section CC are 100 and 559 respectively. Thus, the resulting net porewater pressure response during the storm activity is higher for the 6m storm than the 4m storm.

6.4 Wave Induced Porewater Pressure Response of Island 2

The porewater pressure response at selected sections PP to VV of island 2 at the end of the 6 hour storm with significant wave height of 9m for the two different k_z values of 10^{-3} and 10^{-4} cm/s are shown in Figures 6.19 to 6.25. The results indicate that liquefaction occurs at all sections for the case with 10^{-4} cm/s and at all sections, except PP, for the case with $k_z = 10^{-3}$ cm/s.

It is also apparent that the zone of liquefaction in the case with $k_z = 10^{-4}$ cm/s is deeper than with $k_z = 10^{-3}$ cm/s. However, analyses with $k_z = 10^{-3}$ cm/s indicate higher porewater pressures at depths well below the zone of liquefaction than with $k_z = 10^{-4}$ cm/s. This kind of behaviour can be attributed to the dominant influence of the diffusion of porewater pressure within the profile.

To illustrate the above argument, the flow through the nodal point, in the form $k_z.(du/dz)$, at the particular section QQ predicted by STABW3 analysis is presented in Figure 6.26 for the two cases of k_z value. It appears that at the end of the storm, the effect of the top drainage boundary is felt only up

Figure 6.19; Section-PP; Residual Porewater
Pressure Response At the end of
9m 6 hour Storm.

Figure 5.20; Section-QQ; Residual Porewater
Pressure Response At the end of
9m 6 hour Storm.

Figure 6.21; Section-RR; Residual Porewater
Pressure Response At the end of
9m 6 hour Storm.

Figure 6.22; Section-SS; Residual Porewater
Pressure Response At the end of
9m 6 hour Storm.

Figure **6**.23; Section-TT; Residual Porewater
Pressure Response At the end of
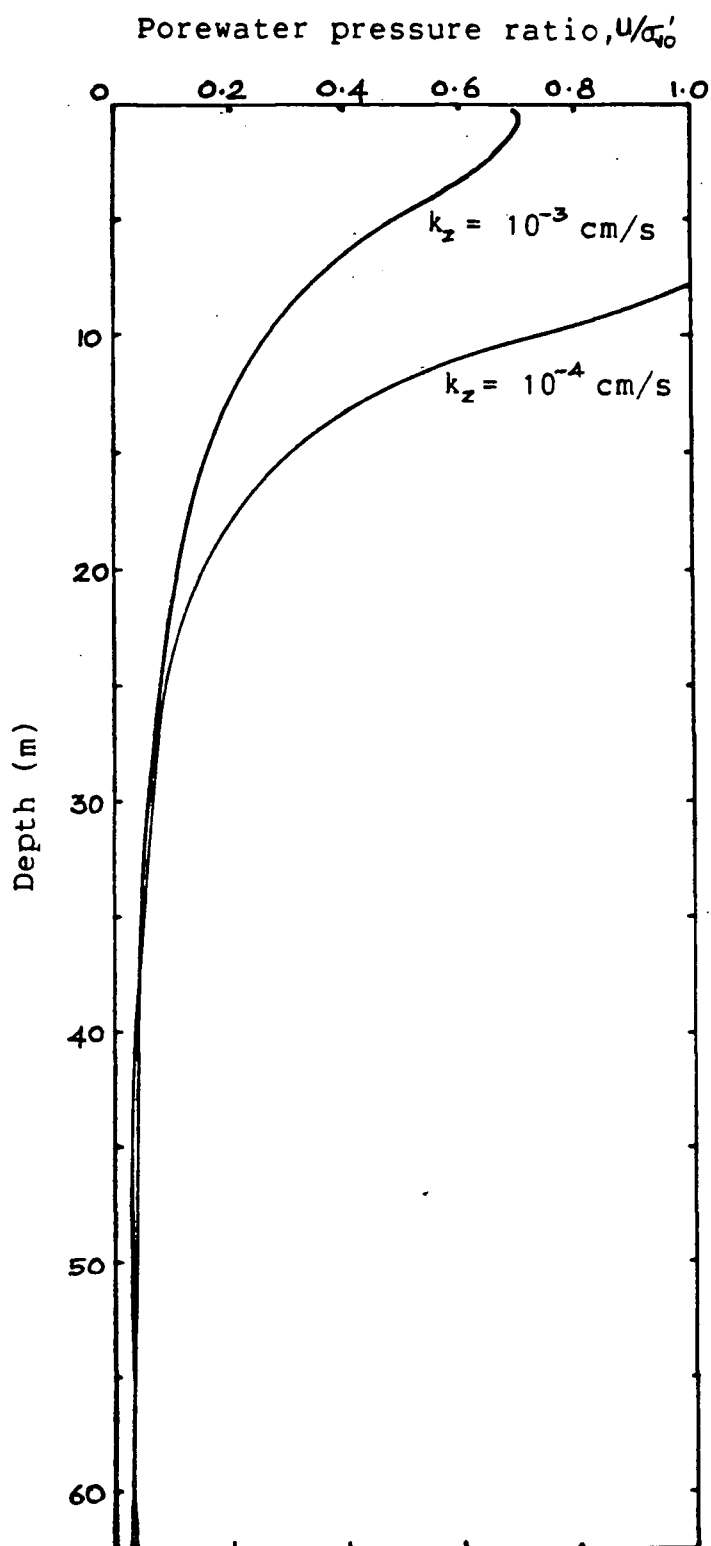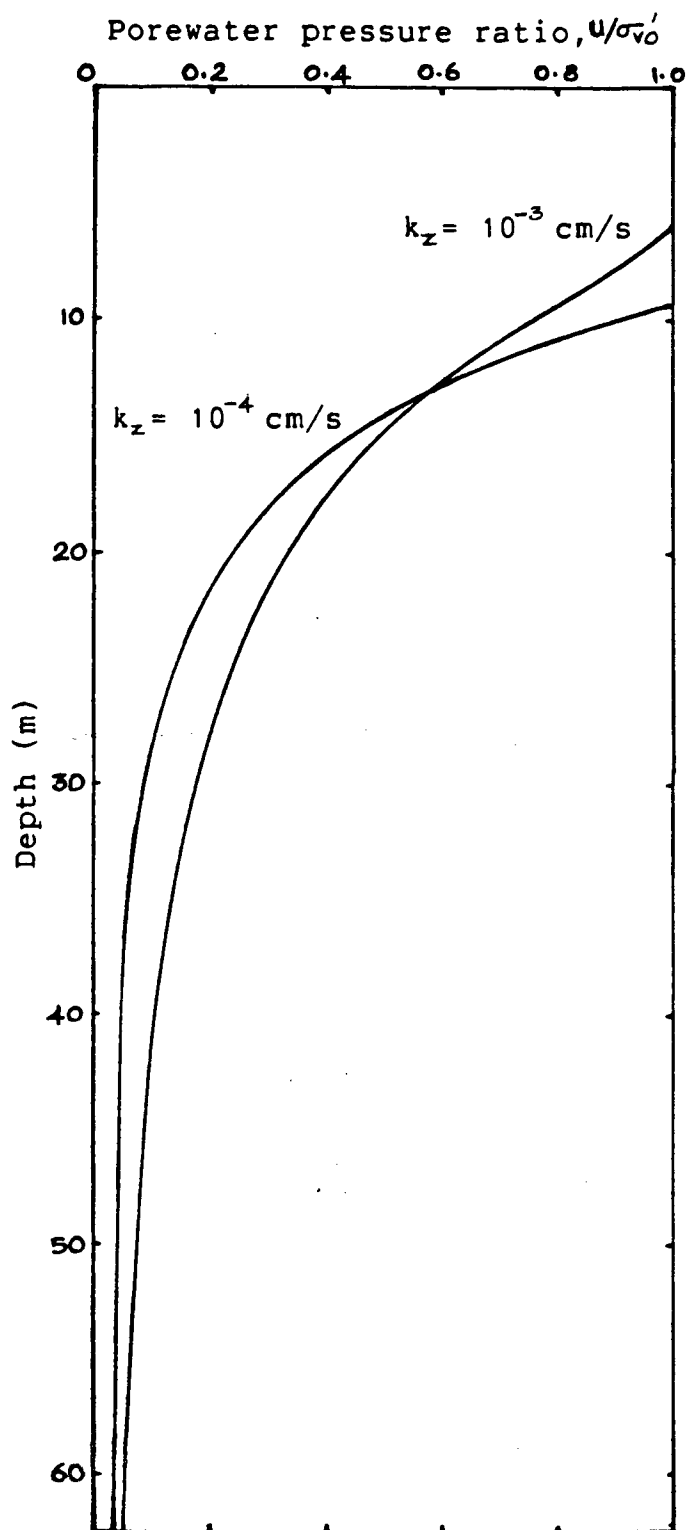9m 6 hour Storm.

Figure 6.24; Section-UU; Residual Porewater
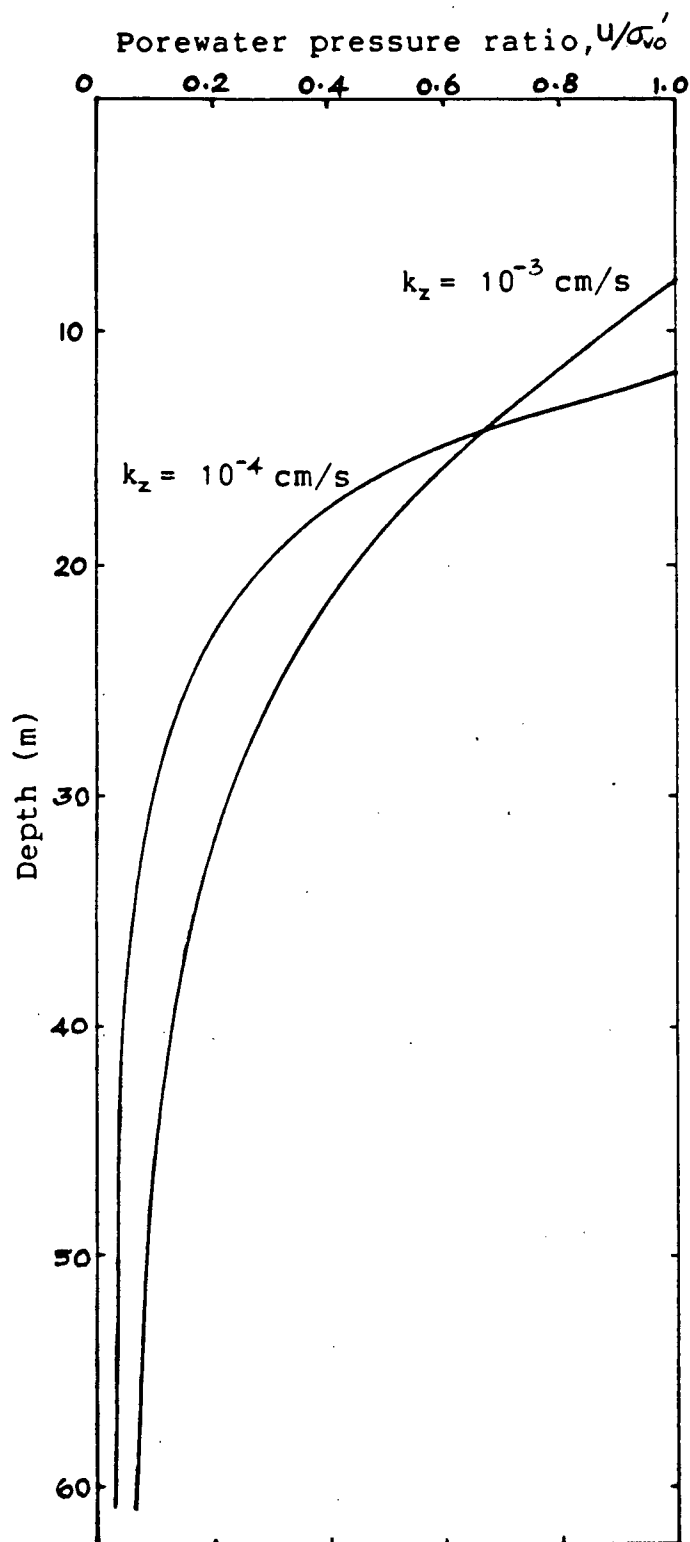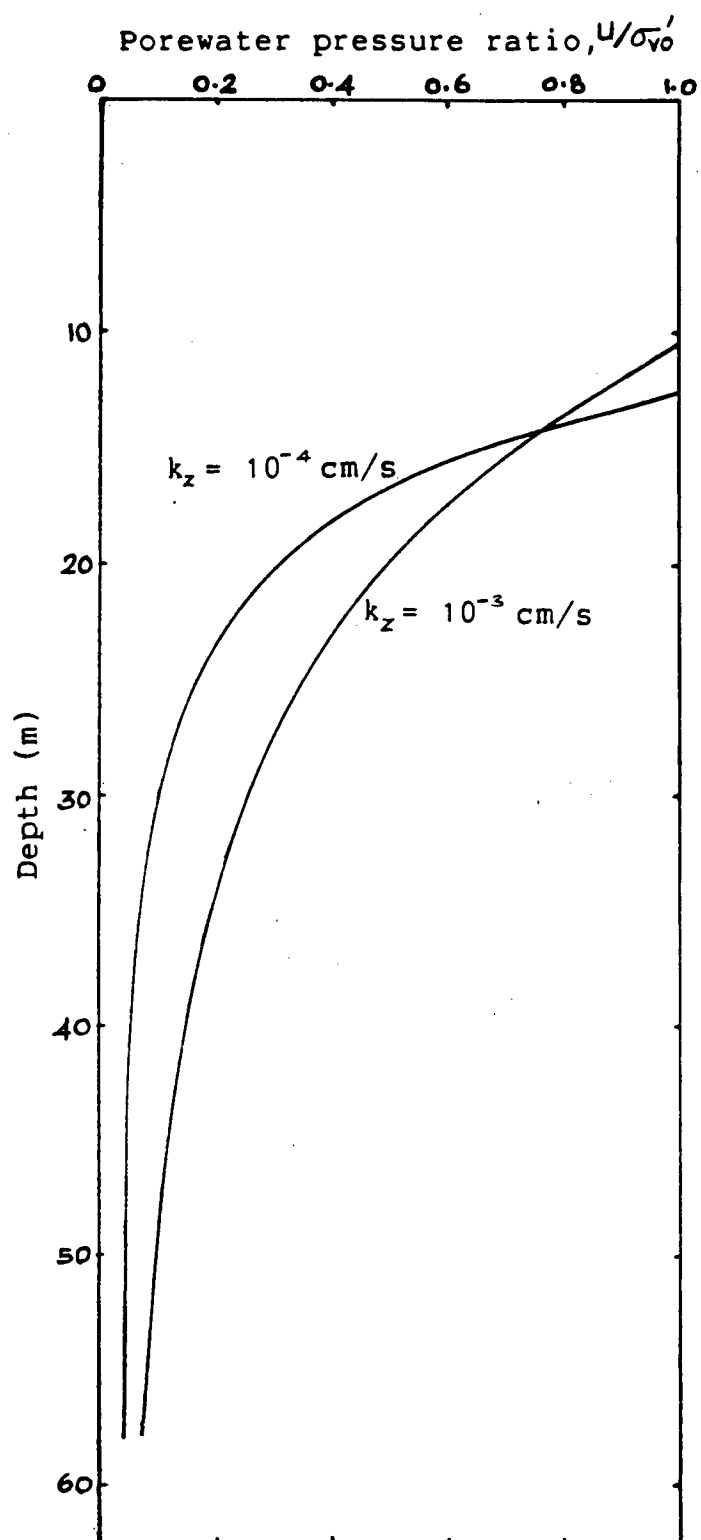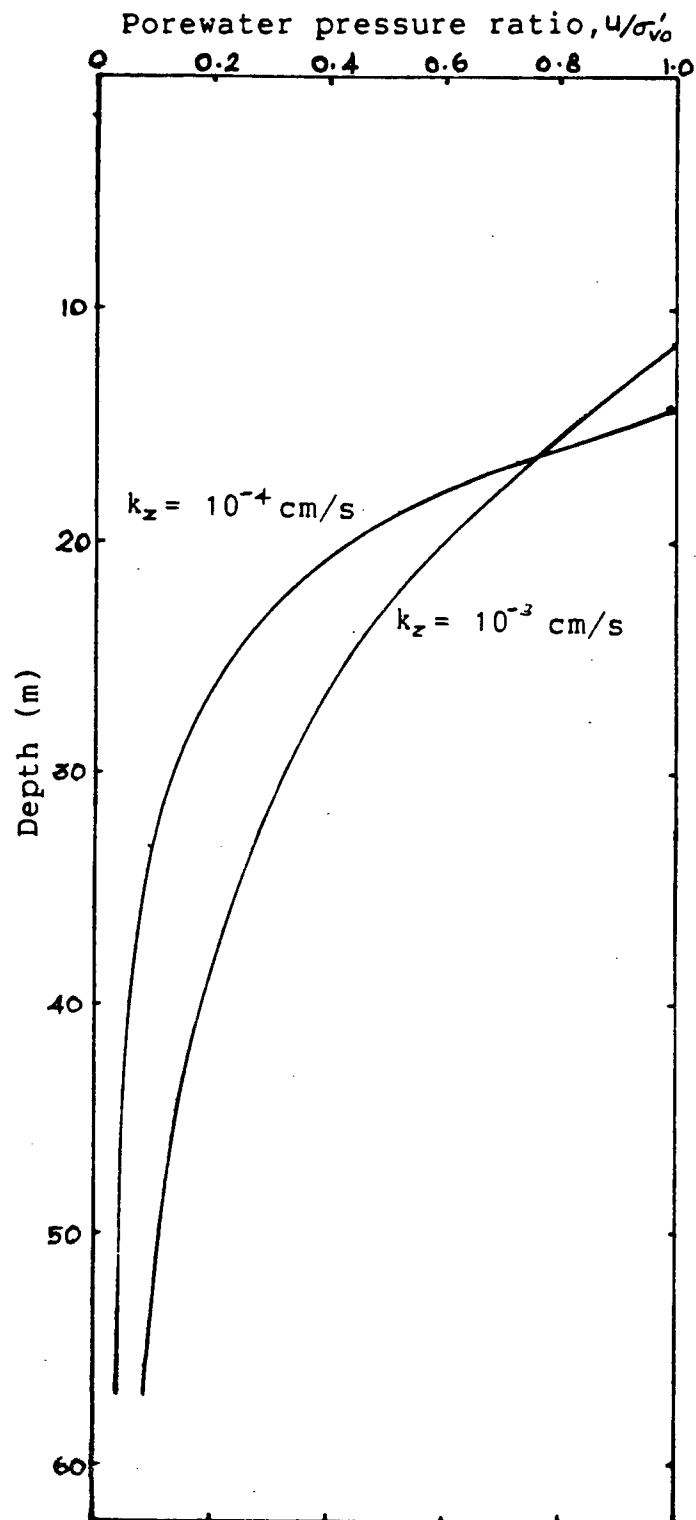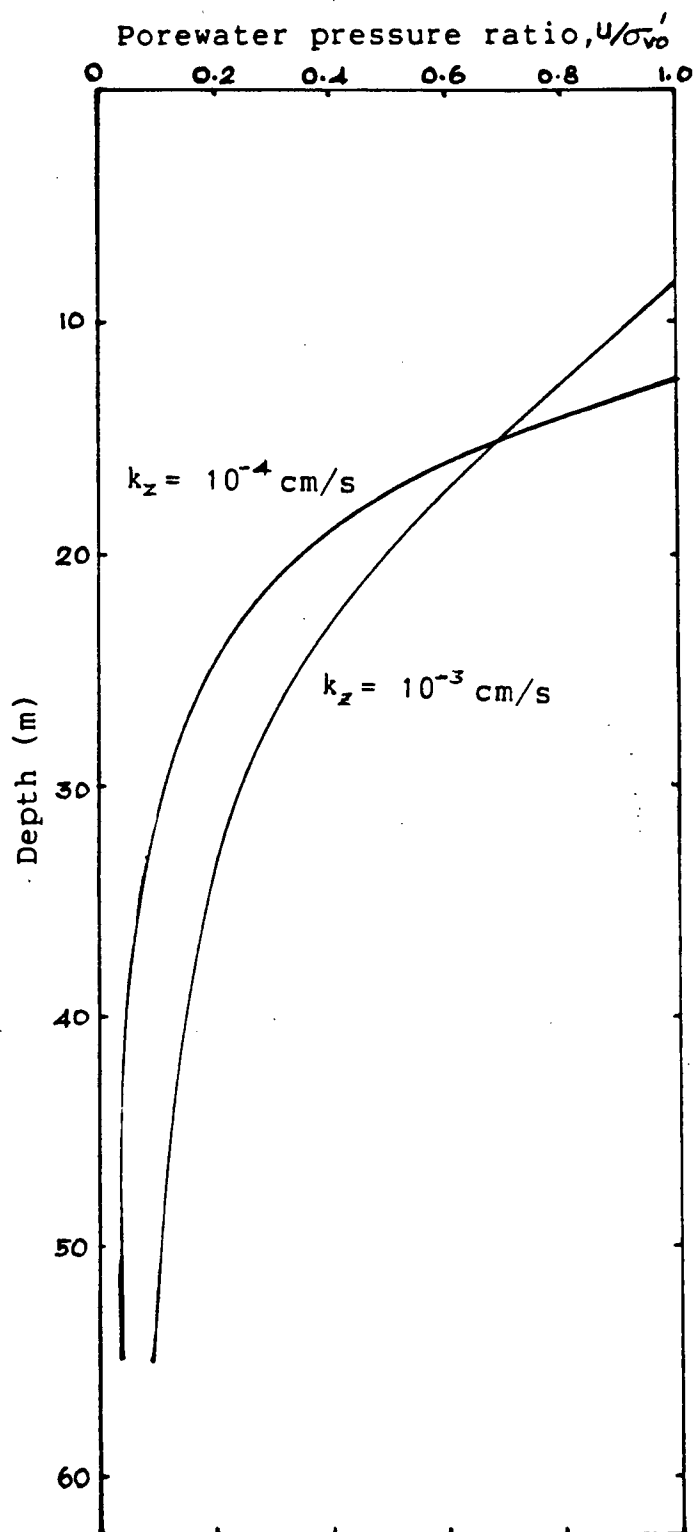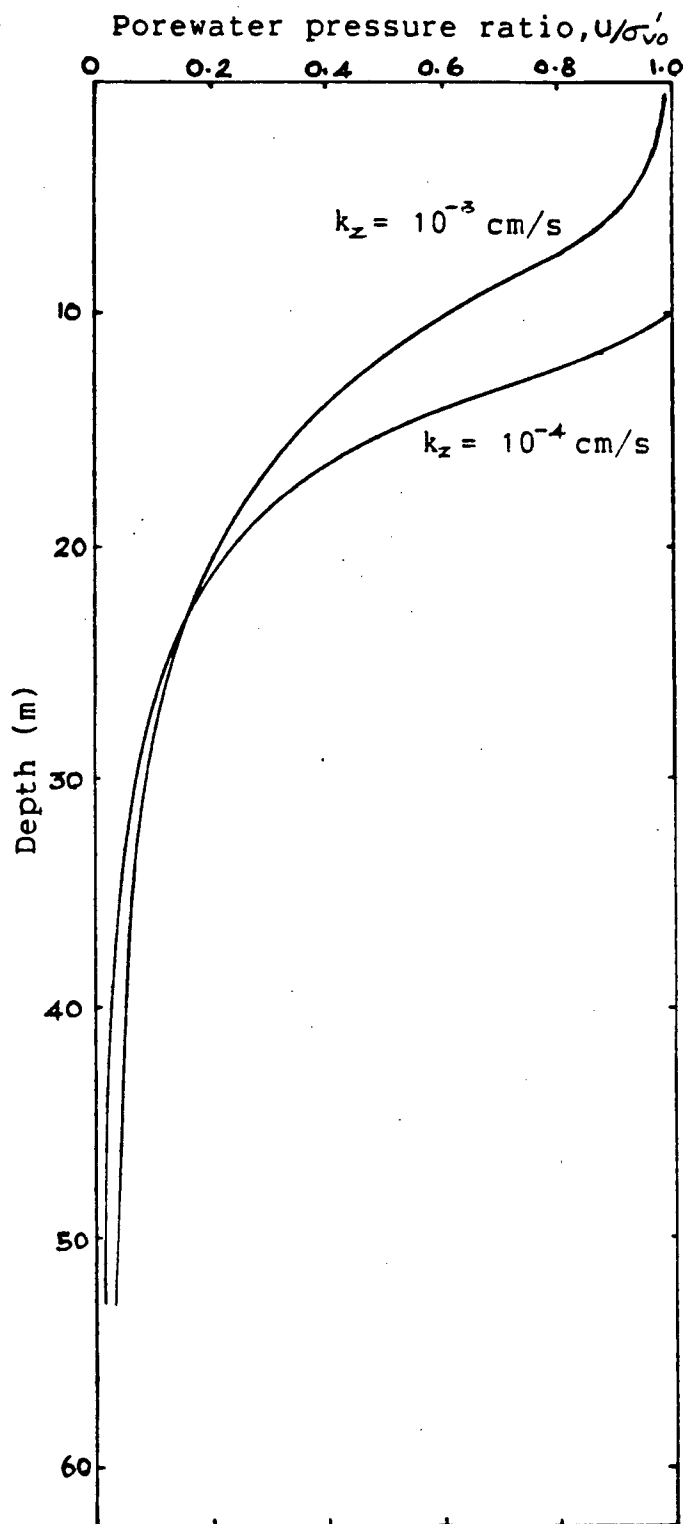Pressure Response At the end of
9m 6 hour Storm.

Figure 6.25; Section-VV; Residual Porewater

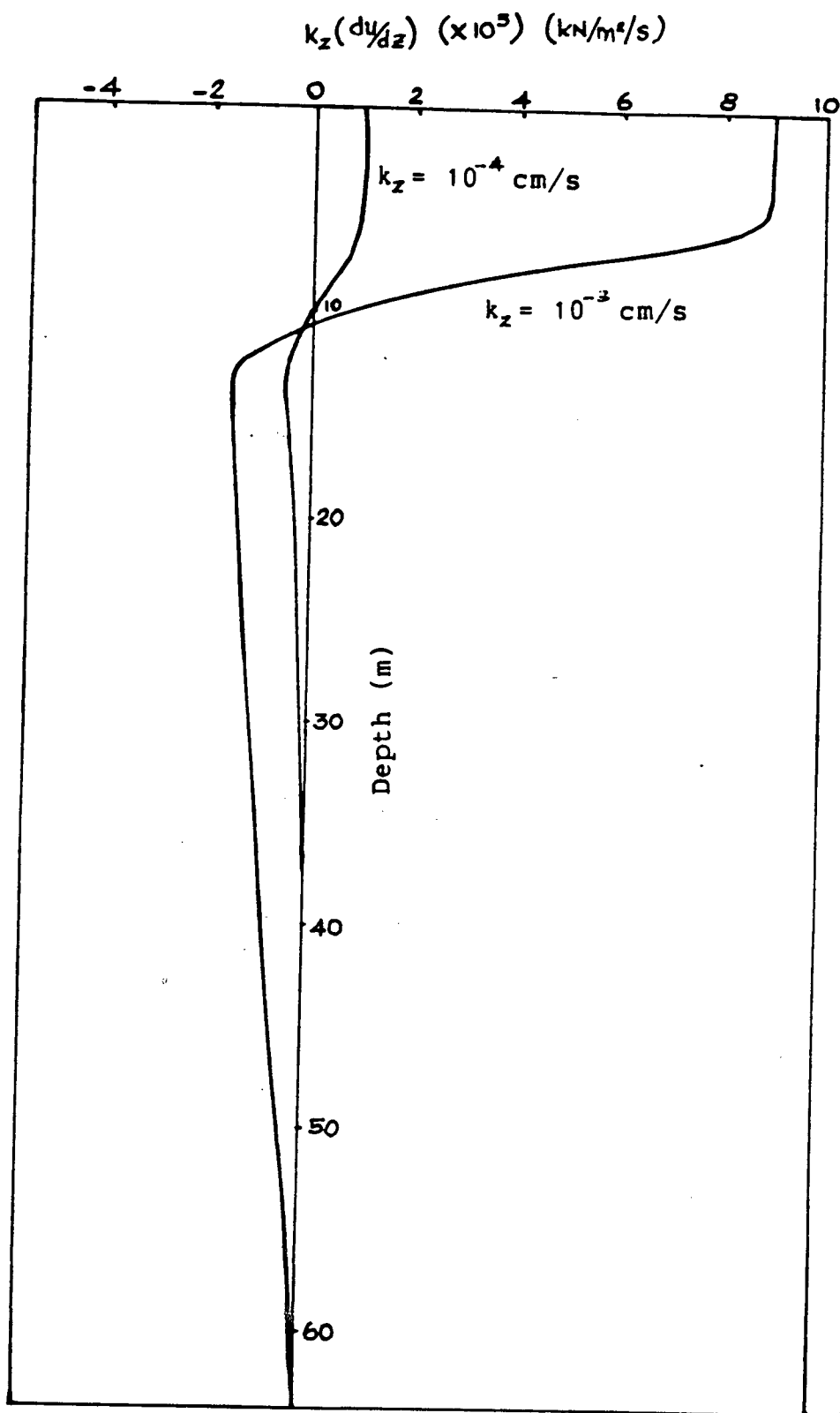Pressure Response At the end of

9m 6 hour Storm.

Figure 6.26; Section-QQ; Flow Through Interface
At the end of 9m 6 hour Storm.

to a certain depth, 10 to 11 m and beyound this depth there is substantial downward flow. It is also seen that in the case with $k_z = 10^{-3}$ cm/s, the flow through the top drainage boundary is much higher, as much as 10 times, than in the case with $k_z = 10^{-4}$ cm/s. However, in both cases, liquefaction occurs presumably because of the higher rate of porewater pressure generation in the top few metres. The depth of liquefaction is shallower in the case with $k_z = 10^{-3}$ cm/s because of higher drainage through the top boundary.

At lower elevations, the difference in the rate of porewater pressure generation for the two values of k_z are marginal because of the fact that N_L remains the same as a result of very low τ/σ'_{vo} values. Hence, the only factor that could influence the porewater pressure response, especially under the circumstance that the effect of the top drainage boundary is not felt effectively at depths, is the difference in diffusion of porewater pressure within the profile. Figure 6.26 clearly indicates that the downward flow at lower elevations is higher in the case with $k_z = 10^{-3}$ cm/s than with $k_z = 10^{-4}$ cm/s. This is because of the higher C_v value associated with it. This increased downward diffusion and high porewater pressures at the top few metres make the porewater pressure higher at lower elevations with $k_z = 10^{-3}$ cm/s.

The maximum porewater pressure response at sections of island 2 at the end of the specified storm is summarized in Table 6.4 for the two values of k_z considered. The results are plotted in Figure 6.27. The porewater pressure response shows

Section	Water depth (m)	(d/H_s)	Maximum pwp Response	
			Liquefaction depth (m)	
			$k_z = 10^{-3}$ cm/s	$k_z = 10^{-4}$ cm/s
PP	6	0.67	0.0	7.0
QQ	8	0.89	6.0	9.0
RR	10	1.11	8.0	11.5
SS	12	1.33	10.5	12.5
TT	14	1.55	11.0	13.5
UU	16	1.78	9.0	12.0
VV	18	2.00	2.0	8.5

Table 6.4; Maximum Porewater Pressure Response At Sections of Island 2 At the End of the 9m 6 hour Storm
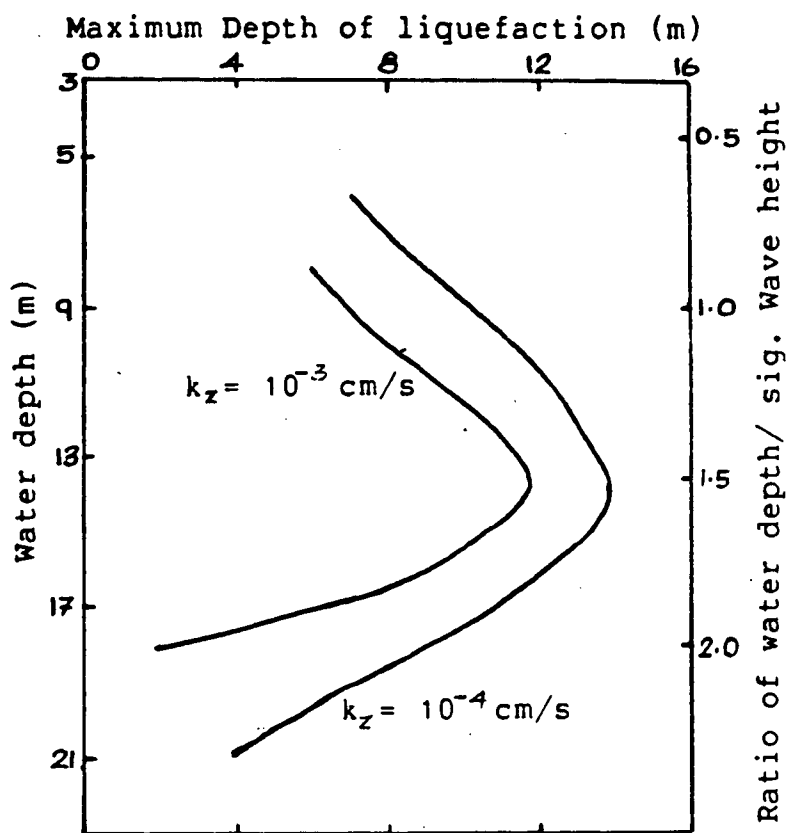
Figure 6.27; Maximum Porewater Pressure Response of Island 2
At the end of 9m 6 hour Storm.

the same kind of trend as before; that is, the response for both cases increases with depth of water until a critical depth is reached and then decreases beyound that depth. The crticical location in this case is around section TT and the critical water depth in terms of the significant wave height of the storm is approximately given by 1.50 H_S. It is also found that, within the limits of data, the location is unique and is not dependent on the drainage characteristics of the berm material. This agrees very well with the results obtained in the analyses involving island 1.

It can be inferred from Figure 6.27 that the depth of water beyound which liquefaction would not occur for the specified storm, depends on the drainage characteristics of the berm material. For the case with k_Z = 10^{-3} cm/s, the depth in terms of significant wave height is 2.10 H_S. It would appear that in the case of k_Z = 10^{-4} cm/s, this depth is increased considerably, as high as to 2.55 H_S. This would mean that liquefaction is possible even at the bottom most section of island 2, as the maximum depth of island 2 is 2.34 H_S.

Additional analyses conducted at section TT of island 2, the closest section to critical location for the 9m, 6 hour storm, reveal that the permeabilities required to limit porewater pressure ratio to 95 to 100% and 65% or less, are 2 x 10^{-3} cm/s and 3 x 10^{-3} cm/s respectively.

6.5 Wave Induced Porewater Pressure Response of Island 3

The porewater pressure response at selected sections HH to NN of island 3 at the end of the specified 12m, 6 hour storm for the two different k_z values of 10^{-3} cm/s and 10^{-4} cm/s are presented in Figure 6.28 to 6.34.

It is observed that liquefaction occurs at all sections in the case with $k_z = 10^{-4}$ cm/s and only at sections II to MM in the case with $k_z = 10^{-3}$ cm/s. The zone of liquefaction predicted for $k_z = 10^{-3}$ cm/s is deeper than for $k_z = 10^{-3}$ cm/s. However, as in the case of analyses involving island 2, higher porewater pressures are predicted at depths below the zone of liquefaction for the case with $k_z = 10^{-3}$ cm/s than for $k_z = 10^{-4}$ cm/s. The explanation for this behaviour has been ·presented in section 6.4.

The maximum porewater pressure response at sections of island 3 at the end of the specified storm for both values of k_z are given in Table 6.5 and the results are plotted in Figure 6.35.

From this figure, it is apparent that the effect of the storm is felt severely at a critical location, where the water depth in terms of the significant wave height is approximately given by 1.50 H_s, regardless of the k_z value. These results agree with the similar results obtained from analyses of islands 1 and 2.

Figure 6.35 suggests that the depth of water beyond which liquefaction would not occur for the k_z values of 10^{-3} cm/s and 10^{-4} cm/s are 2.20 H_s and 2.50 H_s respectively.

Figure 6.28; Section-HH; Residual Porewater

Pressure Response At the end of
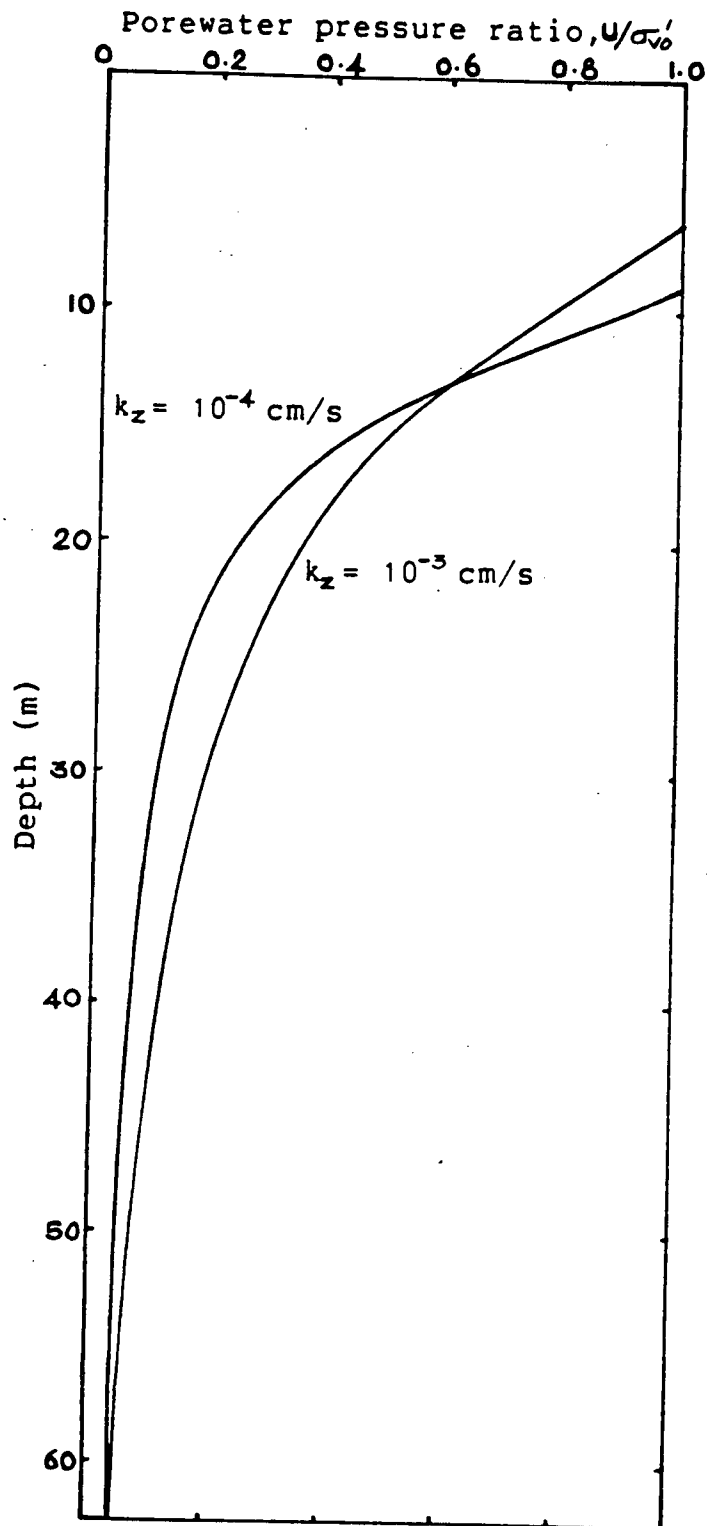
12m 6 hour Storm.

Figure 6.29; Section-II; Residual Porewater
Pressure Response At the end of
12m 6 hour Storm.
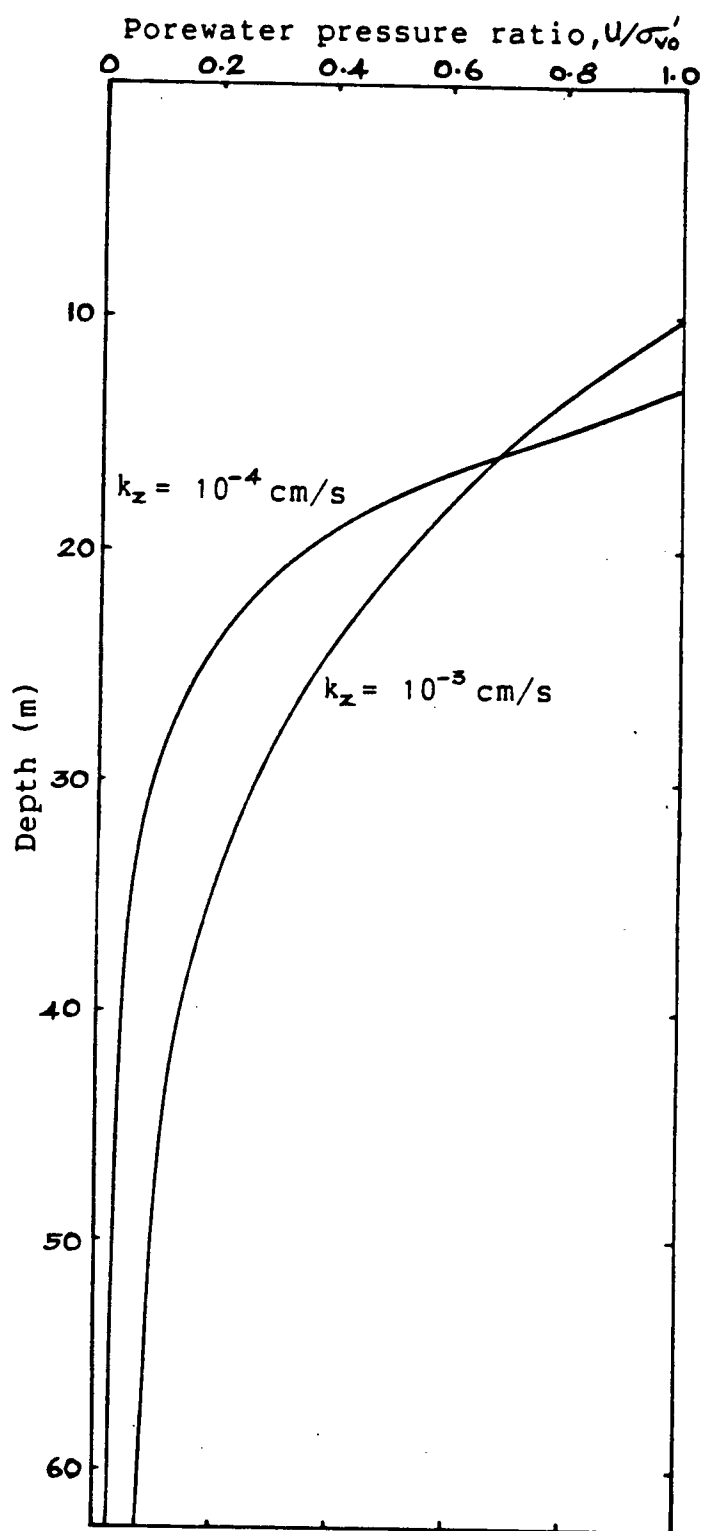
Figure 6.30; Section-JJ; Residual Porewater

Pressure Response At the end of
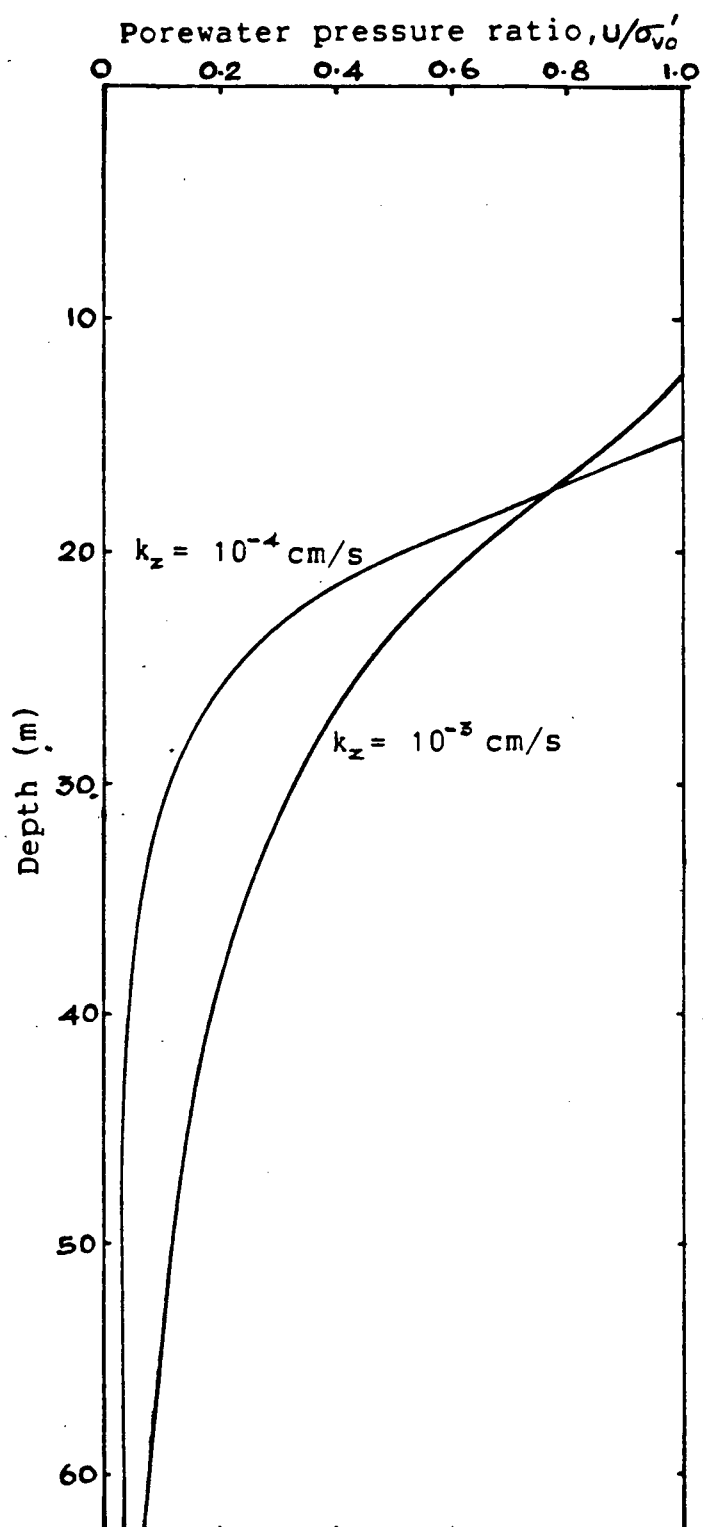
12m 6 hour Storm.

Figure 6.31; Section-KK; Residual Porewater
Pressure Response At the end of
12m 6 hour Storm.
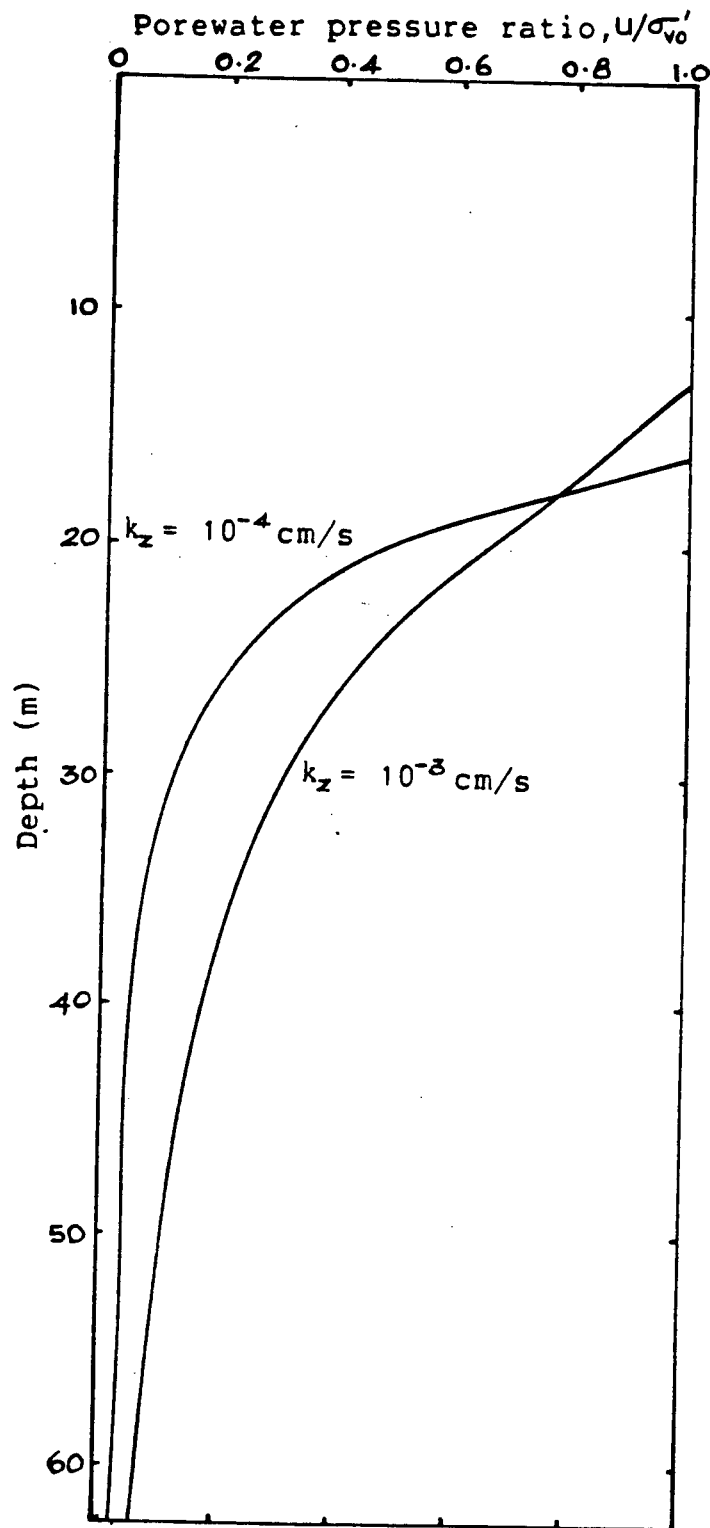
Figure 6.32; Section-LL; Residual Porewater
Pressure Response At the end of
12m 6 hour Storm.

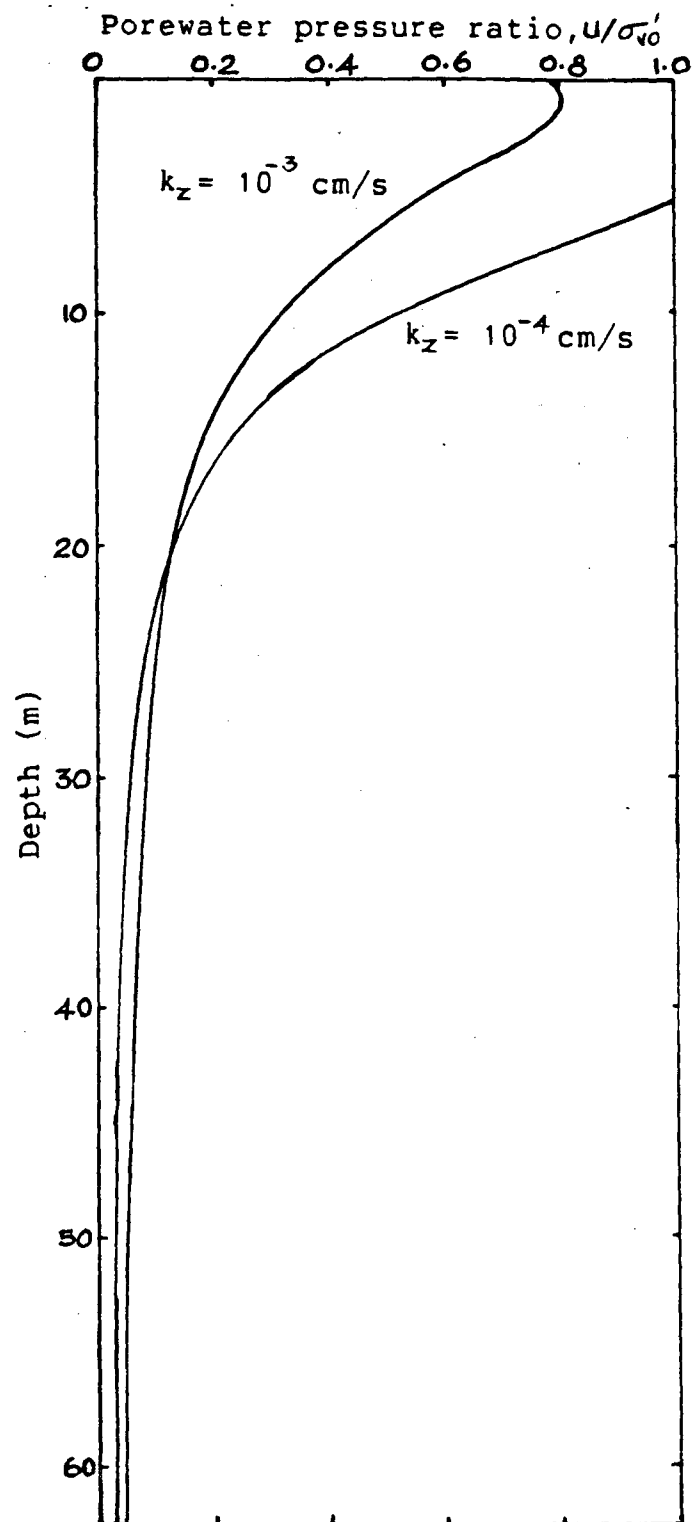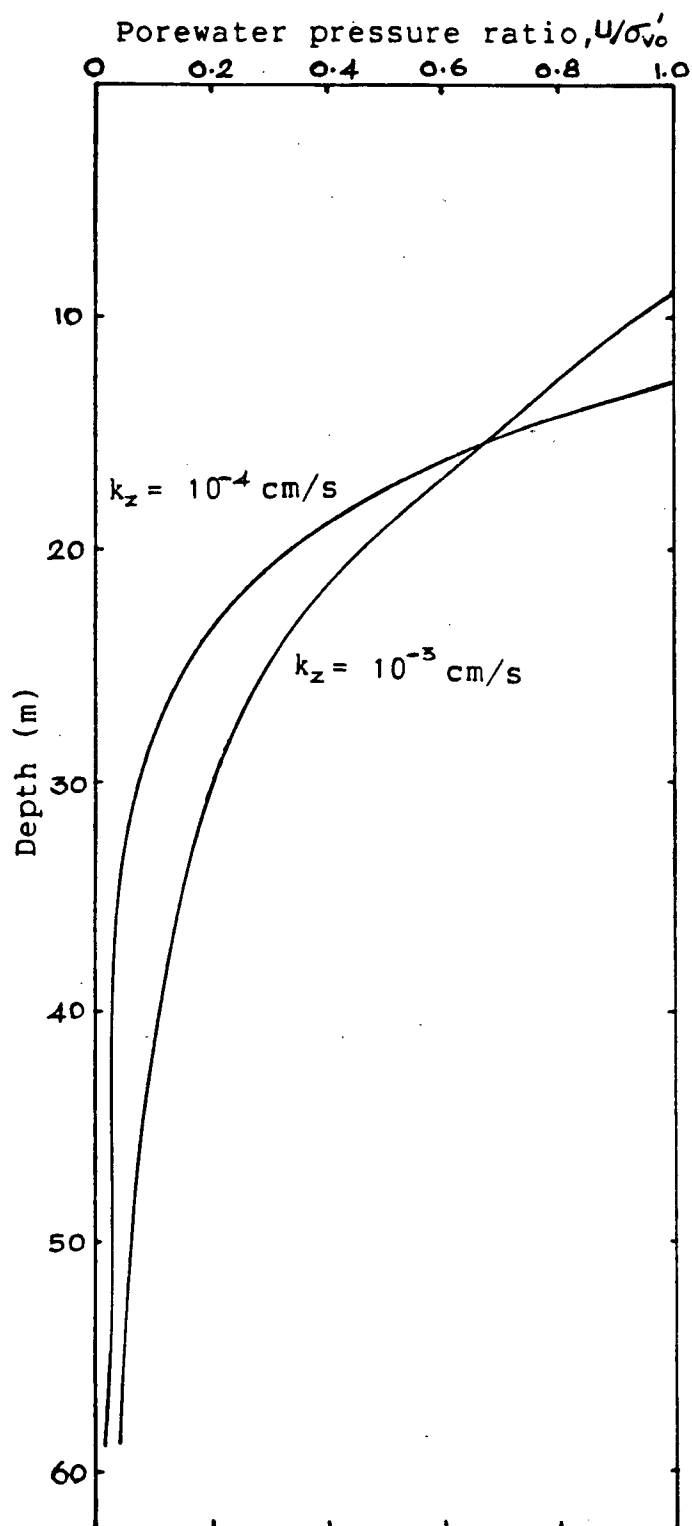Figure **6**.33; Section-MM; Residual Porewater
Pressure Response At the end of
12m 6 hour Storm.
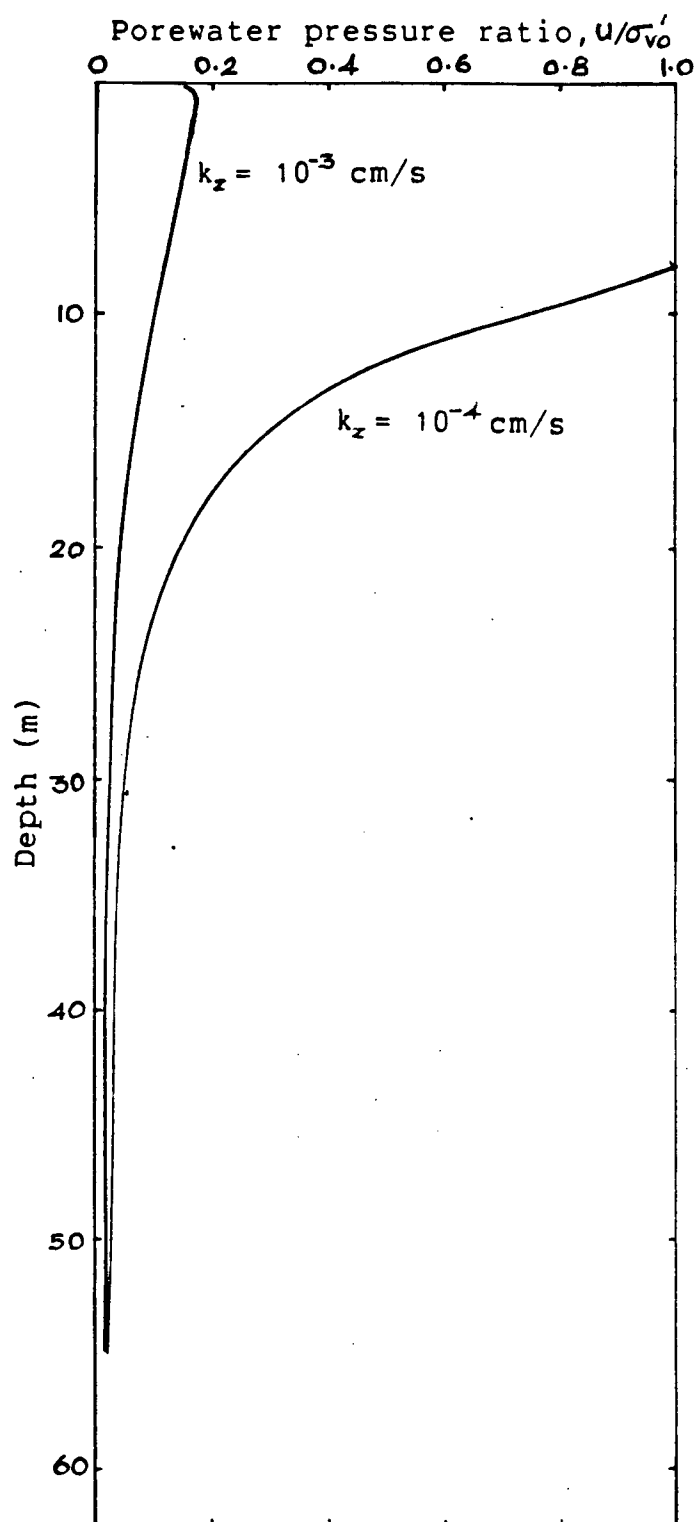
Figure 6.34; Section-NN; Residual Porewater
Pressure Response At the end of
12m 6 hour Storm.

Section	Water depth (m)	(d/H_s)	Maximum pwp Response	
			Liquefaction depth (m)	
			$k_z = 10^{-3}$ cm/s	$k_z = 10^{-4}$ cm/s
HH	6	0.50	0.0	5.0
II	10	0.83	6.0	9.0
JJ	14	1.17	9.0	13.0
KK	16	1.33	12.5	15.0
LL	18	1.50	13.0	16.0
MM	22	1.83	9.0	12.0
NN	26	2.17	0.0	6.5

Table 6.5; Maximum Porewater Pressure Response At Sections
of Island 3 At the End of the 12m 6 hour Storm
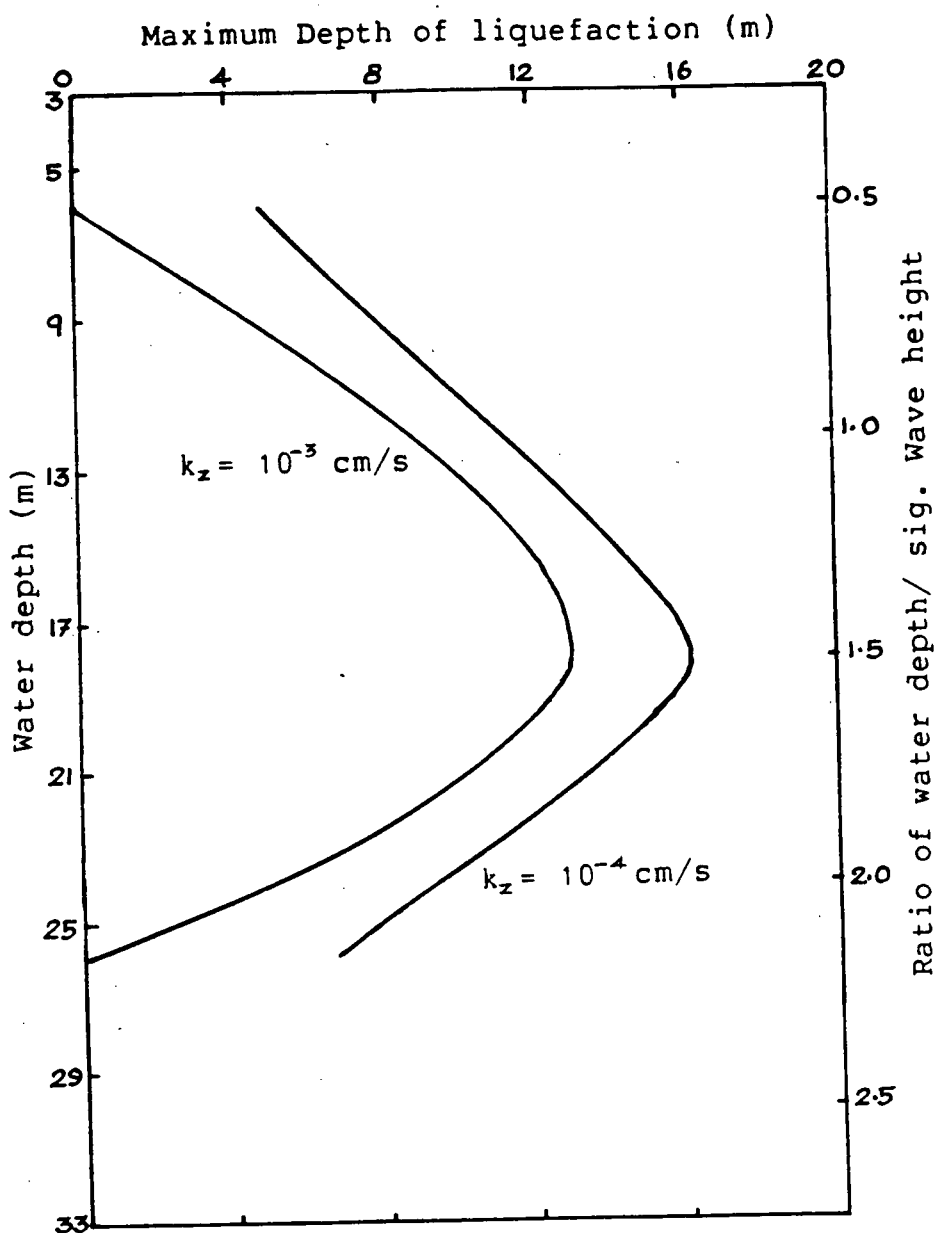
Figure **6**.35; Maximum Porewater Pressure Response of Island 3
At the end of 12m 6 hour Storm.

Additional analyses were conducted at section LL to establish the value of k_z required to prevent liquefaction within the island and also to limit porewater pressure ratio to 65% or less. The respective k_z values are found to be 2.5 x 10^{-3} cm/s and 4.0 x 10^{-3} cm/s.

6.6 Summary and Comparison of Results of Analyses
On Sand Foundation

Based on the results of the analyses involving three islands on sand foundations, the following conclusions and comments are made.

The porewater pressure response during and after the storm strongly depends on the storm characteristics, the drainage and compressibility characteristics of the berm material and the still water depth at sections of interest. Further, at a particular section, the porewater pressure response at a location depends on the depth of that location from the top island surface. As the depth increases, the porewater pressure ratio developed at any instant of time shows a steady decay similar to the distribution of wave induced cyclic stress ratio, τ/σ'_{vo} .

The effect of a storm is felt most strongly at a specific location, regardless of the drainage and compressibility . The water depth to this location is given by 1.50 times the significant wave height. This shows that within the range of data investigated, this critical location is unique for a specified storm and for a severe storm the critical location is

deeper than for a mild storm. For a given storm, the porewater pressure response increases with depth until the critical water depth and decreases beyound the critical water depth.

The permeabilities for a given initial compressibility or the initial co-efficient of consolidation, C_{vo}, required to limit the maximum porewater pressure ratio to a certain specified level depends on the significant wave height and duration of the storm. Table 6.6 shows the permeabilities and the corresponding initial values of the co-efficient of consolidation, required for different storms of duration 6 hours to limit maximum porewater pressure ratio within the islands analysed to just liquefaction (95 - 100%) and to 65%. It is evident from these results that the requirements become tougher as the storm becomes more severe.

As stated earlier, the factor that governs the rate of dissipation and thereby the net porewater pressure response is k_z/m_{vo} or the initial co-efficient of consolidation, C_{vo}, defined as $k/m_{vo} \gamma_w$. Thus, if analyses were to be carried out with combinations of k_z and m_{vo} values such that the ratio k_z/m_{vo} remains the same in each case, then the resulting porewater pressure response to a specified storm would be identical in each case. This principle can be applied to all analyses presented so far.

The predicted maximum depth of liquefaction, that is, the depth of liquefaction at the critical location of each island for the specified storms of duration 6 hours, for the two values of k_z are presented in Table 6.7, along with an estimate

Island	Storm	95-100% (u/σ_{vo}') Limit		65% (u/σ_{vo}') Limit	
No.	H_s (m)	k_z (cm/s)	C_{vo} (m^2/s)	k_z (cm/s)	C_{vo} (m^2/s)
1	4	2.5×10^{-4}	0.85×10^{-2}	3.5×10^{-4}	1.20×10^{-2}
1	6	8.0×10^{-4}	2.70×10^{-2}	1.0×10^{-3}	3.40×10^{-2}
2	9	2.0×10^{-5}	6.80×10^{-2}	3.0×10^{-3}	1.02×10^{-1}
3	12	2.5×10^{-3}	8.50×10^{-2}	4.0×10^{-3}	1.36×10^{-1}

Table 6·6; Drainage Characteristics Requirement To Limit
Porewater Pressure Ratio To Specified Levels For
Different Strorms of Duration 6 Hours.

| Island | Storm | Maximum Depth of Liquefaction (m) | | 'Undrained' |
| | | STAB-W3   Analysis | | |
No.	H_S (m)	$k_z = 10^{-3}$ cm/s	$k_z = 10^{-4}$ cm/s	Analysis
1	4	0.0	6.5	7.5
1	6	0.0	9.0	10.0
2	9	11.0	13.5	13.5
3	12	13.5	16.0	16.0

Table 6·7; Predicted Maximum Depth of Liquefaction At Critical
Locations Different Storms and Permeabilities
For Islands On Sand Foundations.

of depth of liquefaction from analyses assuming undrained conditions. It is interesting to note that for mild storm and higher k_z values, the error involved in estimating maximum depth of liquefaction assuming undrained conditions is high. It is quite possible in some instances that 'undrained' analyses may predict depth of liquefaction to be several metres, whereas analyses incorporating dissipation effects, such as STABW and STABW3 analyses, would predict no liquefaction at all.

The classic example for such a case is the analysis involving 4m, 6 hour storm. It is clearly seen from the results in Table 6.7, that 'undrained' analysis predicted liquefaction at critical section to be as much as to 7m, but STABW3 analyses predicted only 6m for the case with k_z = 10^{-4} cm/s and no liquefaction for the case with k_z = 10^{-3} cm/s. The above example clearly shows the significance of incorporating dissipation effects to avoid unduly conservative estimates of depth of liquefaction during wave loading.

The results also suggest that in cases of severe storms and lower k_z values, such as k_z < 10^{-4} cm/s, the islands are practically undrained in the analyses and the estimates based on 'undrained' analyses and STABW3 analyses are the same. However, for locations other than the critical location, even for low permeabilities, there may be significant errors involved, if the depth of liquefaction is predicted assuming undrained conditions.

If the wave pattern and the drainage characteristics are such that liquefaction occurs at the critical location, then

the depth of water beyound which liquefaction would not occur, is dependent on the drainage characteristics and the wave pattern itself. The results with $k_z = 10^{-4}$ cm/s indicate that the best estimate of the above depth for the 6 hour storm, in terms of the significant wave height is 2.50 H_S. The best estimate of the above depth for the case with $k_z = 10^{-3}$ cm/s is 2.20 H_S. However, these estimates are based on such a limited number of analyses that they should be viewed with caution.

Finally, the results of analyses conducted on islands on sand foundations, indicate liquefaction or high levels of porewater pressures are possible for drainage characteristics of sand generally encountered in practice during moderate wave conditions of practically feasible duration. Thus, it is important to resort to some kind of remedial measures that would bring down the wave induced porewater pressures to acceptable levels. One of the popular and efficient means of suppressing liquefaction potential is to provide coarse, relatively free draining material on top of the island surface, where the island is susceptible to liquefaction. The effect of such measures is examined in the next chapter.

CHAPTER 7

EFFECT OF ROCKFILL COVER ON WAVE INDUCED POREWATER PRESSURES

7.1 Introduction

One of the practical remedial measures to bring down the wave induced porewater pressure to acceptable levels is to provide coarse cover on top of the island surface. This chapter examines the effect of rockfill in reducing the wave induced porewater pressures. The choose of rockfill as a suitable cover has the advantages that it not only reduces the wave induced porewater pressures significantly but also stays intact without being eroded heavily.

For analyses involving cover, the permeability and the thickness of the rockfill cover are taken as 10 cm/s and 1m respectively. Within the limited range of data investigated, the results from the previous chapter suggest that in cases of possible liquefaction, the cover has to be extended to water depths beyond 2.50 H_s in the case with $k_z = 10^{-4}$ cm/s and 2.20 H_s in the case with $k_z = 10^{-3}$ cm/s.

7.2 Effect of Cover on Porewater Pressure Response of
     Island 1 To 6m, 6 hour Storm

Figures 7.1 to 7.7 show the effect of 1m cover of a coarse material on the poreawter pressure response at sections from AA to GG of island 1 at the end of 6m, 6 hour storm for the two different permeabilities of the sand fill. It is

Figure 7.1; Section-AA; Effect of Cover on Porewater Pressure
Response At the end of 6m 6 hour Storm.

Figure 7.2 ; Section-BB; Effect of Cover on Porewater Pressure
Response At the end of 6m 6 hour Storm.

Figure 7.3 ; Section-CC; Effect of Cover on Porewater Pressure
Response At the end of 6m 6 hour Storm.

Figure 7.4; Section-DD; Effect of Cover on Porewater Pressure
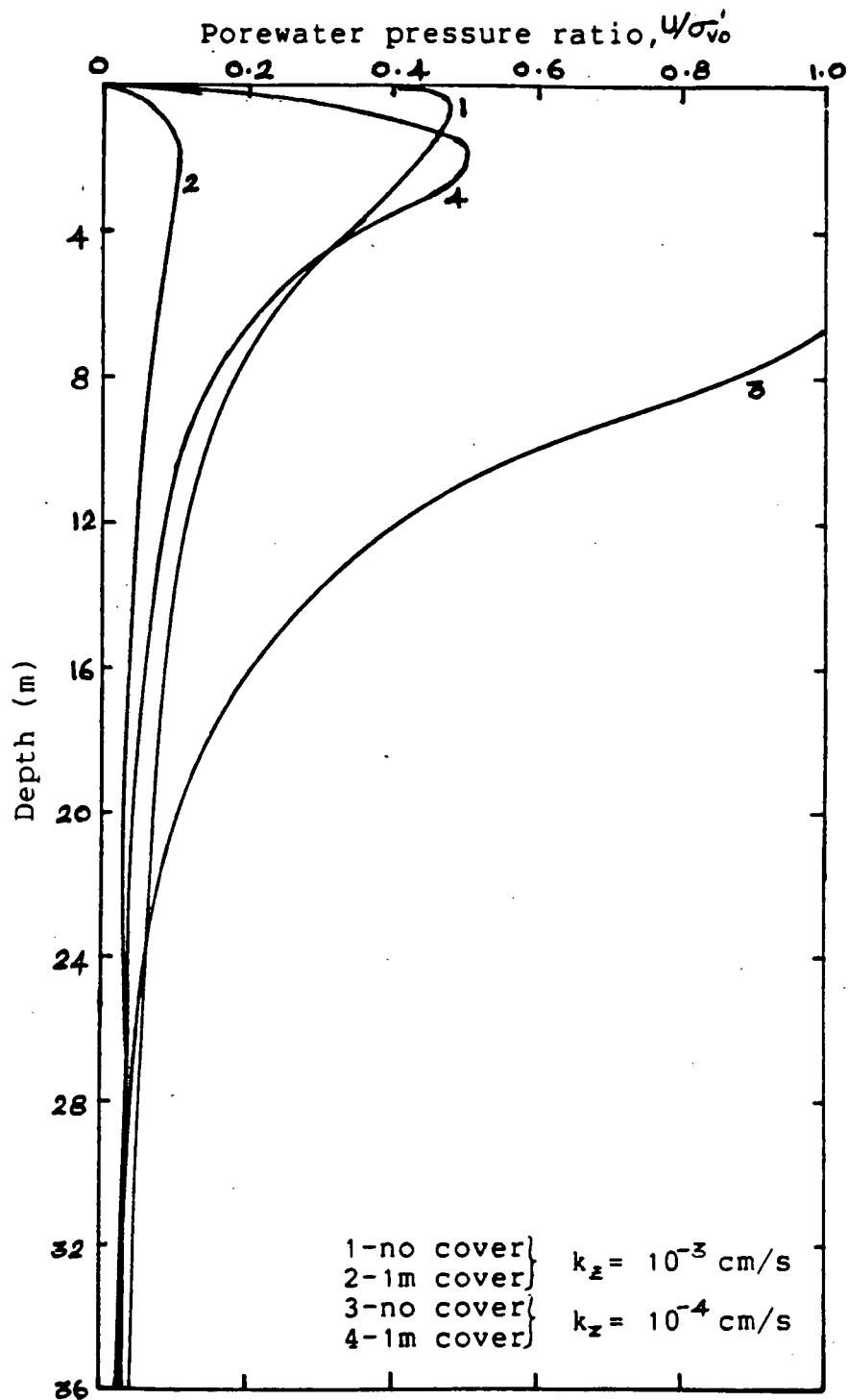Response At the end of 6m 6 hour Storm.

Figure 7.5; Section-EE; Effect of Cover on Porewater Pressure
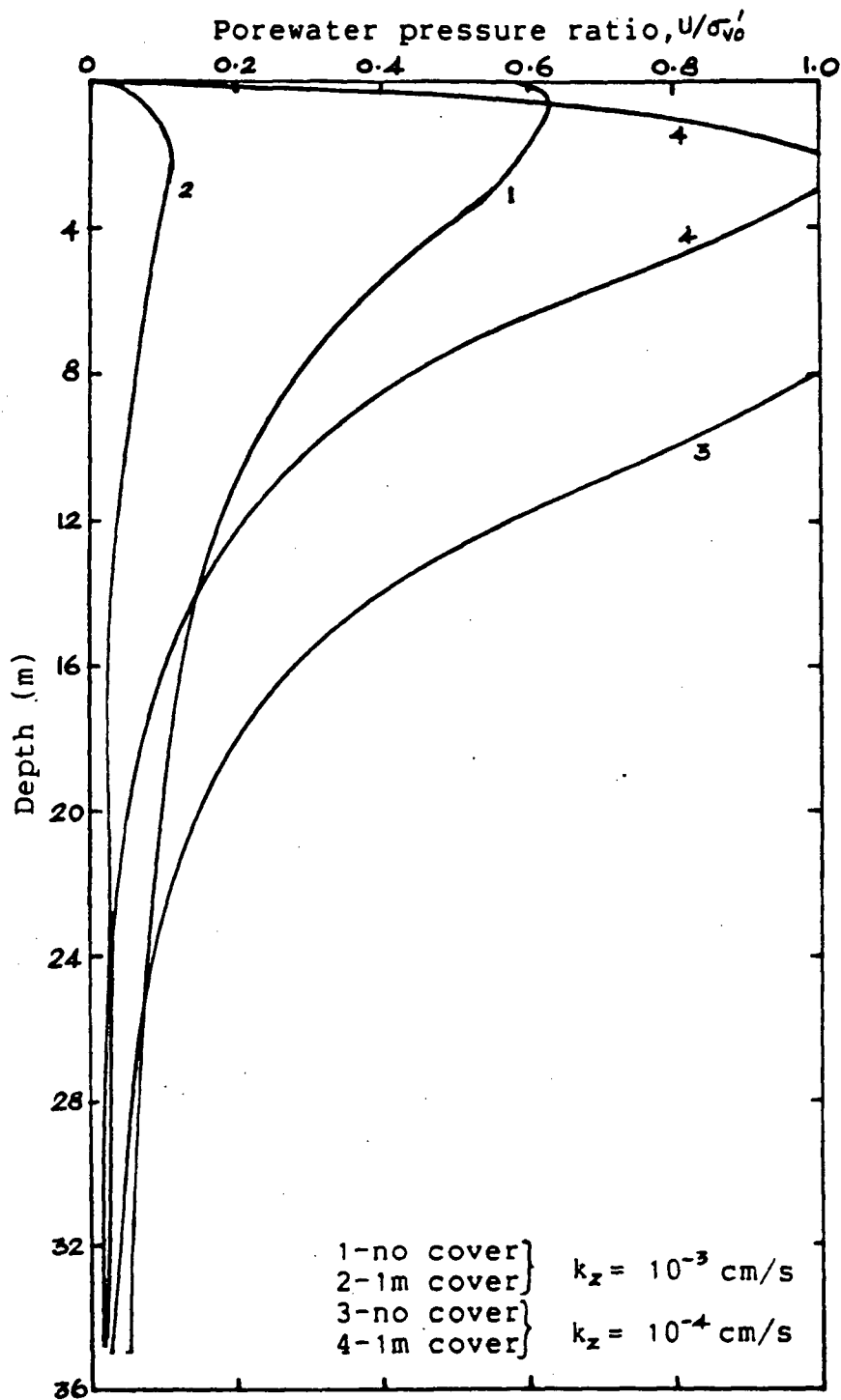Response At the end of 6m 6 hour Storm.

Figure 7.6 ; Section-FF; Effect of Cover on Porewater Pressure
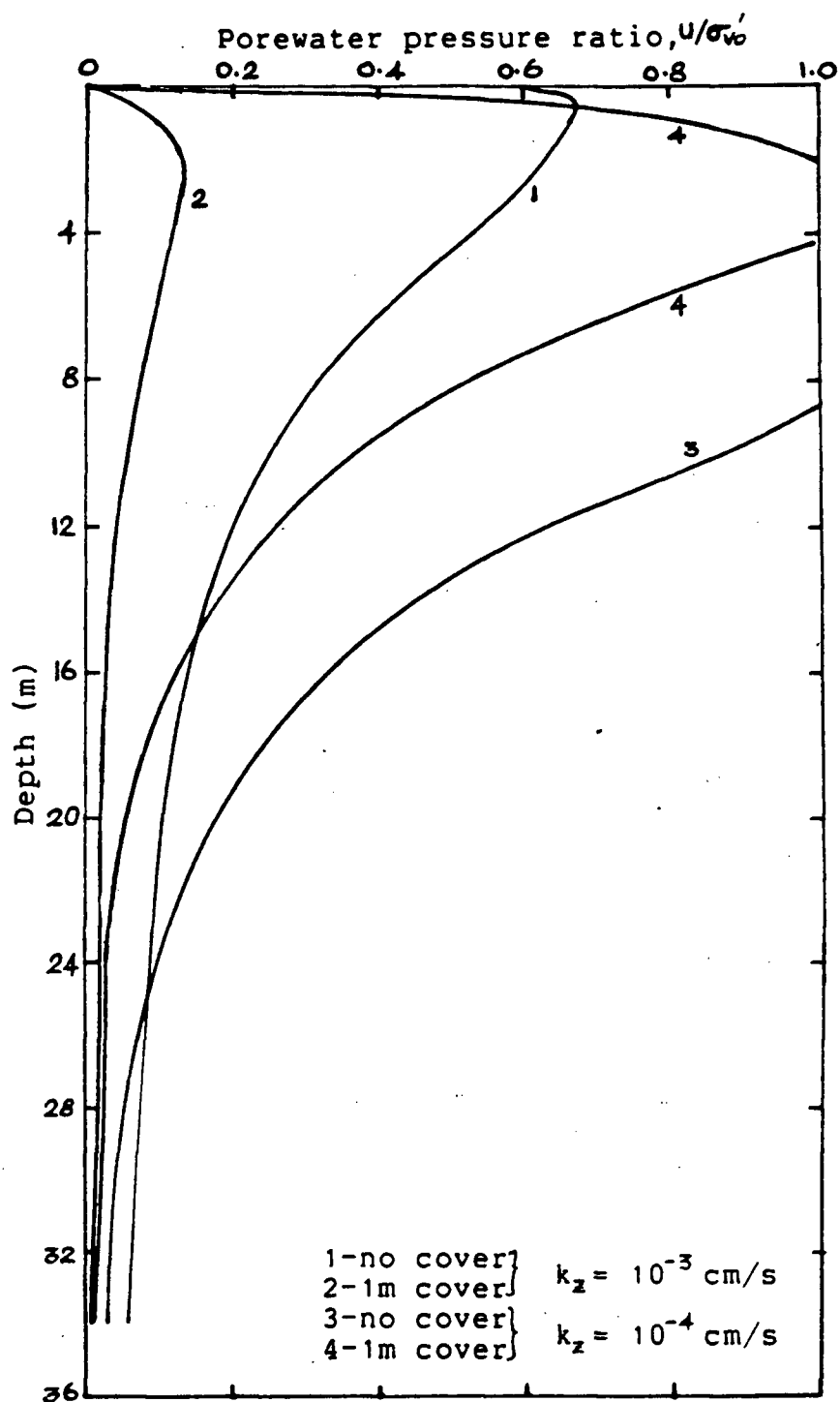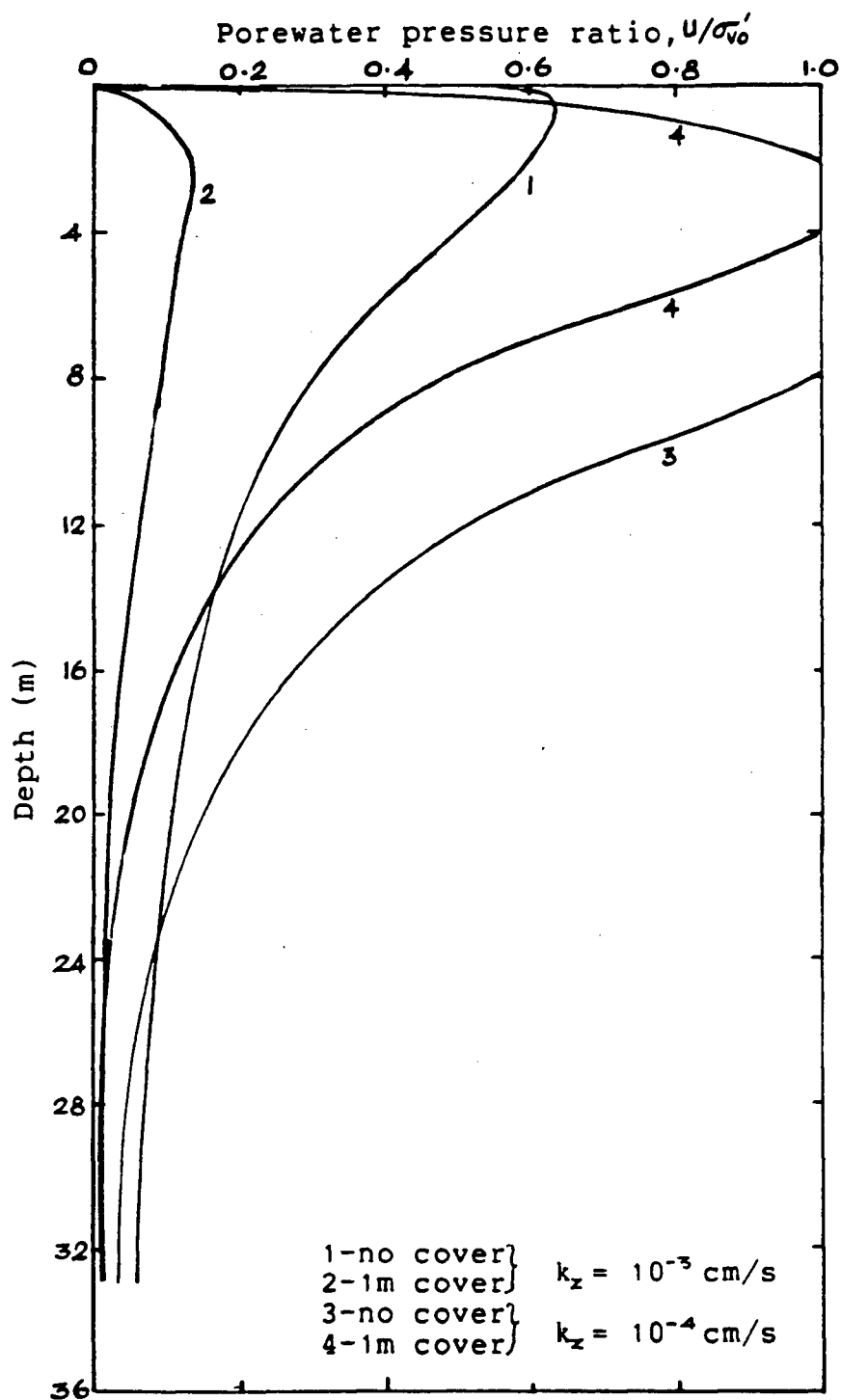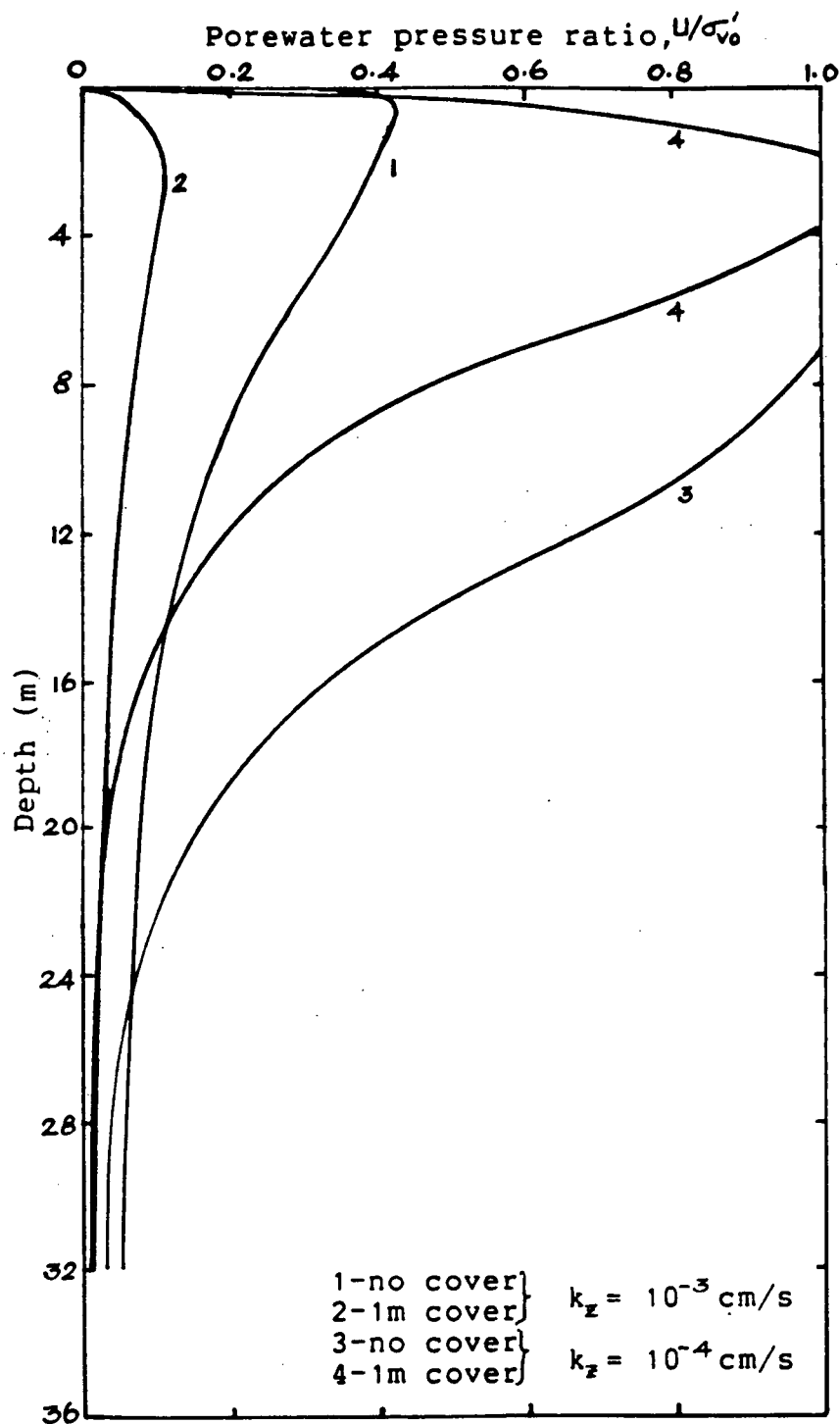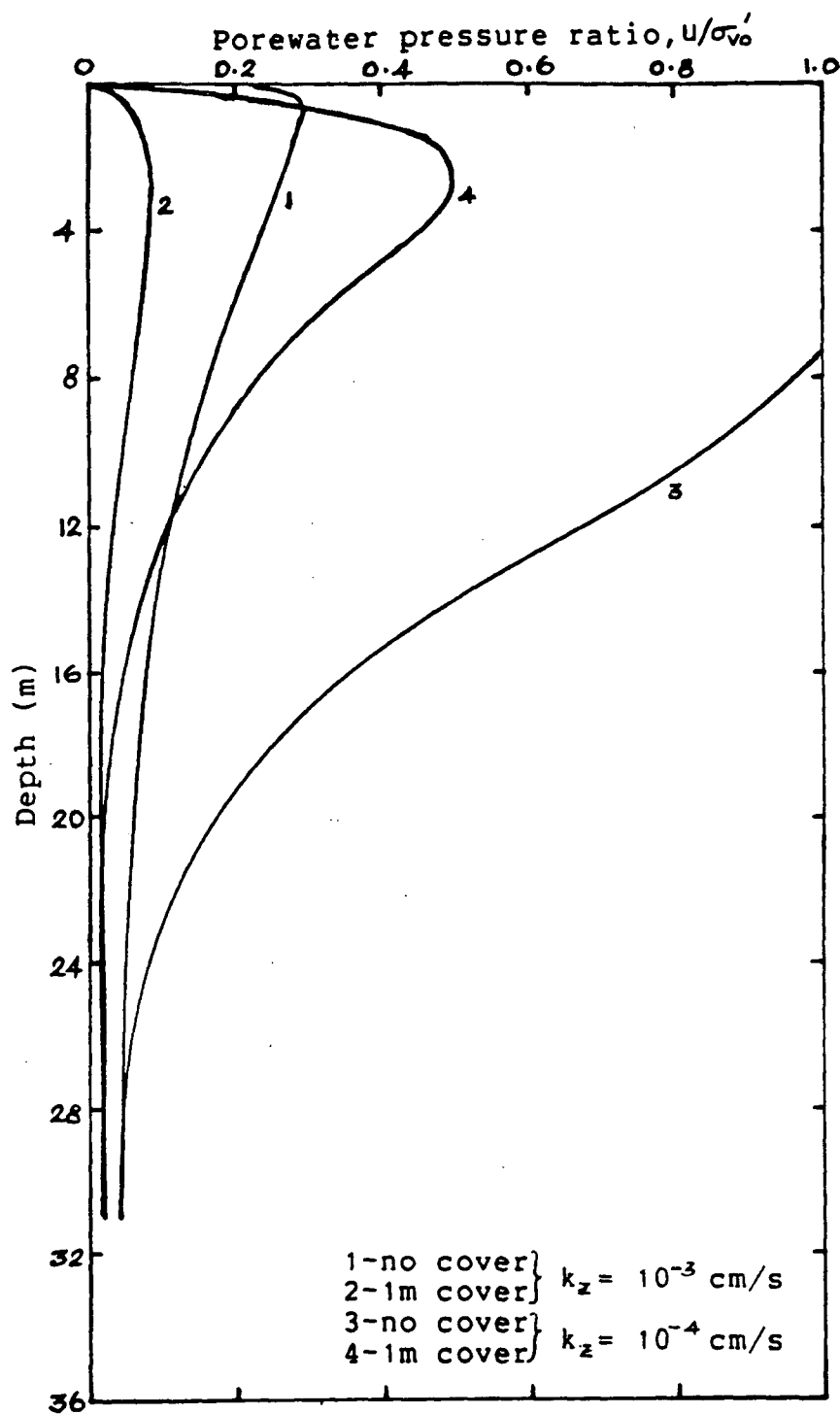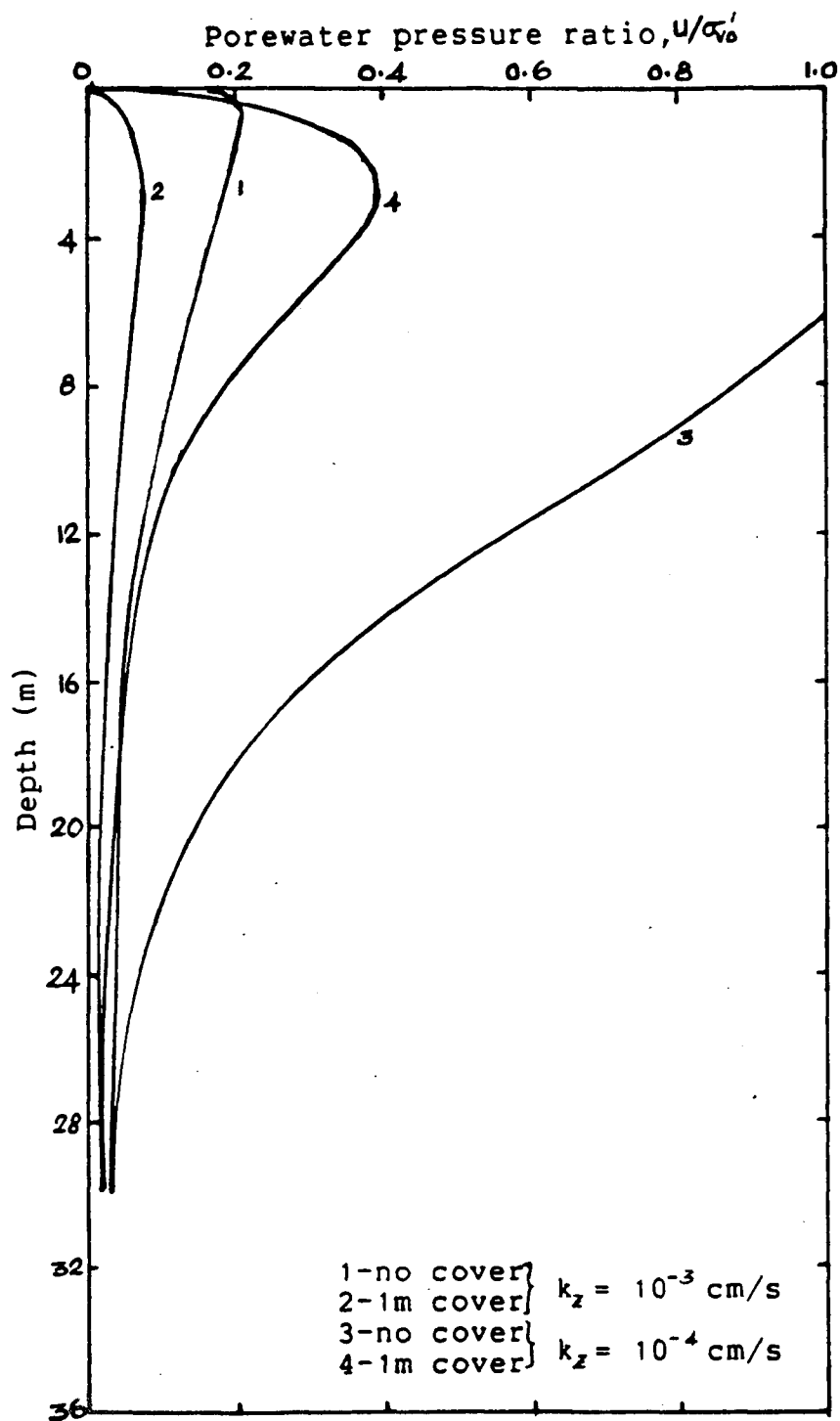Response At the end of 6m 6 hour Storm.

Figure 7.7 ; Section-GG; Effect of Cover on Porewater Pressure
Response At the end of 6m 6 hour Storm.

evident from these figures that the effect of the coarse cover is to reduce the porewater pressure response significantly and in some cases to negligible levels.

Unlike the porewater pressure response without the cover, the response with cover shows that the maximum porewater pressure ratio occurs not at the top, but at some depth from the top of the original island surface and thereafter shows a steady decay. The reduction in porewater pressures at the top few metres is apparently due to the influence of the free draining non-liquefiable cover at top.

It is also seen that the porewater pressure response at the end of the storm is much higher for the case with $k_z = 10^{-4}$ cm/s than with $k_z = 10^{-3}$ cm/s. This is as expected because for the same depth of cover , the porewater pressure response with $k_z = 10^{-3}$ cm/s has to be less because of the more pervious nature of the soil. This also makes it clear that the resulting response for the same depth of cover, depends on the drainage characteristics of the sand fill; the greater the permeability of sand fill, the smaller the maximum porewater pressure response will be.

At section AA, for the case with $k_z = 10^{-4}$ cm/s, analysis shows that with 1m coarse cover the maximum porewater pressure ratio developed at the end of the storm is 51%. In contrast,analysis shows that without 1m coarse cover there would be liquefaction up to a depth 6.5m. In the case with $k_z = 10^{-3}$ cm/s, analyses with and without the cover show that the maximum porewater pressure ratio developed at the end of the

storm are 11% and 47% respectively.

Section CC is of interest, because it is closest to the critical section for the 6m, 6 hour storm. The results of the analysis with 1m cover for the case with k_z = 10^{-4} cm/s indicate that liquefaction is limited to a zone of 1m extent between the depth 2m and 3m, while without cover, soil would liquefy up to a depth of 9m. In the case with k_z = 10^{-3} cm/s, the maximum porewater pressure ratio predicted from analyses with and without cover are 14% and 67% respectively. Similar reductions in porewater pressure response are apparent at all other sections of island 1.

The quantitative comparison of the maximum porewater pressure response at the end of the 6m, 6 hour storm from analyses with and without the 1m top coarse cover for the two values of k_z are summarized in Table 7.1. In the event of liquefaction, that is, porewater pressure ratio of 100%, the figures in brackets indicate the predicted depth of liquefaction.

Results in Table 7.1 show that the suppression in the porewater pressure response is very significant and for the range of permeability above 10^{-3} cm/s, 1m coarse cover is sufficient to bring down the porewater pressures to negligible levels. In direct contrast to this, in the case of k_z=10^{-4} cm/s, the 1m top coarse cover is insufficient to suppress liquefaction at section BB to EE. In these cases, the thickness of the cover has to be increased sufficiently to bring down the wave induced porewater pressure to levels considered to be

Section	Maximum Porewater Pressure Ratio, U/σ'_{vo}, (%)			
	$k_z = 10^{-3}$ cm/s		$k_z = 10^{-4}$ cm/s	
	No Cover	1m Cover	No Cover	1m Cover
AA	47	11	100(6.5)	51
BB	62	12	100(8.0)	100(1.0)
CC	67	14	100(9.0)	100(2.0)
DD	65	14	100(8.5)	100(2.0)
EE	43	13	100(7.0)	100(1.5)
FF	29	9	100(6.5)	50
GG	22	8	100(6.0)	40

Table 7·1; Effect Of Cover On Maximum Porewater Pressure Response At Sections Of Island 1 At the End Of 6m 6 hour Storm.

Note; Figures in brackets indicate the extent of the zone of liquefaction in metres.

safe.

The reduction in porewater pressure response in the case of analyses with coarse cover, may be attributed to the following reasons;

Firstly, the presence of pervious and non-liquefiable cover reduces the build up of the porewater pressure because of the easy drainage at the top. Secondly, the cover reduces the water depth and consequently the wave composition of the storm changes due to the breaking of higher waves. The changes in the wave composition alters the shear stress distribution with depth and in turn, the initial values of N_L required for the estimation of porewater pressure generation, as in equation (3-12), increase. This increase would result in a slower rate of porewater pressure generation. The reduced rate of porewater pressure generation coupled with the increased dissipation effects give rise to the reduced residual porewater pressure responses.

Figure 7.8 clearly illustrates the effect of coarse cover on the rate of residual porewater pressure build up during the 6m, 6 hour storm as compared to the rate of build up without the cover at a depth 3m below the orinigal top surface at section CC. It can be seen from Figure 7.8 that in both cases of k_z values, the rate of porewater pressure build up during the storm activity is reduced considerably in the cases with the coarse cover on top. The reduction is much more apparent in the case with $k_z = 10^{-3}$ cm/s than with $k_z = 10^{-4}$ cm/s.
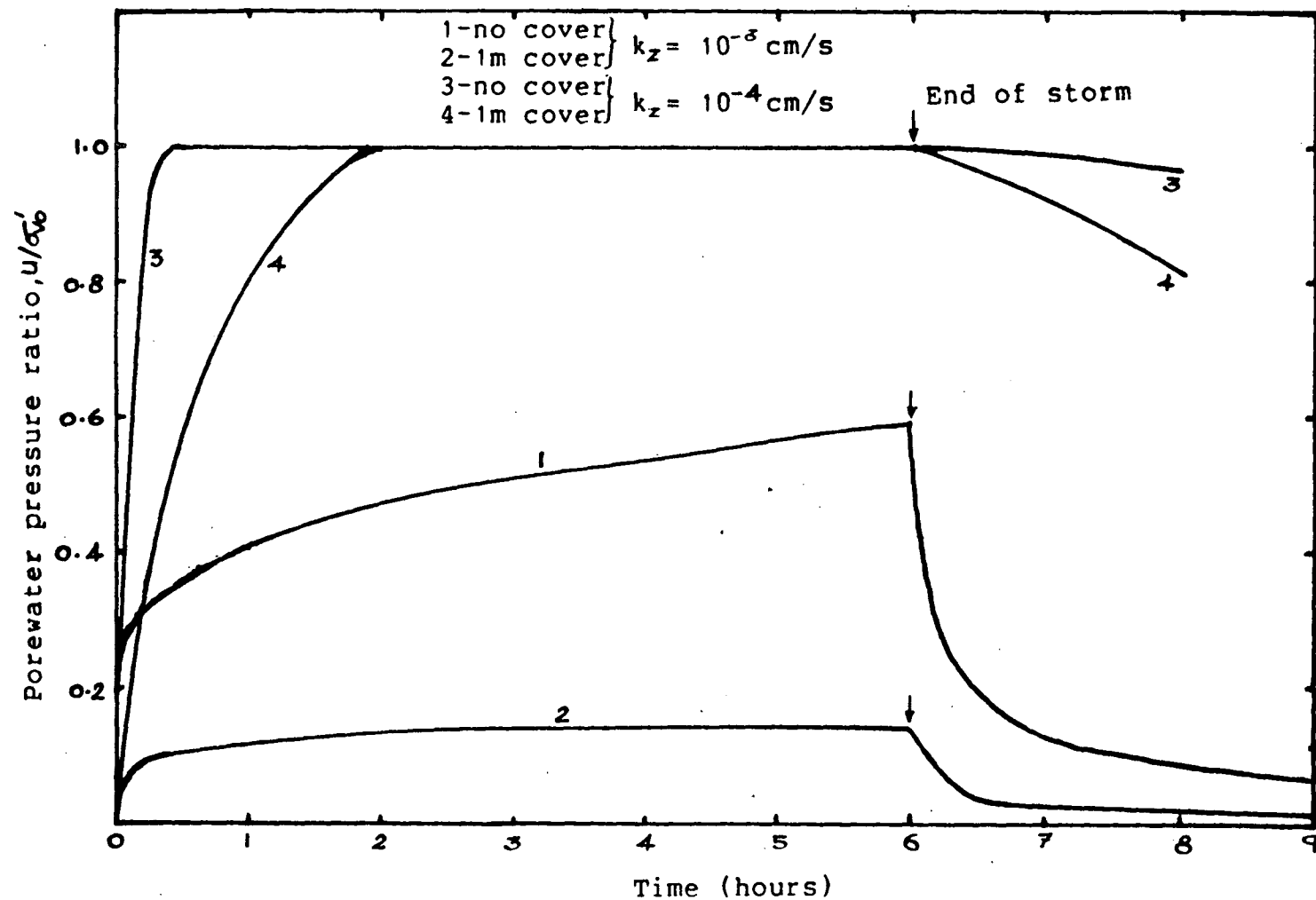
Figure 7·8 ; Effect of Cover on Time History Of Pore Pressure

At 3m Below Original Island Surface At Section CC.

7.2.1 <u>Effect Of Permeability Of Cover Material</u>

Figure 7.9 shows the influence of the permeability of the cover material on the induced porewater pressure response at section AA of island 1 at the end of the 6m, 6 hour storm. It is clearly seen that there is no difference in the response when the permeability of the cover is increased from 10 cm/s to 100 cm/s. Hence it appears that the use of highly pervious materials as cover does not seem to produce any further reductions in the porewater pressure response and the efficient way to reduce porewater pressures to desired levels is to resort to the use of cover with an increased thickness.

Figure 7.9 ; Section-AA; Effect of Cover Permeability on
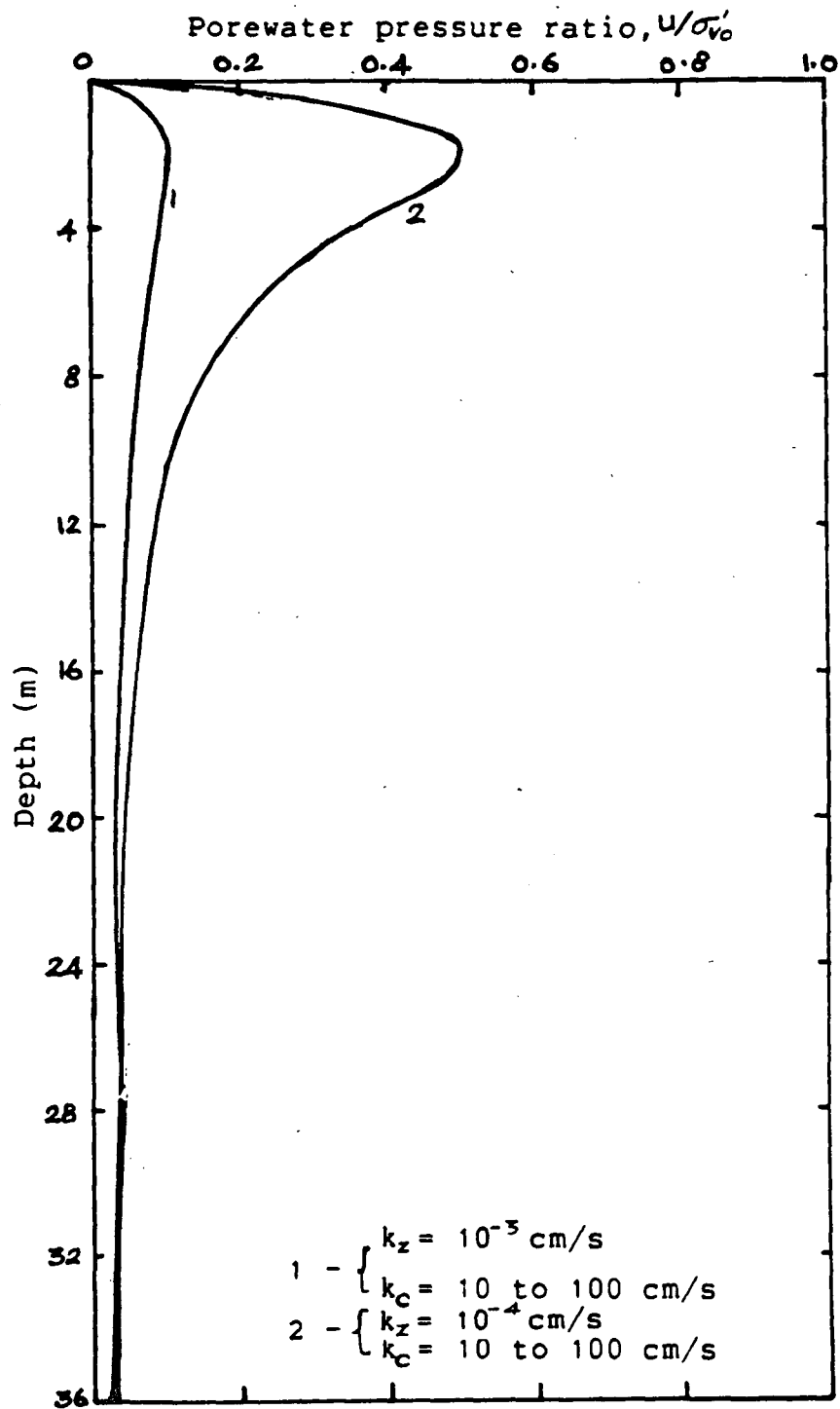
Porewater Pressure Response At the End of

the 6m 6 hour Storm.

7.3 Effect of Cover on Porewater Pressure Response of Island 1 to 4m, 6 hour Storm

Figures 7.10 to 7.12 show the effect of 1m top coarse cover on the porewater pressure response at sections AA, CC and DD of island 1 at the end of 4m, 6 hour storm. The results show that the predicted reductions in porewater pressure response with 1m coarse cover are very significant. For example, at section AA, the critical section for the 4m, 6 hour storm, for k_z = 10^{-4} cm/s, the results from the analysis with the cover shows that maximum porewater pressure ratio developed at the end of the storm is 36%, while analysis without cover shows that there would be liquefaction to a depth of 6.5m.

At the other sections, the resulting porewater pressure response with the 1m cover are negligible for both the cases of permeability.

Table 7.2 compares maximum porewater pressure response with and without the 1m of coarse cover at the end of the 4m, 6 hour storm at sections AA, CC and DD of island 1.

The results suggest that the 1m of coarse cover is sufficient to bring down porewater pressures to safe levels for the range of permeability greater than 10^{-4} cm/s during the 4m, 6 hour storm. In the case of k_z = 10^{-3} cm/s, the need for the coarse cover protection to reduce porewater pressures is not necessary since the developed porewater pressure without the presence of cover are unlikely to exceed 20% during the 4m storm. But if the permeability of the sand fill is around 10^{-4} cm/s, it is essential to have a top coarse cover protection and
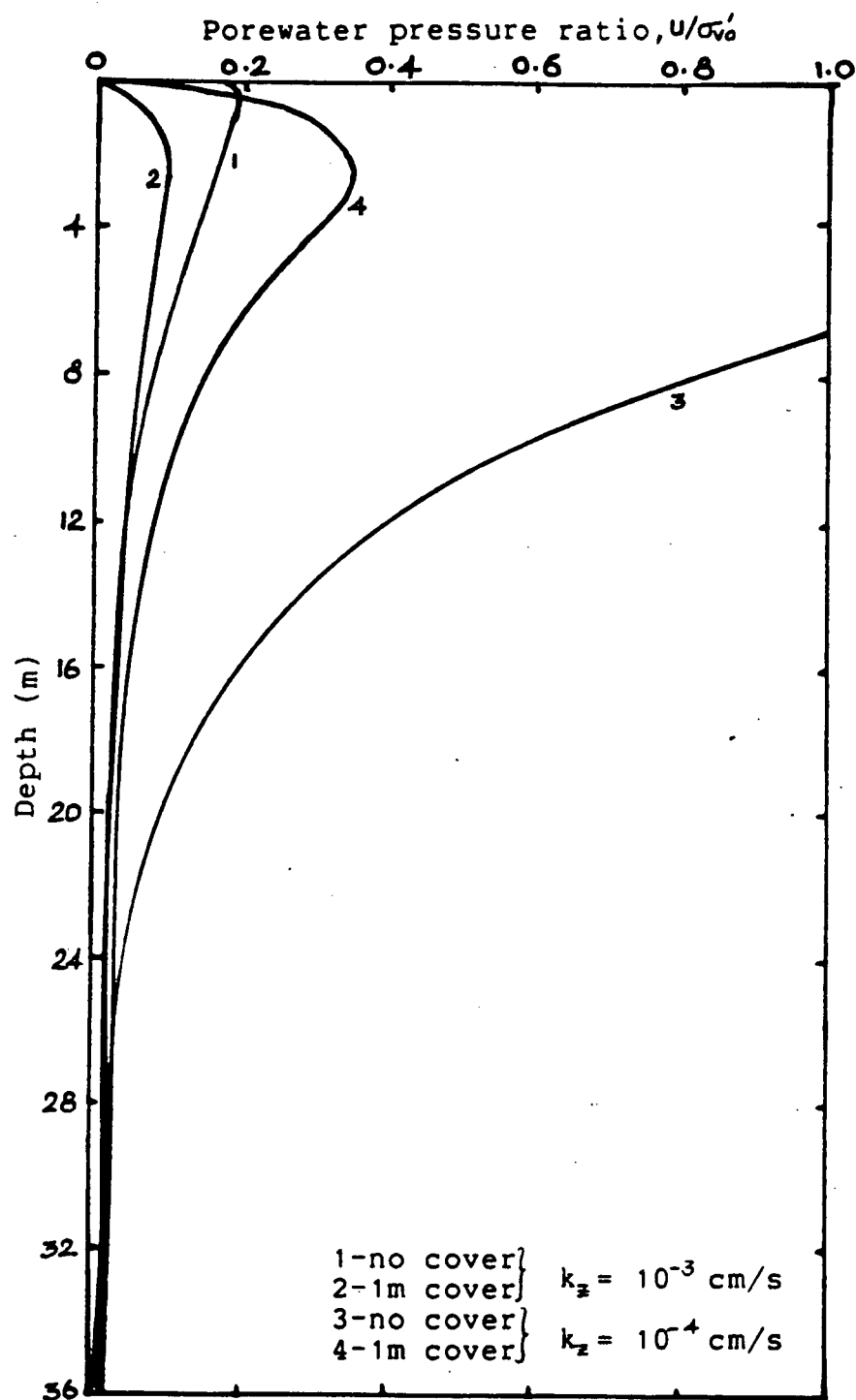
Figure 7.10; Section-AA; Effect of Cover on Porewater Pressure
Response At the End of the 4m 6 hour Storm.

Figure 7·11; Section-CC; Effect of Cover on Porewater Pressure Response At the End of the 4m 6 hour Storm.

Figure 7·12; Section-DD; Effect of Cover on Porewater Pressure Response At the End of the 4m 6 hour Storm.

	Maximum Porewater Pressure Ratio, U/σ'_{vc}, (%)			
Section	$k_z = 10^{-3}$ cm/s		$k_z = 10^{-4}$ cm/s	
	No Cover	1m Cover	No Cover	1m Cover
AA	19	10	100(6.5)	35
CC	13	5	100(5.0)	24
DD	10	4	100(2.0)	18

Table 7·2 ; Effect Of Cover On Maximum Porewater Pressure
Response At Sections Of Island 1 At the End Of
4m 6 hour Storm.

Note; Figures in brackets indicate the extent of the zone of
liquefaction in metres.

a cover of thickness 1m is sufficient to reduce porewater pressures to acceptable limits. As mentioned earlier, the cover has to be extended beyond water depth 10m (as given by 2.50 times H_s) to eliminate the possibility of liquefaction during the 4m storm.

7.4 Effect of Cover on Porewater Pressure
Response of Island 2

The effect of the 1m thick coarse cover on the porewater pressure response at sections PP to VV of island 2 at the end of the specified storm are shown in Figures 7.13 to 7.19.

These figures indicate that there is considerable reduction in the porewater pressure response as a result of the top coarse cover and also the response has the same trend as seen before in the analyses of island 1. In the case with k_z = 10^{-3} cm/s, the results indicate that the effect of 1m cover is to reduce the porewater pressure response to just below liquefaction levels at sections RR, SS and TT and to very negligible levels at other sections. But in the case with k_z = 10^{-4} cm/s, the effect of cover is to reduce the thickness of the zone of liquefaction significantly. In these cases, the liquefaction is limited to a localized zone of a few metres in extent. For example, at section TT, the thickness of the zone of liquefaction is reduced from 13.5m to 7m and the localized zone of liquefaction extends from depth 2m to depth 9m from the original sand berm top surface.
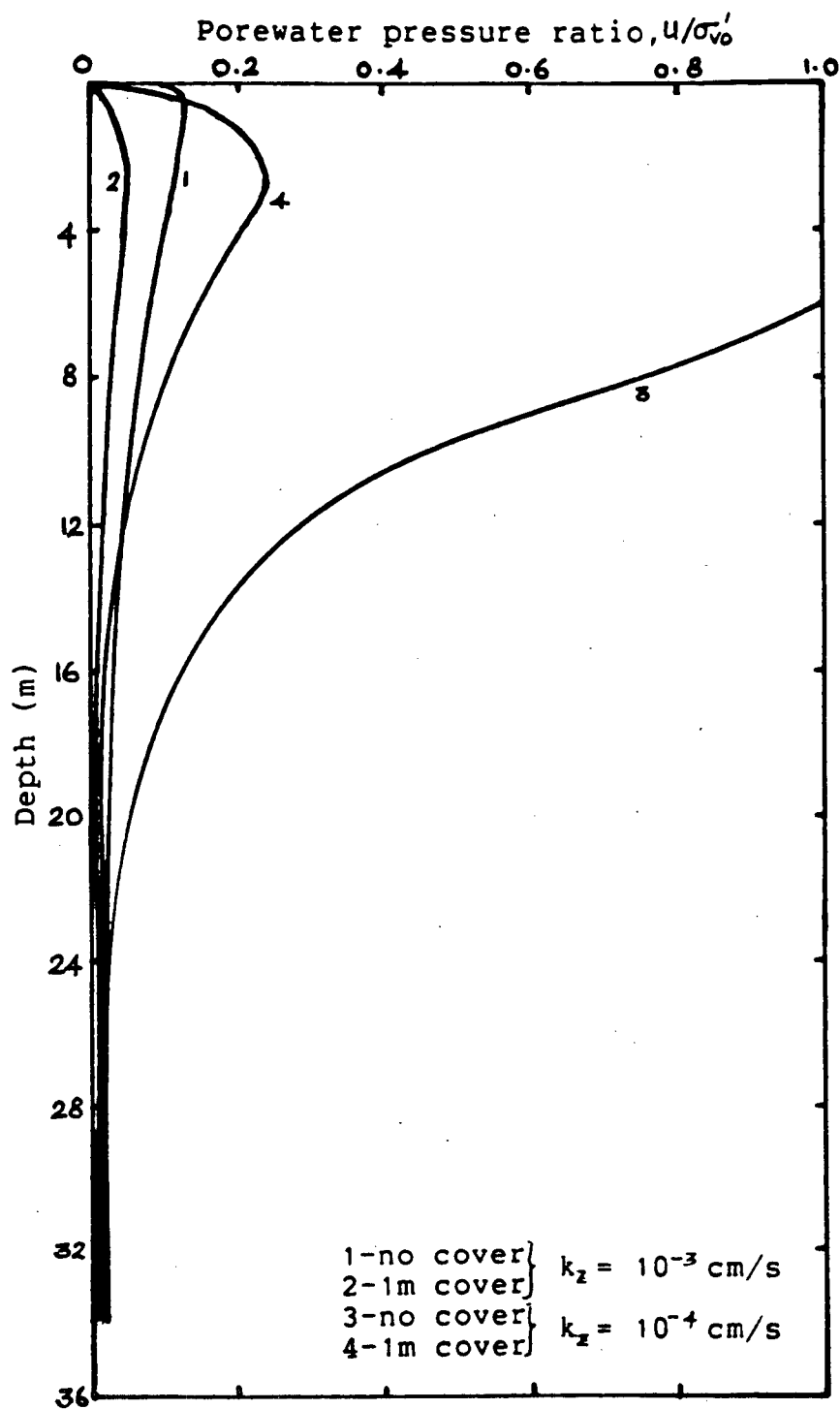
Figure 7.13; Section-PP; Effect of Cover on

Porewater Pressure Response At

the end of 9m 6 hour Storm.

Figure 7.14; Section-QQ; Effect of Cover on
Porewater Pressure Response At
the end of 9m 6 hour Storm.

Figure 7.15; Section-RR; Effect of Cover on
Porewater Pressure Response At
the end of 9m 6 hour Storm.
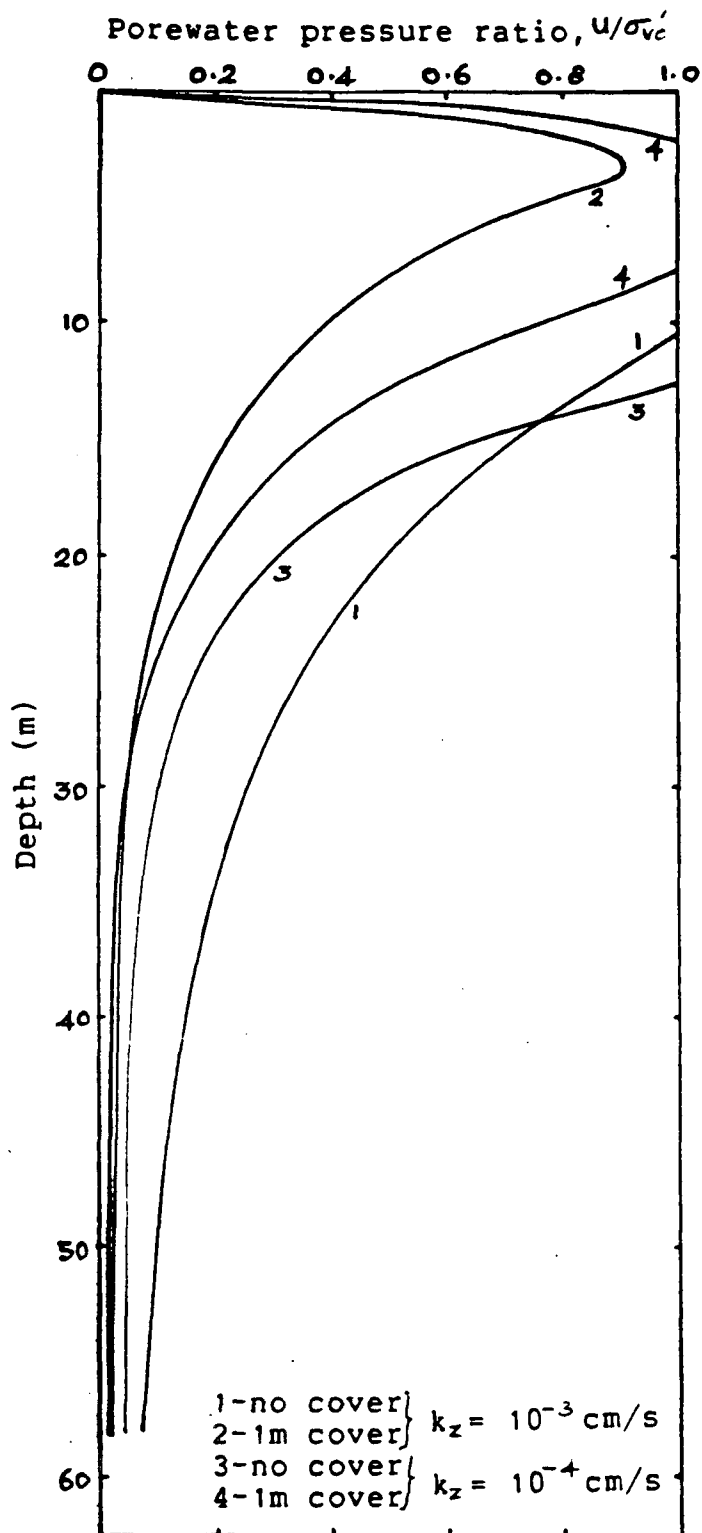
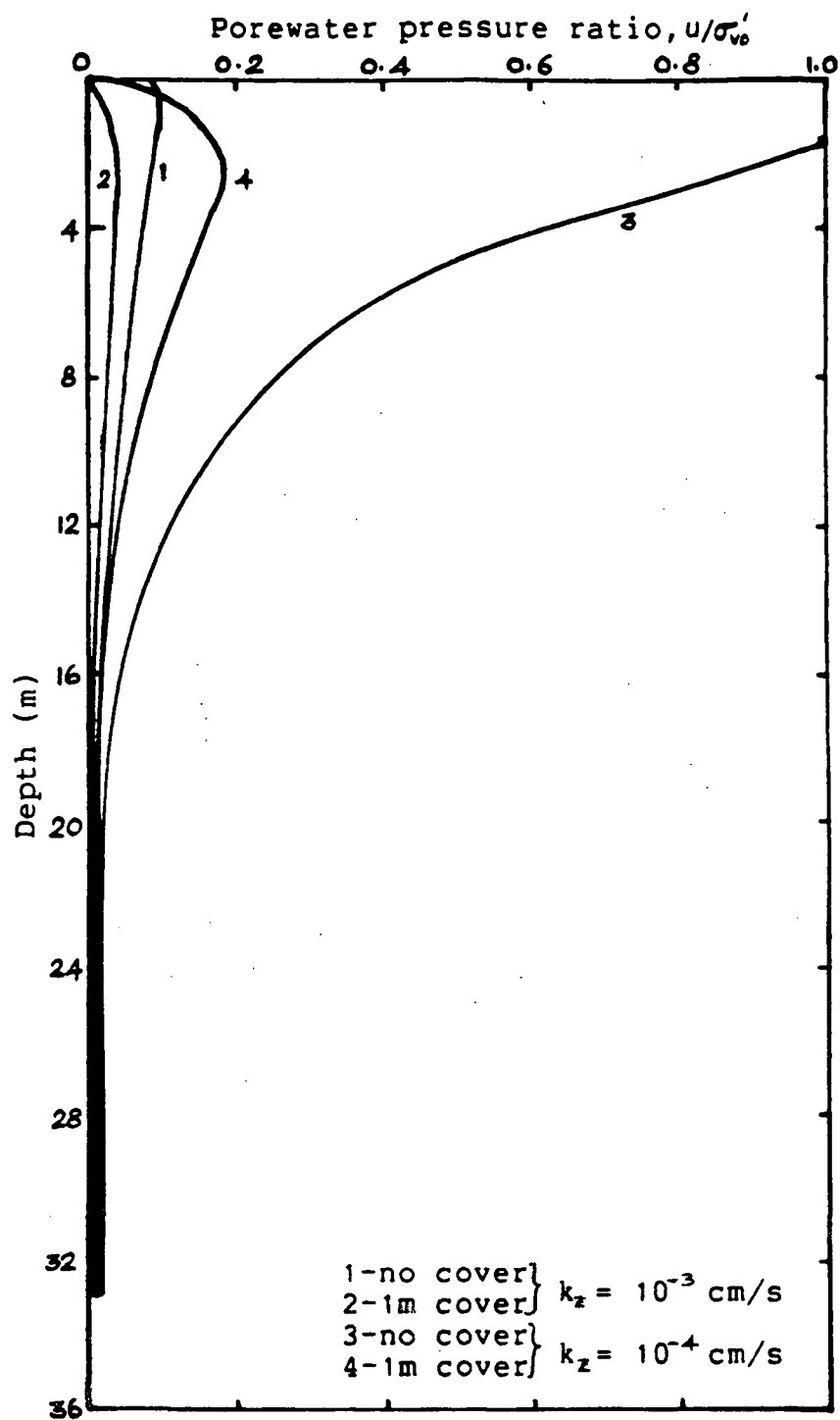Figure 7.16; Section-SS; Effect of Cover on

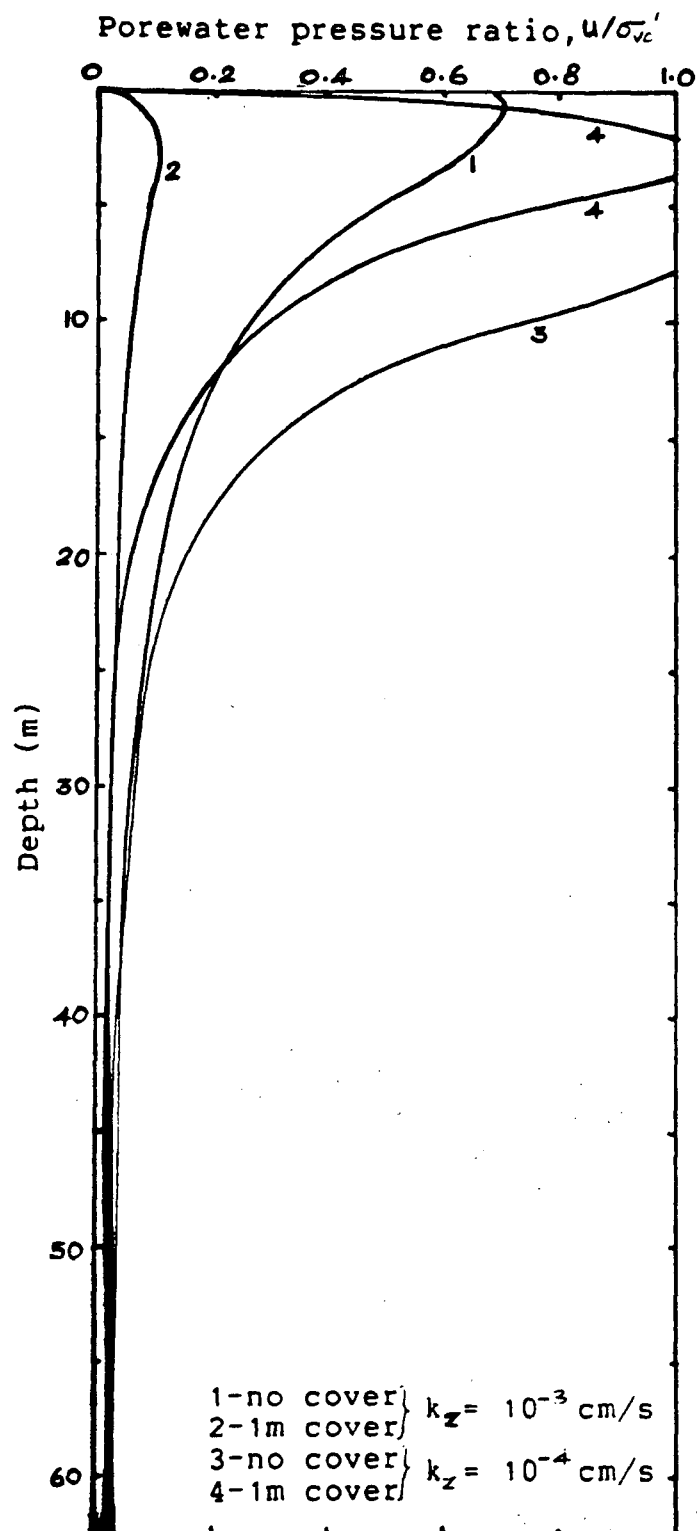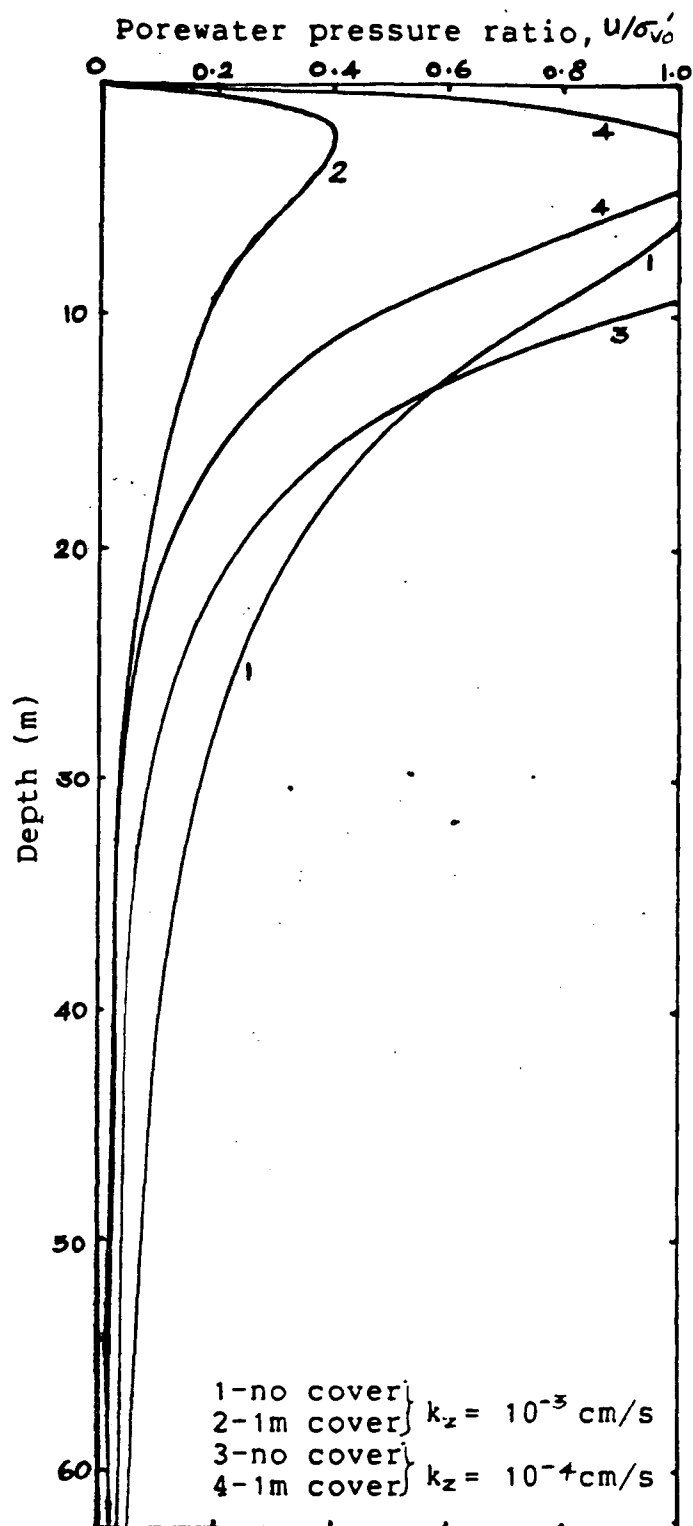Porewater Pressure Response At

the end of 9m 6 hour Storm.
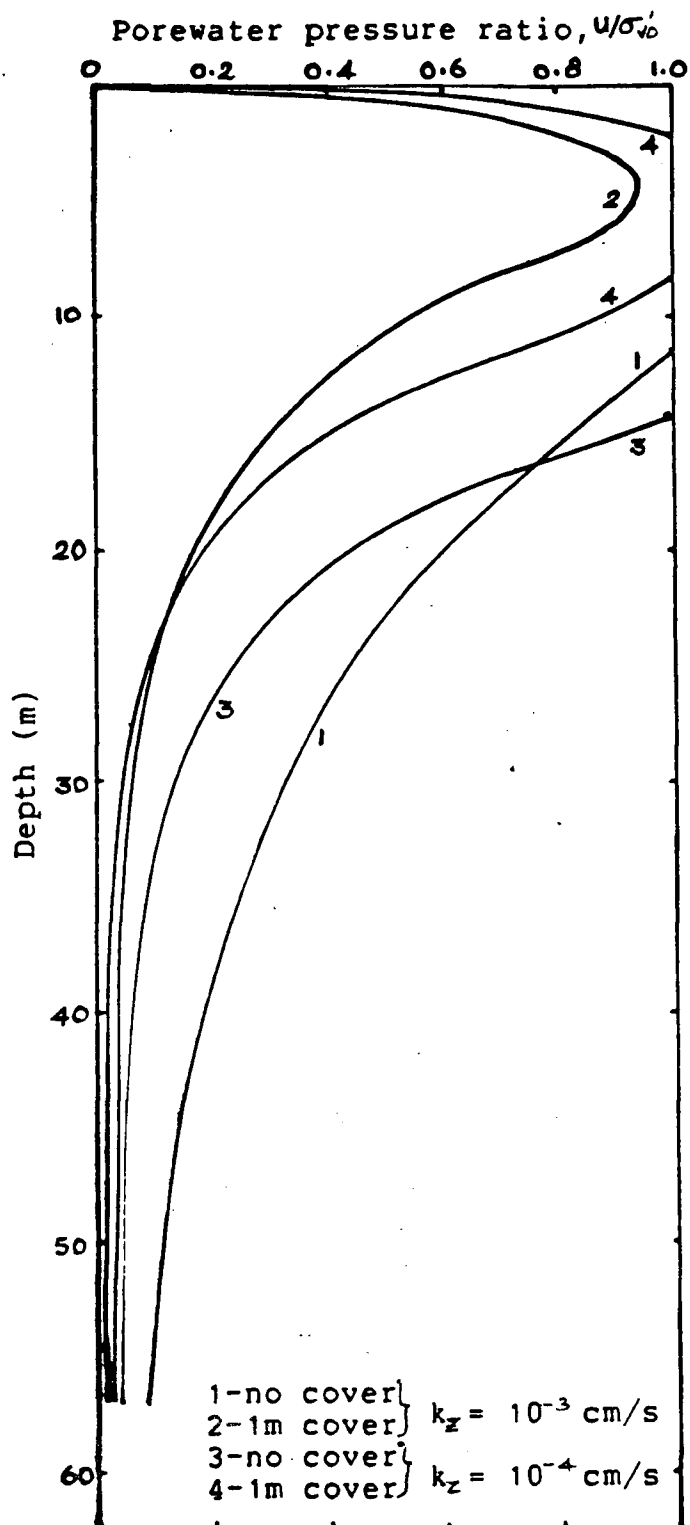
Figure 7.17; Section-TT; Effect of Cover on
Porewater Pressure Response At
the end of 9m 6 hour Storm.
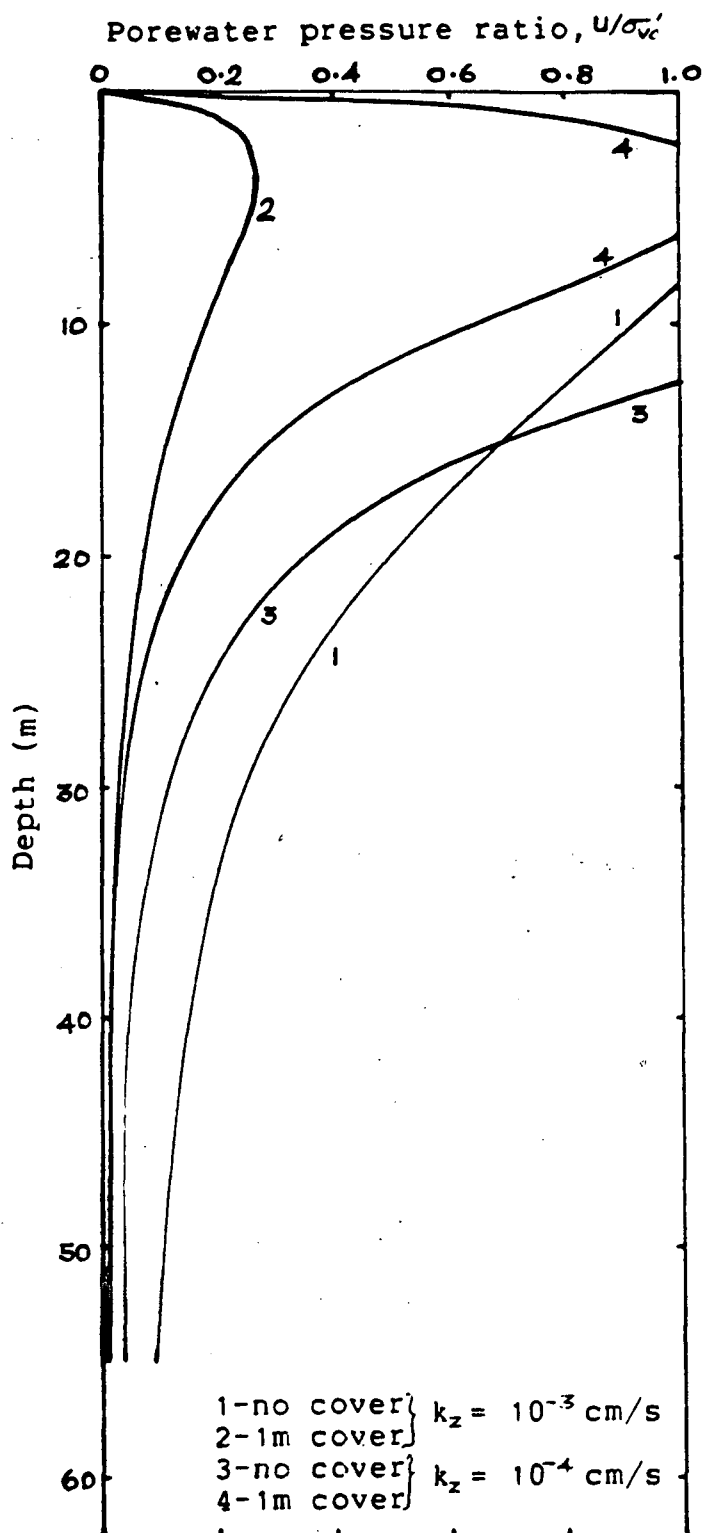
Figure 7.18; Section-UU; Effect of Cover on
Porewater Pressure Response At
the end of 9m 6 hour Storm.
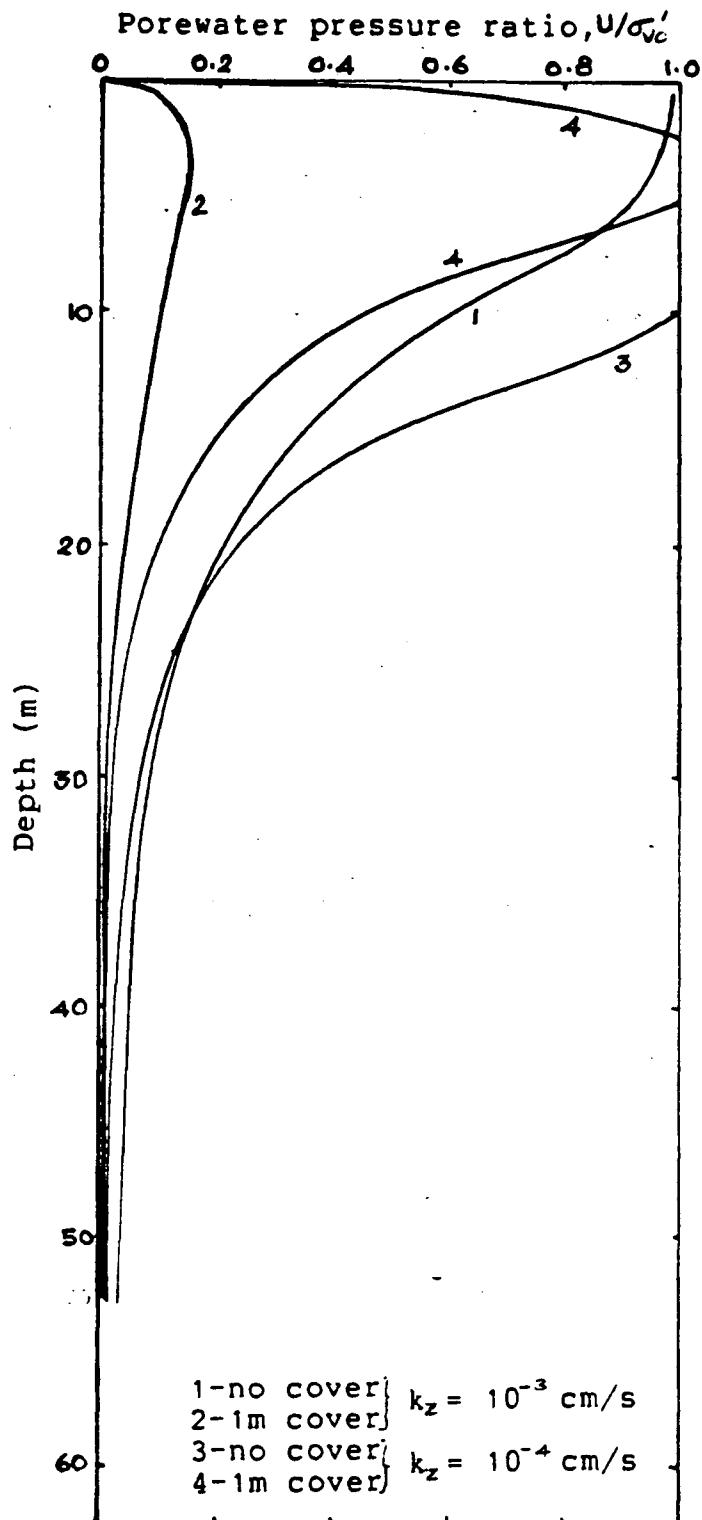
Figure 7.19; Section-VV; Effect of Cover on Porewater Pressure Response At the end of 9m 6 hour Storm.
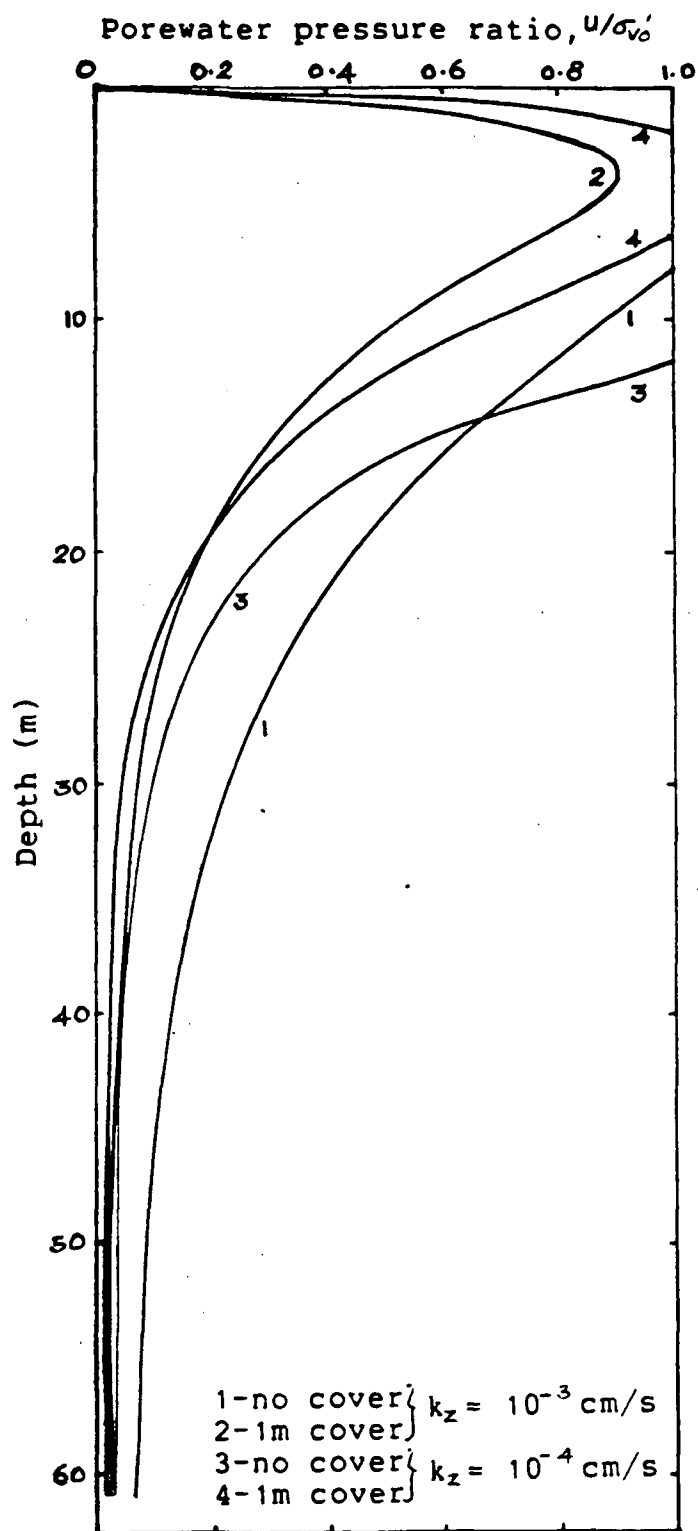
The comparison of maximum porewater pressure response with and without the 1m thick coarse at sections PP to VV of island 2 at the end of the storm is presented in Table 7.3. It is evident from the results that, as in the case without cover, the maximum porewater pressure ratio in the case with cover occurs around section TT. Results also indicate that the cover of 1m thickness is not sufficient to suppress liquefaction when the permeability is 10^{-4} cm/s. An increase in thickness of cover is required to prevent liquefaction in these cases. However, in the case of $k_z = 10^{-3}$ cm/s, a cover thickness of 1m is sufficient only beyond water depth of 14m and an increased cover would be necessary up to water depth 14m to bring down porewater pressures to safer levels during the specified storm activity.

| Section | Maximum Porewater Pressure Ratio, u/σ'_{vo}, (%) | | | |
| | $k_z = 10^{-3}$ cm/s | | $k_z = 10^{-4}$ cm/s | |
	No Cover	1m Cover	No Cover	1m Cover
PP	70	11	100(7.0)	100(2.0)
QQ	100(6.0)	41	100(9.0)	100(2.5)
RR	100(8.0)	90	100(11.5)	100(4.5)
SS	100(10.5)	92	100(12.5)	100(6.0)
TT	100(11.0)	95	100(13.5)	100(7.0)
UU	100(9.0)	27	100(12.0)	100(4.5)
VV	100(2.0)	16	100(8.5)	100(3.0)

Table 7.3 ; Effect Of Cover On Maximum Porewater Pressure
Response At Sections Of Island 2 At the End Of
9m 6 hour Storm.

Note; Figures in brackets indicate the extent of the zone of
liquefaction in metres.

7.5 Effect of Cover on Porewater Pressure

Response of Island 3

Figures 7.20 to 7.26 show the effect of 1m coarse cover on the porewater pressure response at sections HH to NN of island 3 at the end of the specified storm for the two different permeabilities. Even though significant changes in the porewater pressure response is apparent, the results indicate that liquefaction still occurs to considerable depths at sections II to MM for the case when k_z = 10^{-4} cm/s. Liquefaction or high levels of porewater pressure are indicated for the case with k_z = 10^{-3} cm/s at sections JJ to LL.

Table 7.4 shows the maximum porewater pressure response at sections of island 3 at the end of the storm with and without 1m of coarse cover. It appears that 1m of coarse cover is not sufficient to suppress liquefaction during the specified storm for both permeabilities considered. However, in the case of k_z = 10^{-3} cm/s, 1m cover is sufficient beyond water depth 18m (section LL) although increased cover is required for water depths above 18m. In the case of k_z = 10^{-4} cm/s, 1m cover is sufficient only beyond water depth 22 m and for shallower depths the thickness of cover has to be increased.

Porewater pressure ratio, U/σ_{vo}'

Figure 7.20; Section-HH; Effect of Cover on
Porewater Pressure Response At
the end of 12m 6 hour Storm.

Figure 7.2i; Section-II; Effect of Cover on Porewater Pressure Response At the end of 12m 6 hour Storm.

Figure 7.22; Section-JJ; Effect of Cover on

Porewater Pressure Response At

the end of 12m 6 hour Storm.

Porewater pressure ratio, u/σ'_{vc}

1-no cover} $k_z = 10^{-3}$ cm/s
2-1m cover}
3-no cover} $k_z = 10^{-4}$ cm/s
4-1m cover}

Figure 7.23; Section-KK; Effect of Cover on
Porewater Pressure Response At
the end of 12m 6 hour Storm.

Figure 7·24; Section-LL; Effect of Cover on Porewater Pressure Response At the end of 12m 6 hour Storm.
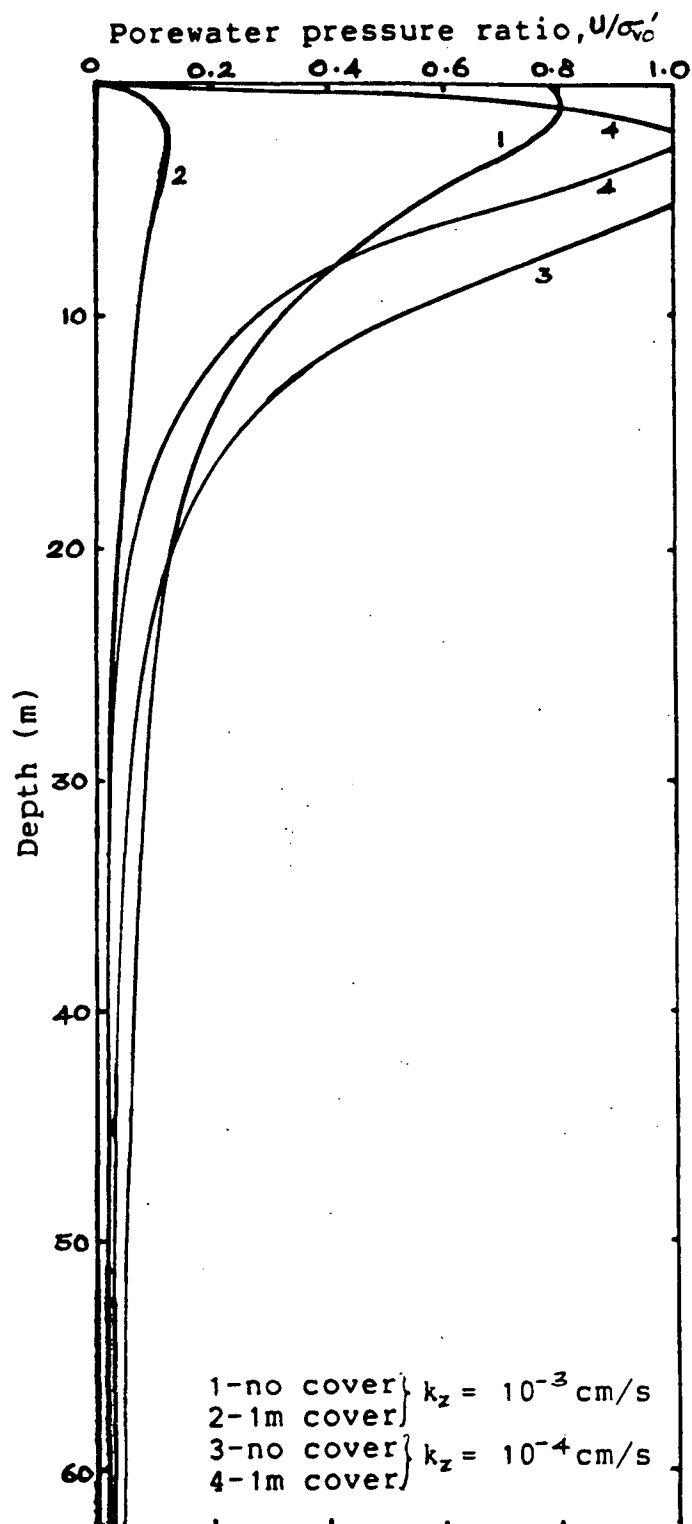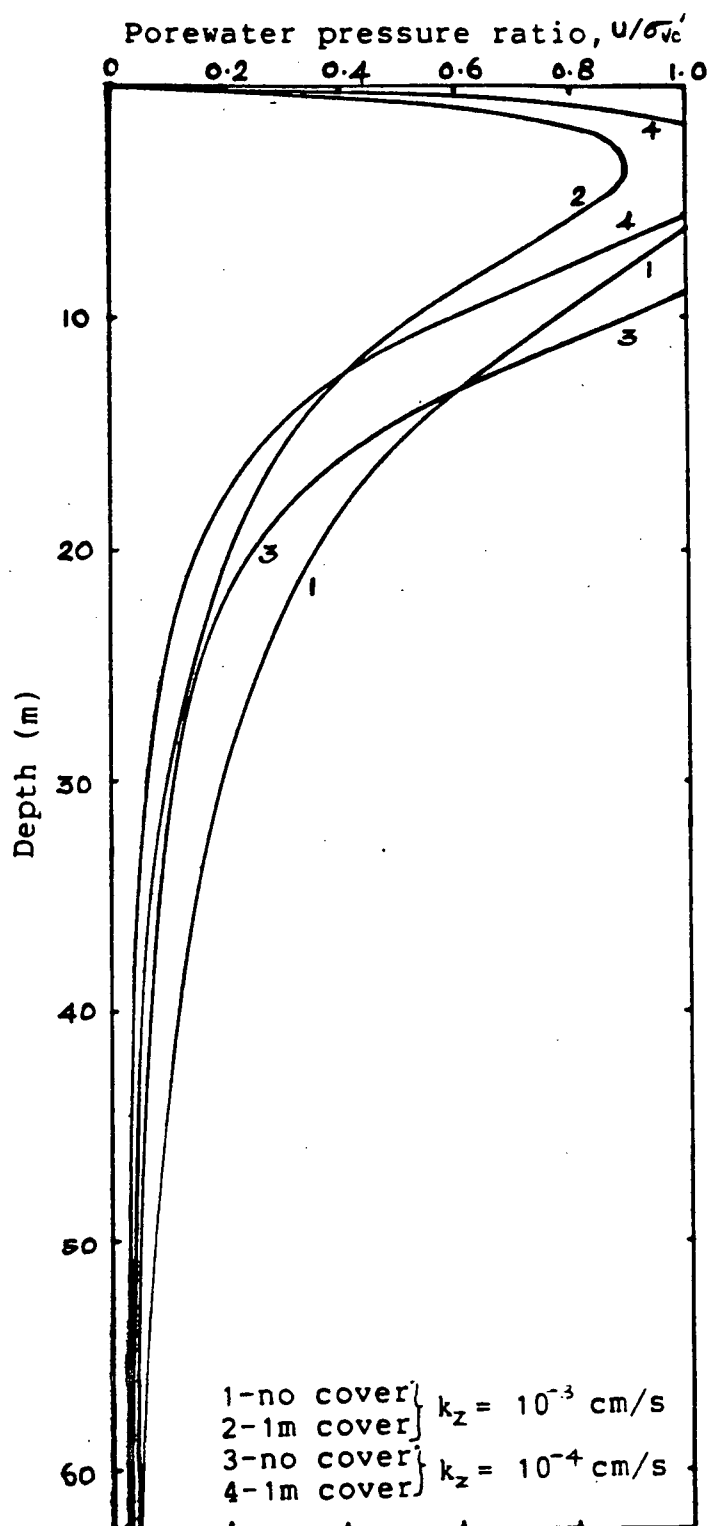
Figure 7.25; Section-MM; Effect of Cover on

Porewater Pressure Response At

the end of 12m 6 hour Storm.

Figure 7.26; Section-NN; Effect of Cover on

Porewater Pressure Response At

the end of 12m 6 hour Storm.

Section	Maximum Porewater Pressure Ratio, u/σ'_{vo}, (%)			
	$k_z = 10^{-3}$ cm/s		$k_z = 10^{-4}$ cm/s	
	No Cover	1m Cover	No Cover	1m Cover
HH	80	12	100(5.0)	100(1.0)
II	100(6.0)	90	100(9.0)	100(4.0)
JJ	100(9.0)	98	100(13.0)	100(6.0)
KK	100(12.5)	100(1.0)	100(15.0)	100(7.0)
LL	100(13.0)	100(2.5)	100(16.0)	100(7.5)
MM	100(9.0)	22	100(12.0)	100(5.0)
NN	18	5	100(6.5)	18

Table 7.4; Effect Of Cover On Maximum Porewater Pressure
Response At Sections Of Island 3 At the End Of
12m 6 hour Storm.

Note; Figures in brackets indicate the extent of the zone of
liquefaction in metres.

CHAPTER 8

EFFECT OF FOUNDATION CONDITIONS ON POREWATER PRESSURES

8.1 Response of Island 1

The porewater pressure response at the end of the 6m, 6 hour storm at sections AA and CC of island 1 sitting on a clay foundation is presented in Figure 8.1 and 8.2 for the case of $k_z = 10^{-3}$ cm/s. These figures show that the porewater pressure response is very much dependent on the undrained shear strength S_u of clay immediately below the sand fill. It is also apparent that the harder the clay, greater the porewater pressure response will be. The limiting magnitude of the porewater pressures is the one corresponding to the rigid base.

For instance, at section AA, the maximum porewater pressure ratio developed at the end of the storm is 66% and 42% for S_u values of 50 kPa and 30 kPa respectively. On the other hand, at section CC, the corresponding maximum induced porewater pressure ratios are 45% and 24% respectively. The limiting wave induced porewater pressures at section AA and CC are 95% and 50% respectively.

The reason for the porewater pressure response being directly dependent on the undrained shear strength is due to the fact that in current engineering practice the shear modulus is related to the undrained shear strength on a one-to -one basis (Seed et al,1970). Any increase in undrained shear strength of the clay increases the shear modulus and hence alters the shear stress distribution with depth in the sand
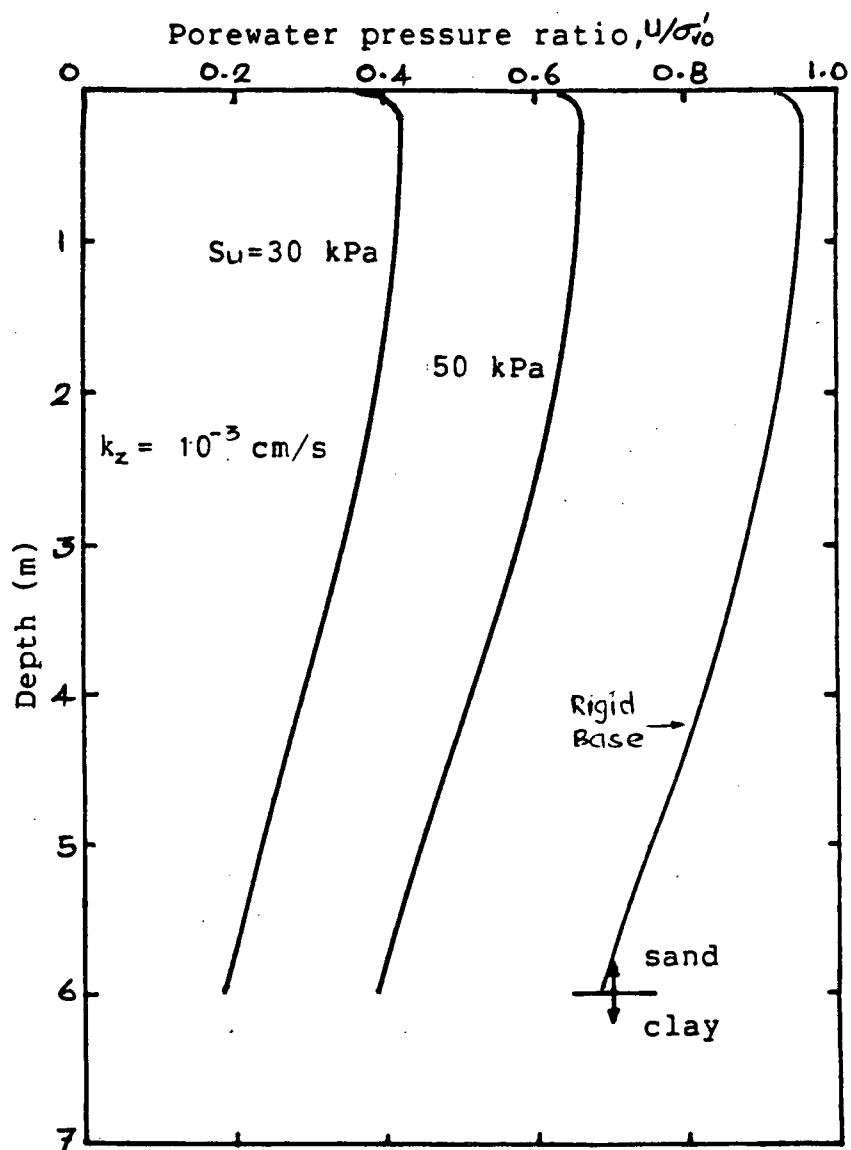
Figure 8·1 ; Section-AA; Residual Porewater Pressure Response
At the end of 6m 6 hour Storm.
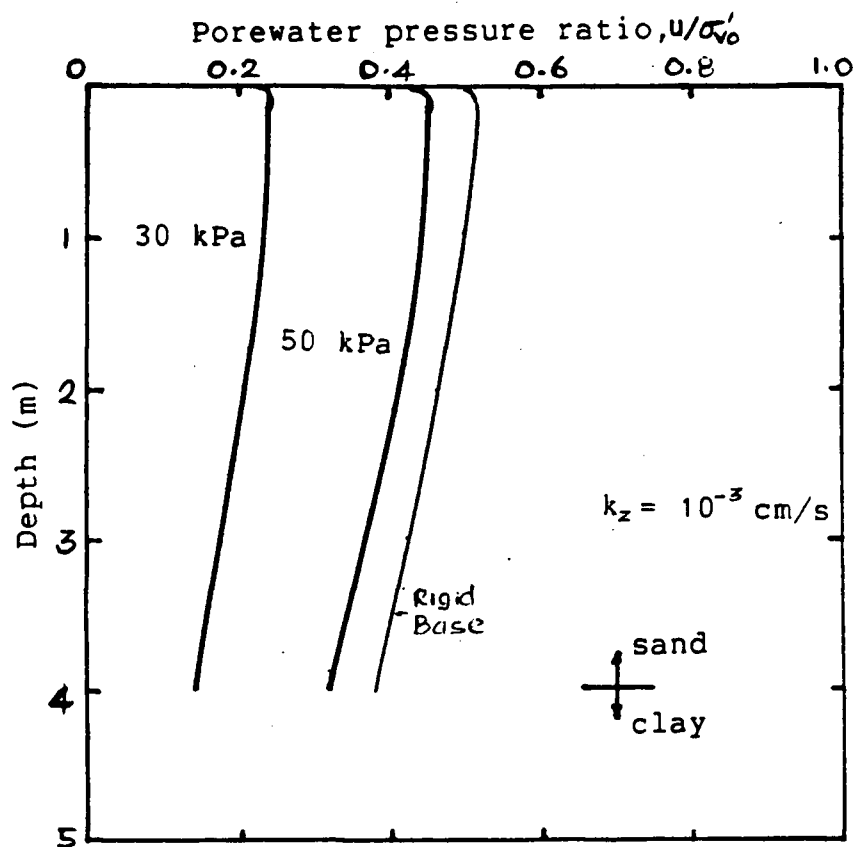
Figure 8.2 ; Section-CC; Residual Porewater Pressure Response
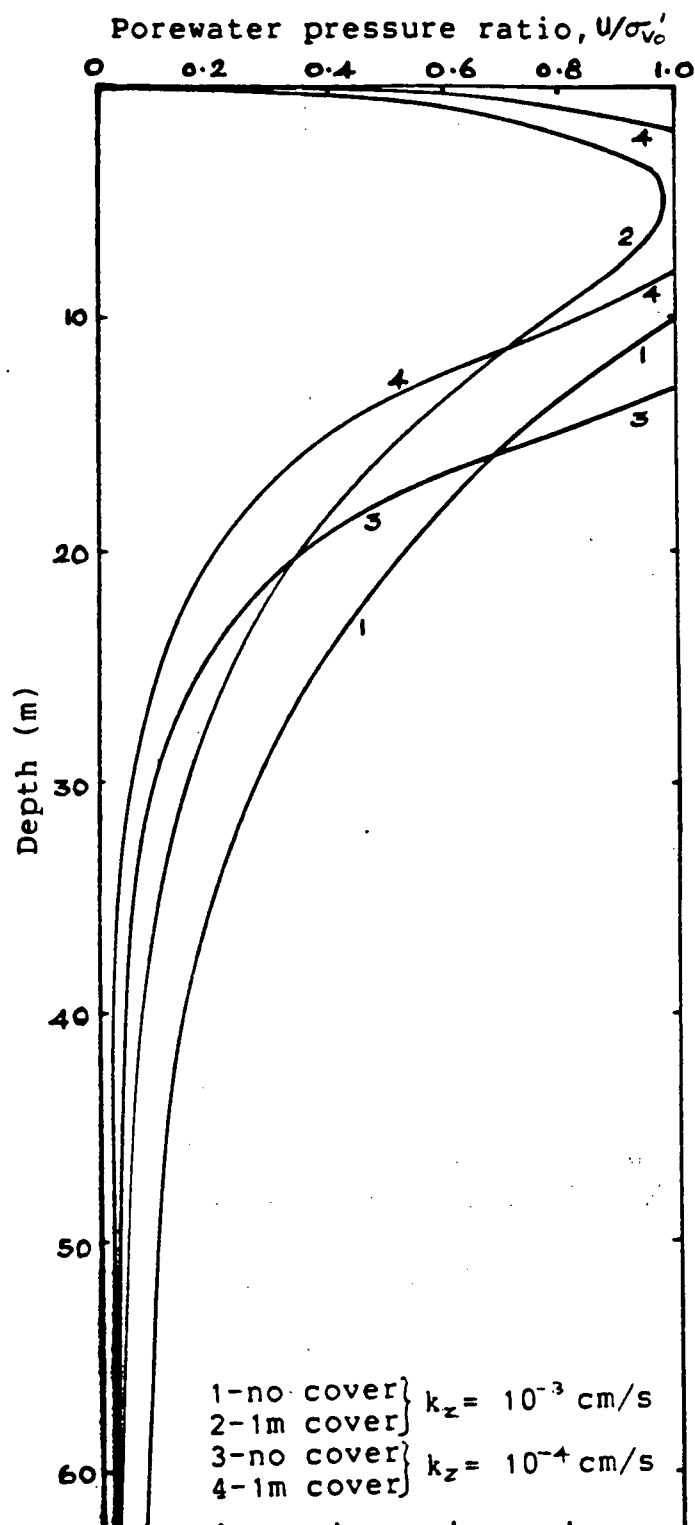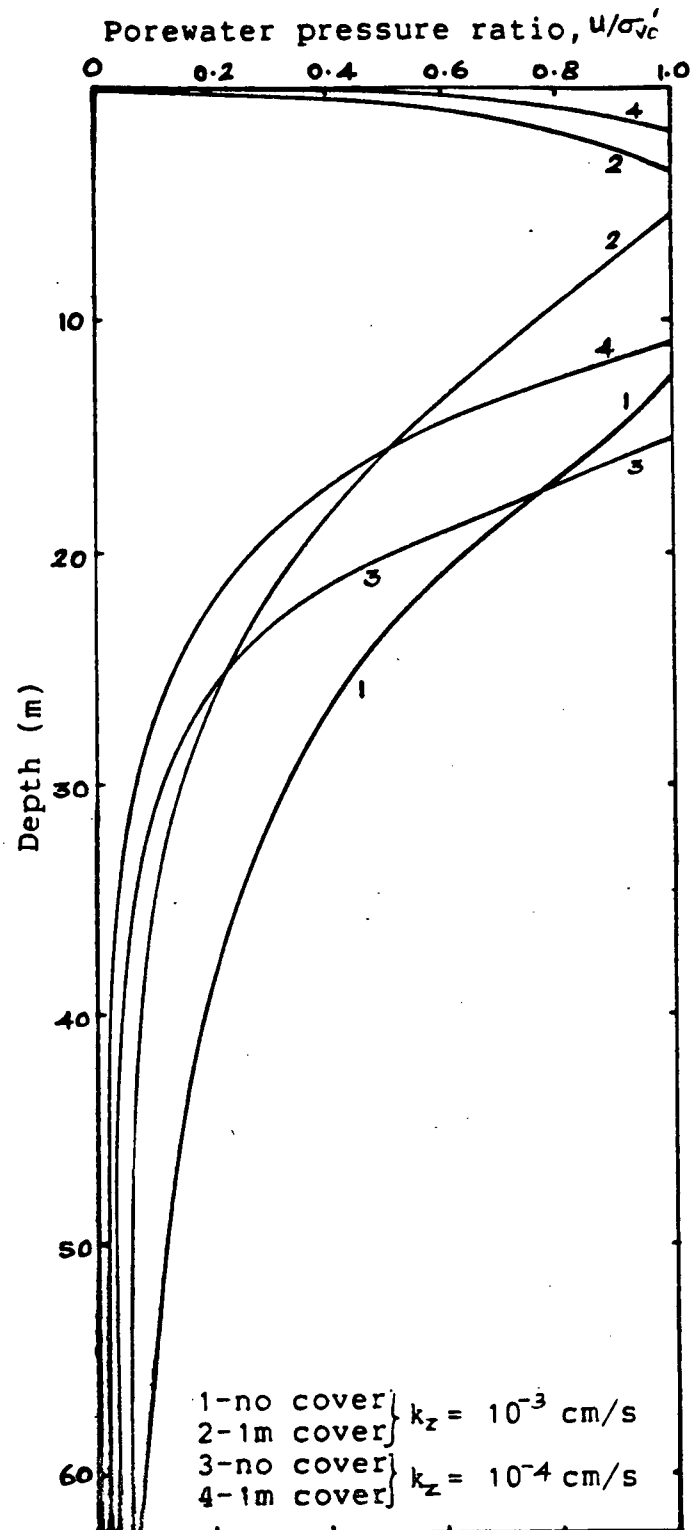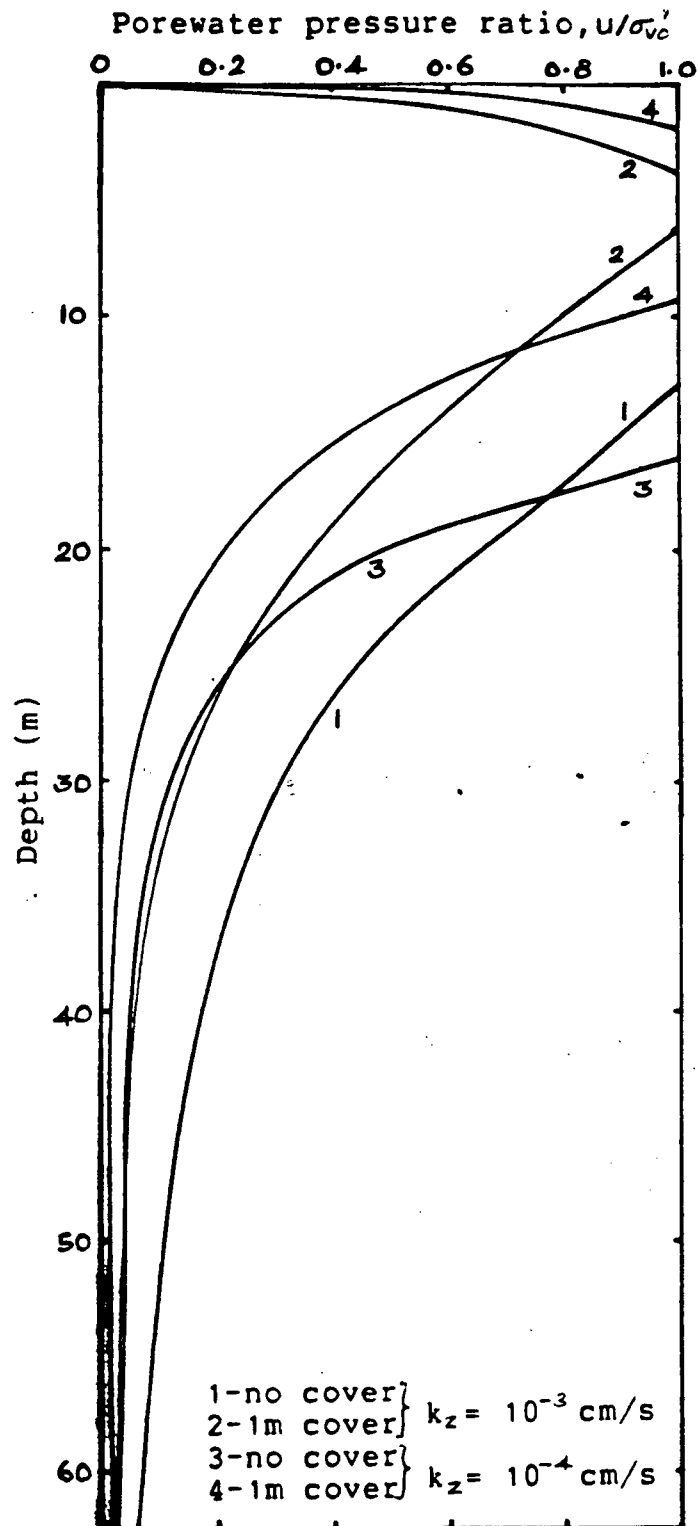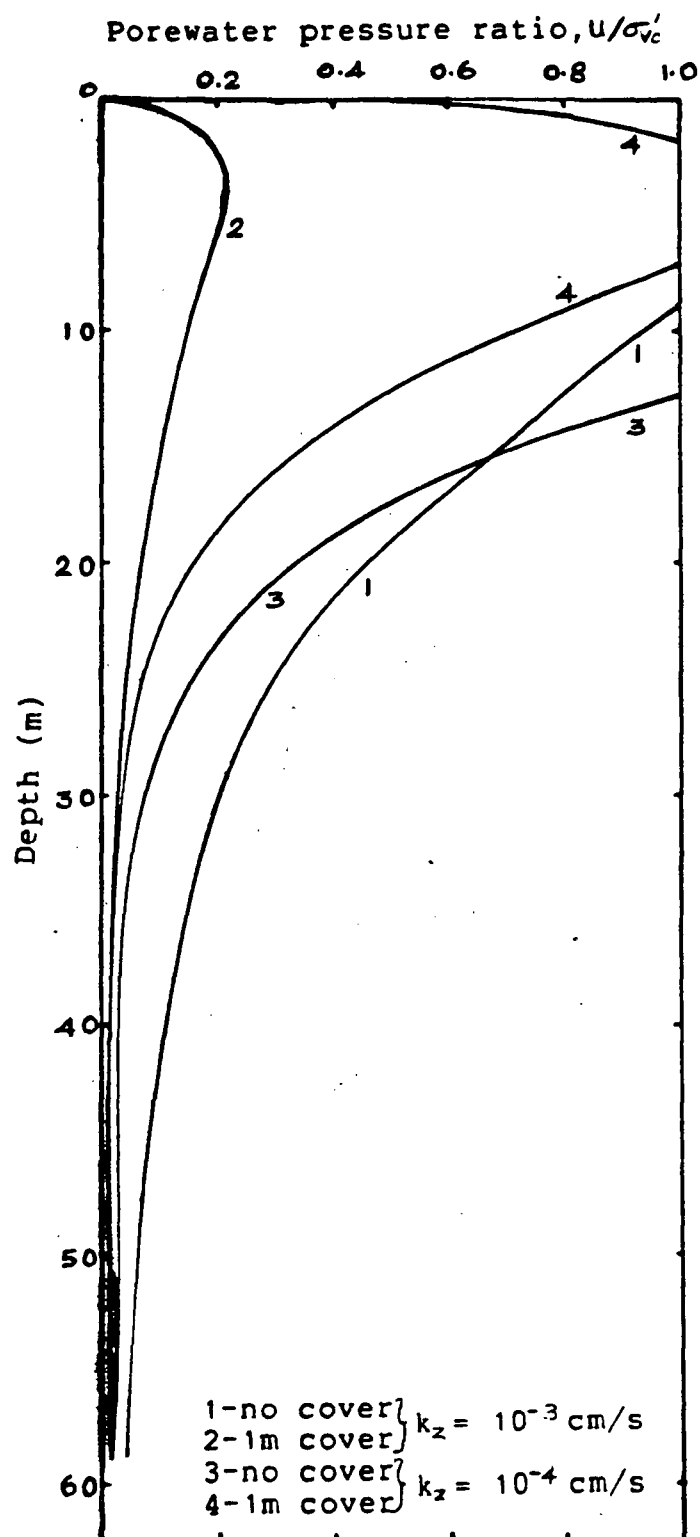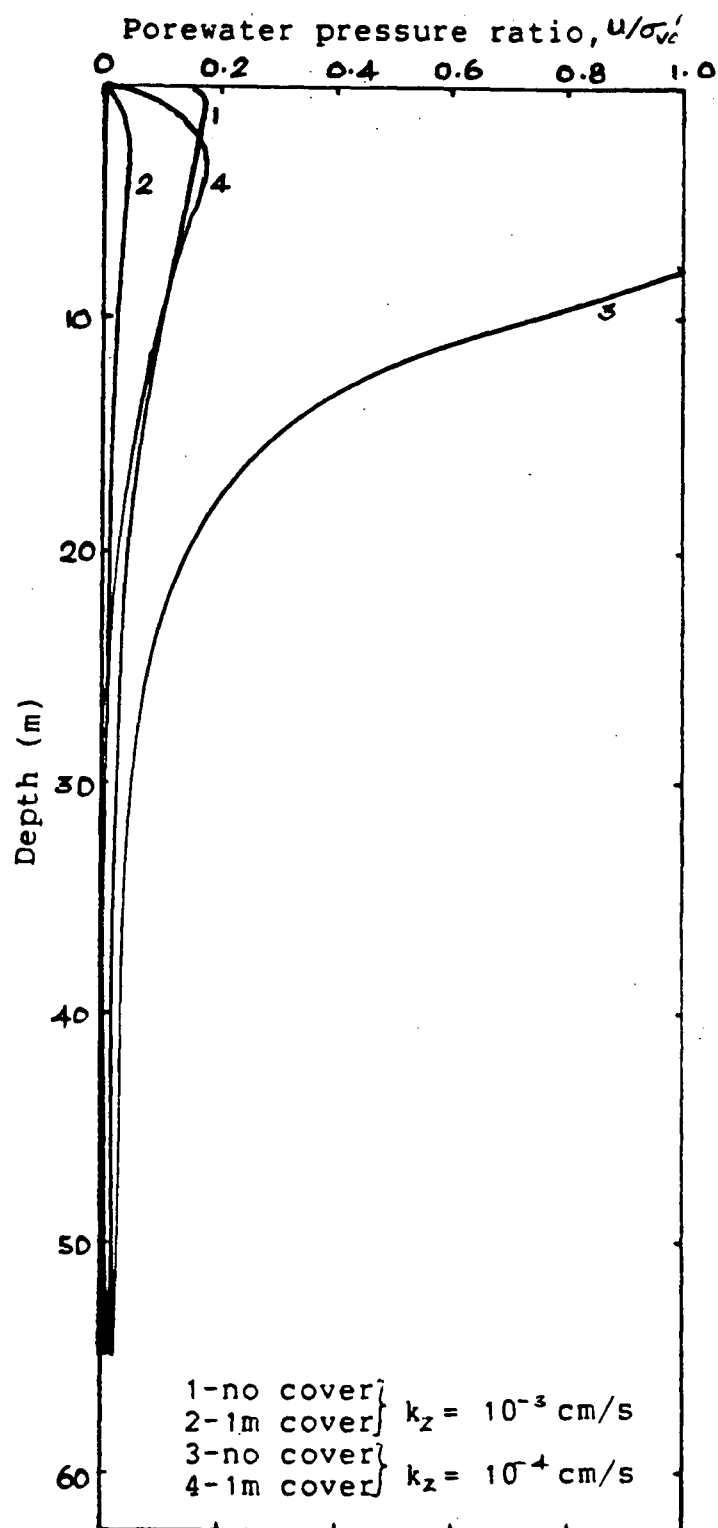At the end of 6m 6 hour Storm.

fill.

Figure 8.3 clearly demonstrates the resulting increase in the shear stress ratio distribution in the sand fill at section AA at the start of the storm, as a result of the increase in undrained shear strength from 30 kPa to 50 kPa. The consequence of the increase in shear stress distribution as in the above case, will be reflected not only on the initial values of N_L but also in the calculation of the number of waves of the equivalent storm N_{eq} in such a manner that N_L values become smaller and N_{eq} value becomes larger.

For example, at section AA, the N_L value corresponding to the first layer of the sand fill for the cases of S_u being 30 kPa and 50 kPa is 10.77 and 10.0 respectively. The corresponding values of N_{eq} are 1076 and 1086 respectively. Now, under these conditions, the factor (N_{eq}/N_L) which governs the rate of porewater pressure generation at any instant of time, increases with increasing S_u and so does the rate of porewater pressure generation (see equation 3-12). This increased rate of porewater pressure generation at the start of the storm results in greater porewater pressure response for the case of higher S_u value.
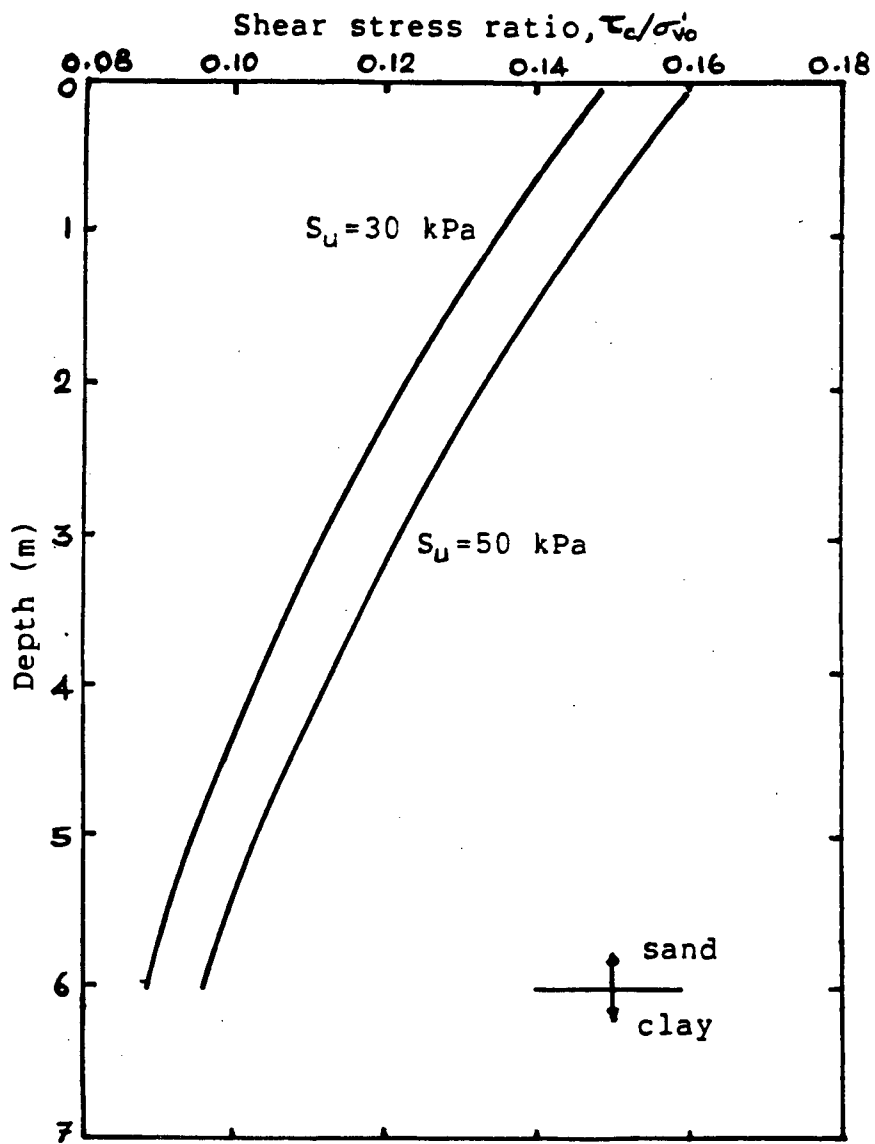
Figure 8.3; Section-AA; Shear Stress Ratio Distribution
At the start of 6m 6 hour Storm.

CHAPTER 9

SUMMARY AND CONCLUSIONS

A simple method of analysis for the determination of wave induced porewater pressures is presented. The method considers both dissipation and generation effects during wave loading. It also considers the effect of increasing porewater pressures on soil properties, namely shear modulus, bulk modulus and volume compressibiliy. The method was incorporated into a finite element computer program STABW3. The program uses a cubic polynomial interpolation function for the porewater pressure field.

The computer program was used to analyse three different artificial islands built up to a set down depth of 6m in water depths 12m, 21m and 31m respectively. The islands were subjected to different patterns of storm waves each of 6 hours duration. The porewater pressures induced in each of the islands by the storm waves were computed for different drainage characteristics of the berm material. The effect of incorporating a non liquefiable coarse cover on top of the island surface on the induced porewater pressure response was also examined. A brief examination of the effect of foundation conditions on the induced porewater pressure response was also reported.

In this study, the relative density of the berm material has been assumed to be 50%. This means that the sand has a

relatively low resistance to liquefaction which tends to dramatise the effect of wave action. Current construction practices tend to give relative density of the range from 50% to 70%. At the higher relative densities, the zone of liquefaction will be greatly reduced and phenomenically the same kind of behavoir will be obtained. Hence, the numerial values cannot be considered to be generally applicable.

The following general conclusions can be drawn from the results of the analyses. These were based on such a limited number of analyses and therefore they have to viewed with caution.

1. For homogeneous island berms on sand foundations, the effect of the waves is felt strongly and severely at a particular location. The water depth, D_c, to this critical location is primarily dependent on the significant wave height, H_s, of the storm and is given approximately by $D_c = 1.50 H_s$ regardless of the drainage characteristics of the berm material.

2. For islands on sand foundations, the water depth beyound which liquefaction would not occur during a storm is dependent on wave parameters and the drainage characteristics of the berm material. For a storm of 6 hours duration and for initial volume compressibility of 3×10^{-5} m^2/kN, the water depth, in terms of H_s, beyound which liquefaction would not occur, is

given approximately by 2.20 H_s and 2.50 H_s for k_z values of 10^{-3} cm/s and 10^{-4} cm/s respectively.

3. For islands on sand foundations, the drainage characteristics of the berm material required to limit the porewater pressure response below liquefaction levels, is dependent on the wave characteristics; the requirements becomes more stringent the more severe the storms.

4. The effect of non liquefiable relatively free draining coarse cover material placed on top of the berm slope is to reduce the porewater pressure response during wave loading. The reduction in porewater pressure response for a given permeability of the berm material is dependent on the cover thickness provided. Moreover, the increase in the permeability of the cover material does not seem to produce further significant reduction in the porewater pressure response. Hence, in order to suppress porewater pressure response to the desired levels, it is more effective to increase the thickness of the coarse cover rather than to resort to the use of much more pervious material as cover.

5. The suitable thickness of cover required to suppress liquefaction at a particular section of interest during a storm depends on the drainage characteristics of the berm material and the wave parameters. The cover thickness required to completely suppress liquefaction for given drainage

characteristics of the berm material, is greater for a severe storm than for a milder storm of the same duration; Again for a given storm, it is higher for less pervious berm material than for more pervious material.

6. For islands on clay foundations, the porewater pressure response during the wave loading is dependent on the undrained shear strength of the clay immediately below the sand berm. The harder the clay foundation, the higher the porewater pressure response will be, up to the limiting magnitude corresponding to a rigid base.

REFERENCES

1. Bercha, F.G and Stenning, D.G (1979),"Arctic Offshore Deepwater Ice-Stucture Interactions", Proceedings, Eleventh Annual Offshore Technology Conference, Houston, Texas, Paper No. 3632, Vol.4, pp. 2377-2386.

2. Biot, M.A (1941),"General Theory Of Three Dimensional Consolidation", Journal Of Applied Physics, Vol.12, February, pp. 155-164.

3. Boone, D.J (1980), "The Construction Of An Artificial Drilling Island in Intermediate Water Depths in the Beaufort Sea", Proceedings, Tweleveth Annual Offshore Technology Conference, Houston, Texas, Paper No. 3873, Vol.4, pp. 187-195.

4. Brown, A.D and Barrie, K.W (1975), "Artificial Island Construction in the Shallow Beaufort Sea", Third International Conference on Port and Ocean Engineering under Arctic Conditions, University Of Alaska, Fairbanks, Alaska, pp. 705-718.

5. Byrne, P.M (1981), "CE 581, Graduate Course Lectures", Department of Civil Engineering, University of British Columbia, Vancouver, B.C.

6. Cornforth, D.H (1974),"One Dimensional Curves -of a Medium Sand", Geotechnique, Vol.24, No.4, December, pp. 678-683.

7. Croasdale, K.R and Marcellus, R.W (1978), "Ice and Wave Action on Artificial Islands in the Beaufort Sea", Canadian Journal of Civil Engineering, Vol.5, pp 98-114.

8. De Jong, J.J.A and Bruce, J.C (1978), "Design and Construction of a Caisson Retained Island, Drilling Platform for the Beaufort Sea", Proceedings, Tenth Annual Offshore Technology Conference, Houston, Texas, Paper No. 3294, Vol.3, pp. 2111-2120.

9. De Jong, J.J.A, Stigter, C and Steyn, B (1975), "Design and Building of Temporary Artificial Islands in the Beaufort Sea", Third International Conference on Port and Ocean Engineering under Arctic Conditions, University of Alaska, Fairbanks, Alaska, pp. 753-789.

10. Duncan, J.M, Byrne, P.M, Wong, K.S and Marby, P (1980), "Strength, Stress-Strain and Bulk Modulus Parameters for Finite Element Analyses of Stresses and Movements in Soil Masses", Report No. UCB/GT/80-01, University of California, Berkeley, August.

11. Finn, W.D.Liam, Iai, S and Ishihara, K (1982), "Performance of Artificial Offshore Islands Under Wave and Earthquake Loading; Field Data Analyses", Proceedings, Fourteenth Annual Offshore Technology Conference, Houston, Texas, Paper No.4220, Vol.I, pp. 661-671.

12. Finn, W.D.Liam and Lee, M.K.W (1979), "Seafloor Stability Under Seismic and Wave Loading", Proceedings, Soil Dynamics in the Marine Environment, ASCE National Convention and Exposition, Boston, Mass., April 2-6, Preprint 3604, pp 1-25.

13. Finn, W.D.Liam, Lee, K.W and Martin, G.R (1977), "An Effective Stress Model for Liquefaction", Journal of Geotechnical Engineering Division, ASCE, Vol.103, No.GT6

14. Finn, W.D.Liam, Martin, G.R and Lee, M.K.W (1978), "Comparison of Dynamic Analyses for Saturated Sands", Proceedings, ASCE Earthquake Engineering and Soil Dynamics Conference and Exhibit, Pasadena, California, June.

15. Finn, W.D.Liam, Siddharthan, R and Martin, G.R (1980), "Wave Induced Instability in Ocean Floor Sands", ASCE Annual Convention and Exposition, Florida, Oct. 27-31, Preprint 80-638.

16. Finn, W.D.Liam, Siddharthan, R and Yogendrakumar, M (1983), "Response of Caisson Retained and Tanker Islands to Waves and Earthquakes", Thirty Sixth Canadian Geotechnical Conference, Vancouver, June.

17. Garratt, D.H and Kry, P.R (1978), "Construction of Artificial Islands as Beaufort Sea Drilling Platforms", Journal of Canadian Petroleum Technology, April-June.

18. Hayley, D.W (1979), "Site Evaluation for Artificial Drilling Islands in the Beaufort Sea", First Canadian Conference on Marine Geotechnical Engineering, Vol.I.

19. Hayley, D.W and Sangster, R.H.B (1974), "Geotechnical Aspects of Arctic Offshore Drilling Islands", Twenty Seventh Canadian Geotechnical Conference, Edmonton, November.

20. Henkel, D.J (1970), "The Role of Waves in Causing Submarine Landslides", Geotechnique 20, No.1, pp. 75-80.

21. Hogben, N (1976) "Wave Loads on Structures", Proceedings, Conference on Behaviour of Offshore Structures, BOSS'76, Trohnheim, Vol.I, pp 187-219

22. Isaacson, M.de.St.Q (1979), "Wave Forces on Rectangular Caissons", Proceedings, Civil Engineering in the Oceans IV, ASCE, San Francisco, Vol.I, pp.161-171.

23. Kent, D.D, Graham, B.W and Sangster, R.H.B (1979), "Geotechnical Design of a Caisson Retained Island for Exploration Drilling in the Beaufort Sea", First Canadian Conference on Marine Geotechnical Engineering, Vol.I pp. 429-437.

24. Lee, K.W (1975),"Mechanical Model for the Analysis of Liquefaction of Horizontal Soil Deposits", Ph.D Thesis, University of British Columbia, Vancouver, B.C, Canada.

25. Lee, K.L and Albaisa. A (1974), "Earthquake Induced Settlements in Saturated Sands", Journal of Geotechnical Engineering Division, Vol.100, No.GT4, April, pp. 387-406.

26. Lee, K.L and Chan, K (1972), "Number of Equivalent Significant Cycles in Strong Motion Earthquakes", Proceedings, International Conference on Microzonation, Seattle, Vol.II, pp. 609-627.

27. Lee, Michael.K.W and Finn, W.D.Liam (1975), "DESRA-1; Program for Dynamic Effective Stress Response Analysis of Soil Deposits Including Liquefaction Evaluation", Soil Mechanics Series No.36, Department of Civil Engineering, University of British Columbia, Vancouver, B.C.

28. Lee, Michael.K.W and Finn, W.D.Liam (1978), "DESRA-2; Program for Dynamic Effective Stress Response Analysis of Soil Deposits With Energy Transmitting Boundary Including Assessment Liquefaction Potential", Soil Mechanics Series No.38, Department of Civil Engineering, University of British Columbia, Vancouver, B.C.

29. Leidersdorf, C.B, Potter, R.E and Goff, R.D (1981), "Slope Protection for Artificial Exploration Islands Off Prudhoe Bay", Proceedings, Thirteen Annual Offshore Technology Conference, Houston, Texas, Paper No. 4112, Vol.3, pp. 437-447.

30. Macleod, N.R and Butler, J.H (1979), "The Evaluation of Dredging Materials for Island Construction in the Beaufort Sea", Proceedings, Eleventh Annual Offshore Technology Conference, Houston, Texas, Paper No. 3633, Vol.4, pp. 2387-2398.

31. Madsen, O.S (1978), "Wave Induced Pore Pressures and Effective Stresses in a Porous Bed", Geotechnique 28, No.4, December, pp. 377-393.

32. Martin, G.R, Finn, W.D.Liam and Seed, H.B (1975), "Some Fundamental Aspects in Liquefaction Under Cyclic Loading", Journal of the Geotechnical Engineering Division, ASCE, Vol.101, No.GT5, May, pp. 423-438.

33. Martin, P.P and Seed, H.B (1978),"APOLLO", Report No. UCB/EERC 78-21, University of California, Berkeley, California, May.

34. Nataraja, M.S and Singh, H (1979), "Simplified Procedure for Ocean Wave Induced Liquefaction Analysis", Proceedings, Fourth Conference on Civil Engineering in the Oceans, San Francisco, pp. 948-963.

35. Nordenstrom, N, Olsen, O.A, Loken, A.E and Torset, O.P (1978), "Prediction and Application of Wave Loads in Design of Offshore Structures", Fifth Preprint, International Ocean Development Conference, Tokyo, Japan, September, pp. 1-28.

36. Potter, R.E and Goff, R.D (1980), "The Design and Construction of Beaufort Sea Drilling Islands - Sag Delta 7 and 8", The Energy-Sources Technology Conference and Exhibition, Houstion, Texas, January.

37. Riley, J.G (1974), "How Imperial Built First Arctic Island", Petroleum Engineer International, Vol.46, No.1, pp. 25-28.

38. Riley, J.G (1975), "The Construction of Artificial Islands in the Beaufort Sea", Proceedings, Seventh Annual Offshore Technology Conference, Houston, Texas, Paper No. 2167, Vol.1,

39. Sarpakaya, T and Isaacson, M (1981), "Mechanics of Wave Forces on Offshore Structures", Von Nostrand Reinhold Company, New York.

40. Seed, H.B (1979), "Soil Liquefaction and Cyclic Mobility Evaluation for Level Ground During Earthquakes", Journal of the Geotechnical Engineering Division, ASCE, Vol.105, No.GT2, February, pp. 201-255.

41. Seed, H.B and Idriss, I.M (1970), "Soil Moduli and Damping Factors for Dynamic Response Analysis", EERI Report No. 70-10, College of Engineering, University of Califronia, Berkeley, December.

42. Seed, H.B, Idriss, I.M, Makdisi, F and Banerjee, N (1975), "Representation of Irregular Stress Time Histories by Equivalent Uniform Stress Series in Liquefaction Analysis", Report No. EERC 75-29, University of California, Berkeley, California, October.

43. Seed, H.B and Rahman, M.S (1977), "Analysis for Wave Induced Liquefaction in Relation to Ocean Floor Stability", Report No. UCB/TE-77/02, College of Engineering, University of California, Berkeley, December.

44. Siddharthan, R (1981), "Stability of Buried Pipelines Subjected to Wave Loading", M.A.Sc Thesis, University of British Columbia, Vancouver, May.

45. Siddharthan, R and Finn, W.D.Liam (1979,1982),"STABW; Analysis of Instability Induced in Seafloor Sands by Cumulative Effects of Storm Waves", Unpublished.

46. Sleath, J.F.A (1970), "Wave Induced Pressures in Beds of Sand", Journal of Hydraulic Division, ASCE, Vol.96, No. HY2, February, pp.367-378.

47. Stenning, D.G and Schumann, C.G (1979), "Arctic Production Monocone", Proceedings, Eleventh Annual Offshore Technology Conference, Houston, Texas, Paper No. 3630, Vol.4, pp. 2357-2366.

48. Yamamoto, T (1978), "Sea Bed Instability From Waves", Proceedings, Tenth Annual Offshore Technology Conference, Houston, Texas, Paper No. 3262, Vol.3, pp. 1819-1824.